ACTA UNIVERSITATIS SZEGEDIENSIS

ACTA PHYSICA ET CHEMICA

NOVA SERIES

TOMUS XIX

FASCICULUS 3

AUSHAF 19 (3) 189—317 (1973)

HU ISSN 0001—6721

SZEGED, HUNGARIA

1973

ACTA UNIVERSITATIS SZEGEDIENSIS

ACTA PHYSICA ET CHEMICA

NOVA SERIES

TOMUS XIX FASCICULUS 3

AUSHAF 19 (3) 189—317 (1973)

HU ISSN 0001—6721

SZEGED, HUNGARIA

1973

Adiuvantibus

M. BARTÓK, L. CSÁNYI, P. FEJES, F. GILDE, P. HUHN, I. KETSKEMÉTY, F. MÁRTA, L. SZALAY et F. SZÁNTÓ

redigit

KÁLMÁN KOVÁCS

Edit

Facultas Scientiarum Naturalium Universitatis Szegediensis de Attila József nominatae

Editionem curant

J. ANDOR, G. BERNÁTH et Á. SÜLI

Nota

Acta Phys. et Chem. Szeged

Szerkeszti

KOVÁCS KÁLMÁN

A szerkesztőbizottság tagjai:

BARTÓK M., CSÁNYI L., FEJES P., GILDE F., HUHN P., KETSKEMÉTY I., MÁRTA F., SZALAY L. és SZÁNTÓ F.

Kiadja

a József Attila Tudományegyetem Természettudományi Kara

(Szeged, Aradi Vértanúk tere 1.)

Szerkesztőbizottsági titkárok:

ANDOR J., BERNÁTH G. és SÜLI Á.

Kiadványunk rövidítése:

Acta Phys. et Chem. Szeged

FACTORIZATION OF THE GROUP O_4 AND THE HYDROGEN ATOM

By

F. J. GILDE

Institute of Theoretical Physics, Attila József University, Szeged

(Received July 21, 1973)

The relation between $SU_2 \otimes SU_2$ and O_4 is studied with a method different from the usual way, leading to the well-known results of classical quantum mechanics for the hydrogen atom.

The quantum mechanical role of continuous groups is scarcely to be overestimated since WIGNER's classical work [1]. He obtained his first success by the interpretation of the angular momentum, connecting this physical quantity with the rotation group. Later on other continuous groups became of great importance, too. May it suffice to point to the group SU_3, very important in the theory of elementar particles. Investigation into the symmetry of the hydrogen atom began early. FOCK [2], then BARGMANN [3] pointed out that the hydrogen atom has a symmetry higher than O_3, namely, O_4 symmetry. In this connection GYÖRGYI [4] obtained important results. All this points to the circumstance that the group O_4 deserves further attention from the point of view of physical applications. GYÖRGYI's mentioned results can be not only formulated in an other way [5] but also developed with respect to applications. A good review of the problem is given by MICHEL [6].

The semi-simple Lie-groups [7] can be classified according to the classification of the correnponding Lie-algebras. Accordingly, the group O_n is not simple in the case of even n, *i.e.* its algebra has a commutative ideal; this means that, for *e.g* $n=4$, O_4 can be factorized. In this paper we study this factorization and, on this basis, give the irreducible representation of the group. This conception seems also to be more convenient from the point of view of applications.

Factorization of the group O_4

Let us start from the group SU_2. This consists of all unitary matrices of determinant $+1$ of the two-dimensional complex vector space. The group SU_2 is closely connected with the rotation group of the real three-dimensional space. More precisely, there are two matrices differing in sign which correspond to a rotation of the first kind in SU_2; this circumstance will be, however, neglected in the following as irrelevant.

The irreducible representations of SU_2 can be obtained in the well-known way [1]. The irreducible representations can be distinguished by a number j ($j=0, 1/2, 1, \ldots$).

Let us denote be D_j the corresponding representation, which is of dimension $2j+1$. The defining representation belongs to $j=1/2$. The connection with the rotation group can be built up through the representation D_1.

The rotation group O_3 of the three-dimensional space can be parametrized is several equivalent ways: besides the Eulerian angles, the rotations can be characterized also by a vector the length of which is determined by the angle of rotation $\varphi(0 \leqq \varphi < \pi)$ and its direction by the polar angles of $\Phi(0 \leqq \Phi < 2\pi)$ and $\Theta(0 \leqq \Theta < \pi)$.

Starting from given groups, a further group can be defined by direct product. The direct product $G = G_1 \otimes G_2$ of two groups G_1 and G_2 is a set the elements of which consist of all pairs (g_1, g_2), where $g_1 \in G_1$, $g_2 \in G_2$. Among the elements of the resulting set, multiplication can be defined by

$$(g_1, g_2)(g_1', g_2') = (g_1 g_1', g_2 g_2'). \tag{1}$$

For this multiplication G is a group. Let us recall the pertinent algebraic theorems: (i) the representations of a direct product are given by the direct product of the representations of the factor groups; (ii) the trace of the direct product of two matrices is the product of the two traces; (iii) the representation of a direct product built up from irreducible factors is irreducible.

Accordingly, the direct product $SU_2 \otimes SU_2$ is a group with six parameters. Let us denote the parameters by Φ, Θ, φ and Φ', Θ', φ', respectively. The defining representation of the direct product is obtained by the direct product of the defining representations. Let A be a matrix of the defining representation SU_2

$$A = \begin{pmatrix} \alpha & \beta \\ -\beta^* & \alpha^* \end{pmatrix}, \quad \alpha\alpha^* + \beta\beta^* = 1, \tag{2}$$

where α and β are otherwise arbitrary complex numbers. Another element (with primed parameters) is

$$B = \begin{pmatrix} a & b \\ -b^* & a^* \end{pmatrix}, \quad aa^* + bb^* = 1. \tag{3}$$

The set of all matrices

$$T = A \otimes B = (t_{ij}) = \begin{pmatrix} \alpha a & \alpha b & \beta a & \beta b \\ -\alpha b^* & \alpha a^* & -\beta b^* & \beta \alpha^* \\ -\beta^* \alpha & -\beta^* b & \alpha^* a & \alpha^* b \\ \beta^* b^* & -\beta^* a^* & -\alpha^* b^* & \alpha^* a^* \end{pmatrix} \tag{4}$$

gives the defining representation of $SU_2 \otimes SU_2$.

The matrices T can be considered as transformations of the complex vector space spanned by the basis vectors e_1, e_2, e_3, e_4. The elements of this space are linear expressions of the following form

$$v = c_1 e_1 + c_2 e_2 + c_3 e_3 + c_4 e_4. \tag{5}$$

By T, the components c_i of vector v transform according to

$$c_i' = \sum_{j=1}^{4} t_{ij} c_j \equiv t_{ij} c_j, \quad (i = 1, 2, 3, 4). \tag{6}$$

Making use of the properties of SU_2, we obtain

$$c_1' c_4' - c_2' c_3' = c_1 c_4 - c_2 c_3, \tag{7}$$

i.e. an invariant expression. Introducing the quantities

$$x_1 = \frac{c_1+c_4}{2},\ x_2 = -i\frac{c_1-c_4}{2},\ x_3 = \frac{c_2-c_3}{2},\ x_4 = -i\frac{c_2+c_3}{2} \tag{8}$$

for which

$$x_i x_i = c_1 c_4 - c_2 c_3, \tag{9}$$

thus $x_i x_i$ will also be invariant.

The transformations of the x_i-s can be obtained from Eq. (8) (see Appendix I). By these transformations real x_i-s are converted into real ones. Therefore the quantities $x=(x_1, x_2, x_3, x_4)$ can be considered as vectors of a real four-dimensional space, and the T-s as their transformations. According to Eqs. (7) and (9), these transformations leave the length of the vector invariant.

The elements of the group O_4 consist of all real 4×4 matrices which leave the $x_i x_i$ invariant. Accordingly, all elements of $SU_2\otimes SU_2$ belong to O_4: $SU_2\otimes SU_2\subseteq O_4$. If all elements of O_4 have a corresponding element in $SU_2\otimes SU_2$, then the relation will become an isomorphism. As a proof, let us calculate the infinitesimal elements of both groups and the infinitesimal operators of the commutation relations (Appendix II). The commutation relations and structure constants of both groups are identical. Thus both groups are isomorphic at least for infinitesimal quantities.

Representations and their decompositions

The above connections between $SU_2\otimes SU_2$ and O_4 being valid, the representations of the former will be representations of the latter as well. An irreducible representation of $SU_2\otimes SU_2$, being derived from two irreducible representations of SU_2, can be characterized by two numbers $(j;j')$. The dimensions of the representation $(2j+1)(2j'+1)$ can be found for some cases in Table I. Especially, the dimensions of the irreducible representations pertaining to $j'=j$ are the squares of the natural numbers. The irreducible representations of O_4 are given by the matrices $D_j\otimes D_{j'}$.

The question of decomposing according to O_3 the representations $D_j\otimes D_{j'}$ of O_4, which in general are clearly reducible representations of O_3, seems to be of importance with respect to applications.

This problem can be solved on the analogy of the procedure used for finite groups. Instead of summing for all elements of the group, which plays an important role for finite groups, integration is to be used in the case of continuous groups [8].

Table I

j' \ j	0	1/2	1	3/2	2
0	1	2	3	4	5
1/2	2	4	6	8	10
1	3	6	9	12	15
3/2	4	8	12	16	20
2	5	10	15	20	25

Let the number $f(g)$ correspond to an element $g \in G$, then the corresponding integral will be

$$\frac{1}{V} \int_G f(g)\, dV(g), \tag{10}$$

where V is the volume of the parameter space, and $dV(g)$ the volume element around g. In the case of group O_3, the latter can be written [1] as

$$dV(g) = g(E) 2(1-\cos \Phi) \sin \varphi \, d\Phi \, d\Theta \, d\varphi \tag{11}$$

where $g(E)$ is the so called weight function. Especially, with $g(E)=1$ we obtain

$$V = 8\pi^2. \tag{12}$$

The expressions $f(g)$, important for the problem, are mostly matrix elements and traces of the representations. For these the following theorems are valid. The traces of the irreducible representations j and j' fulfil the orthogonality relation [8]

$$\frac{1}{V} \int_G \chi_j(g) \chi_{j'}^*(g)\, dV(g) = \delta_{jj'}. \tag{13}$$

A reducible representation D can be decomposed into the direct sum of irreducible representations in the form

$$D = n_1 D_{j_1} \oplus \ldots \oplus n_k D_{j_k} \tag{14}$$

where n_i is the multiplicity of the irreducible representation i. If the trace of the representation D is $\chi(g)$, then

$$n_i = \frac{1}{V} \int_G \chi(g) \chi_{j_i}^*(g)\, dV(g). \tag{15}$$

Let D be an irreducible representation of O_4, and D_{j_i} one of O_3, then Eq. (15) gives the number of the corresponding irreducible components. By these the decomposition in Eq. (14) is determined; some of the decompositions are presented in Table II.

Table II

Decompositions of $D_{j'} \otimes D_j$

$D_{j'}$ \ D_j	D_0	$D_{1/2}$	D_1	$D_{3/2}$	D_2
D_0	D_0	$D_{1/2}$	D_1	$D_{3/2}$	D_2
$D_{1/2}$	$D_{1/2}$	$D_0 \oplus D_1$	$D_{1/2} \oplus D_{3/2}$	$D_1 \oplus D_2$	$D_{3/2} \oplus D_{5/2}$
D_1	D_1	$D_{1/2} \oplus D_{3/2}$	$D_0 \oplus D_1 \oplus D_2$	$D_{1/2} \oplus D_{3/2} \oplus D_{5/2}$	$D_1 \oplus D_2 \oplus D_3$
$D_{3/2}$	$D_{3/2}$	$D_1 \oplus D_2$	$D_{1/2} \oplus D_{3/2} \oplus D_{5/2}$	$D_0 \oplus D_1 \oplus D_2 \oplus D_3$	$D_{1/2} \oplus D_{3/2} \oplus D_{5/2} \oplus \oplus D_{7/2}$
D_2	D_2	$D_{3/2} \oplus D_{5/2}$	$D_1 \oplus D_2 \oplus D_3$	$D_{1/2} \oplus D_{3/2} \oplus D_{5/2} \oplus \oplus D_{7/2}$	$D_0 \oplus D_1 \oplus D_2 \oplus \oplus D_3 \oplus D_4$

Group O_4 and the hydrogen atom

The hydrogen atom is of O_4 symmetry, therefore its eigenfunctions transform according to the irreducible representations of O_4, and its eigenvalues can be arranged according to the latter. The irreducible representations of O_4 can be characterized by the numbers (j, j'), but not all combinations have a real physical meaning; only the case $j'=j$ is realized. Except for the case $j'=j=0$, the irreducible representations are not unidimensional (Table I); the corresponding states are degenerate. What are the differences between the corresponding states?

From the infinitesimal operators belonging to group O_4 the combination

$$C = A_1^2+A_2^2+A_3^2+B_1^2+B_2^2+B_3^2 \tag{16}$$

(CASIMIR operator) can be formed. This is commutable with every A_i and B_i. The operator C is connected with the energy of the hydrogen atom [5]. This operator is commutable with $B^2 = B_1^2+B_2^2+B_3^2$, which is in similar connection with O_3, as C with O_4. The relations

$$[C, B^2] = 0, \quad [B^2, B_3] = 0, \quad [C, B_3] = 0 \tag{17}$$

will hold. There exist no further combinations of the infinitesimal operations which, joint to the operators C, B^2, B_3, would give a mutually commutable set. Thus there exist only three such operators. B^2 is connected with the absolute value of the angular momentum, and B_3 (respectively iB_3) with the third component of the latter. These results are well known from classical quantum mechanics.

Appendix I

From Eq. (6), using Eq. (4), detailed expressions for the c_i'-s can be obtained. Substituting these in Eq. (8) and rearranging, the x_i'-s can be found:

$$\begin{aligned}
x_1' &= x_1\frac{\alpha a-\beta^*b^*+\alpha^*a^*-\beta b}{2}+x_2 i\frac{\alpha a-\beta^*b^*+b\beta-\alpha^*a^*}{2}+\\
&+x_3\frac{-\beta^*a^*-\alpha b-\alpha^*b^*-\beta a}{2}+x_4 i\frac{\alpha^*b^*-\alpha b-\beta^*a^*+\beta a}{2},\\
x_2' &= x_1 i\frac{-\beta^*b^*-\alpha a+\beta b+\alpha^*a^*}{2}+x_2\frac{\beta^*b^*+\alpha a+\beta b+\alpha^*a^*}{2}+\\
&+x_3 i\frac{\alpha b-\beta^*a^*+\beta a-\alpha^*b^*}{2}+x_4\frac{\beta a-\alpha^*b^*-\alpha b+\beta^*a^*}{2},\\
x_3' &= x_1\frac{b^*\alpha+\beta^*a+\alpha^*b+\beta a^*}{2}+x_2 i\frac{\alpha b^*+\beta^*a-\alpha^*b-\beta a^*}{2}+\\
&+x_3\frac{\alpha a^*-\beta^*b+\alpha^*a-\beta b^*}{2}+x_4 i\frac{\alpha a^*-\beta^*b+\beta b^*-\alpha^*a}{2},\\
x_4' &= x_1 i\frac{\beta^*a-\alpha b^*+\alpha^*b-\beta a^*}{2}+x_2\frac{\alpha b^*-\beta^*a+\alpha^*b-\beta a^*}{2}+\\
&+x_3 i\frac{-\alpha a^*-\beta^*b+\beta b^*+\alpha^*a}{2}+x_4\frac{\alpha a^*+\beta^*b+\beta b^*+\alpha^*a}{2}.
\end{aligned} \tag{18}$$

Appendix II

The elements of the defining representation of SU_2 can be also expressed by φ, Φ, Θ

$$\alpha = \cos\frac{\varphi}{2} - i\sin\frac{\varphi}{2}\cos\Phi,\ \beta = -e^{i\Theta}\sin\frac{\varphi}{2}\sin\Phi. \tag{19}$$

An element will be infinitesimal if the angle of rotation φ is infinitesimal for Φ and Θ. In the case of small φ, Eq.-s (19) can be written in the form

$$\delta\alpha = 1 - i\frac{\varphi}{2}\cos\Phi,\ \delta\beta = -\frac{\varphi}{2}\sin\Phi e^{i\Theta} \tag{20}$$

and, for the other factor as

$$\delta a = 1 - i\frac{\varphi'}{2}\cos\Phi',\ \delta b = -\frac{\varphi'}{2}\sin\Phi' e^{i\Theta}. \tag{21}$$

Substituting these into Eq. (18) and neglecting the terms of second and higher order, we obtain

$$\delta T' = \begin{pmatrix} 1 & a_3 & -a_1 & a_2 \\ -a_3 & 1 & b_2 & b_1 \\ a_1 & -b_2 & 1 & b_3 \\ -a_2 & -b_1 & -b_3 & 1 \end{pmatrix} \tag{22}$$

where the notations

$$\begin{aligned} a_1 &= -\frac{\varphi}{2}\sin\Phi\cos\Theta - \frac{\varphi'}{2}\sin\Phi'\cos\Theta', \\ a_2 &= \frac{\varphi}{2}\sin\Phi\sin\Theta - \frac{\varphi'}{2}\sin\Phi'\sin\Theta', \\ a_3 &= \frac{\varphi}{2}\cos\Phi + \frac{\varphi'}{2}\cos\Phi' \end{aligned} \tag{23}$$

and

$$\begin{aligned} b_1 &= -\frac{\varphi}{2}\sin\Phi\cos\Theta + \frac{\varphi'}{2}\sin\Phi'\cos\Theta', \\ b_2 &= \frac{\varphi}{2}\sin\Phi\sin\Theta + \frac{\varphi'}{2}\sin\Phi'\sin\Theta', \\ b_3 &= \frac{\varphi}{2}\cos\Phi - \frac{\varphi'}{2}\cos\Phi' \end{aligned} \tag{24}$$

are used. The corresponding infinitesimal operators can be calculated from

$$\left(\frac{\partial\delta T'}{\partial a_i}\right)_{a_i=0,\ b_i=0} = A_i,\ \left(\frac{\partial\delta T'}{\partial b_i}\right)_{a_i=0,\ b_i=0} = B_i. \tag{25}$$

Then, the commutation relations will be

$$\begin{aligned} A_i A_j - A_j A_i &= B_k \\ A_i B_j - B_j A_i &= A_k \\ B_i A_j - A_j B_i &= A_k \\ B_i B_j - B_j B_i &= B_k \end{aligned} \qquad (ijk = 123, 231, 312) \tag{26}$$

and

$$A_i B_i - B_i A_i = 0 \qquad (i = 1, 2, 3). \tag{27}$$

Let a matrix g of O_4 be

$$g = \begin{pmatrix} a_{11} & a_{12} & a_{13} & a_{14} \\ a_{21} & a_{22} & a_{23} & a_{24} \\ a_{31} & a_{32} & a_{33} & a_{34} \\ a_{41} & a_{42} & a_{43} & a_{44} \end{pmatrix} \tag{28}$$

for which

$$a_{ni} a_{nk} = \delta_{ik} \qquad (i, k = 1, 2, 3, 4), \tag{29}$$

this means 10 relations for 16 real a_{ik}. Let us write these in the form

$$a_{ik} = \delta_{ik} + c_{ik} \tag{30}$$

and let the c_{ik} be infinitesimal. Then

$$c_{ki} = -c_{ik}, \quad c_{ii} = 0, \tag{31}$$

therefore the infinitesimal form of Eq. (28), using the notation

$$\begin{aligned} c_{12} &= \varepsilon_3, \quad c_{13} = -\varepsilon_1, \quad c_{14} = \varepsilon_2, \\ c_{23} &= \delta_2, \quad c_{24} = \delta_1, \quad c_{34} = \delta_3 \end{aligned} \tag{32}$$

will be

$$g = \begin{pmatrix} 1 & \varepsilon_3 & -\varepsilon_1 & \varepsilon_2 \\ -\varepsilon_3 & 1 & \delta_2 & \delta_1 \\ \varepsilon_1 & -\delta_2 & 1 & \delta_3 \\ -\varepsilon_2 & -\delta_1 & \delta_3 & 1 \end{pmatrix}. \tag{33}$$

The infinitesimal operators will be given by

$$\left(\frac{\partial g}{\partial \varepsilon_i}\right)_{\varepsilon_i = 0,\, \delta_i = 0} = A_i', \quad \left(\frac{\partial g}{\partial \delta_i}\right)_{\varepsilon_i = 0,\, \delta_i = 0} = B_i'. \tag{34}$$

For these the same commutation relations will hold as for A_i-s and B_i-s.

References

[1] *Wigner, E.:* Gruppentheorie, Friedr. Vieweg & Sohn Akt.-Ges., Braunschweig (1931).
[2] *Fock, V.:* Z. Physik **98**, 145 (1935).
[3] *Bargmann, V.:* Z. Physik **99**, 576 (1936).
[4] *Györgyi G.:* Magyar Fizikai Folyóirat **15**, 505 (1967).
[5] *Bander, M., C. Itzykson:* Rev. Mod. Phys. **38**, 330, 346 (1966).
[6] *Michel, L.*, in: Group Representation in Mathematics and Physics (ed. V. Bargmann). Springer-Verlag, Berlin (1970) p. 36. ss.
[7] *Pontrjagin, L. S.:* Topological Groups, Princeton University Press, Princeton, (1958).
[8] *Boerner, H.:* Darstellungen von Gruppen, Springer-Verlag, Berlin (1967).

РАЗЛОЖЕНИЕ ГРУППЫ O_4 И АТОМ ВОДОРОДА

Ф. Й. Гилде

Изучена связь между группами $SU_2 \otimes SU_2$ и O_4 новым методом, отличающимся от известного, и получены результаты классической квантовой механики для атома водорода.

O_4 REPRESENTATIONS AND THE SPECTRA OF HYDROGEN AND HELIUM

By

M. G. BENEDICT AND F.J. GILDE

Institute of Theoretical Physics, Attila József University, Szeged

(Received 21 July 1973)

The correspondence between some of the representations of the O_4 group and the hydrogen levels is stated again. The speciality of the occurring representations is pointed out. The helium states are obtained using $O_4 \otimes O_4 \otimes S_2$.

The group theoretical classification of hadrons based on the assumption that mesons and baryons form SU_3 multiplets has proved very fruitful. But only some of the irreducible representations of SU_3 appear really as physical states. Supposing that quarks exist, the speciality of these representations would be clear. But, as there have not been found any quarks yet, it is still a puzzle why these and not other representations do actually occur in nature. So it may be interesting to study the speciality of the occurring representations in the case of other well-known problems.

As it was shown by FOCK [1, 2], the Schrödinger equation of the hydrogen atom can be transformed into an integral equation in the space of the square integrable functions $\Psi(\vec{\xi})$ ($\vec{\xi} \in S^3$) on the four-dimensional unit sphere S^3. The Hamiltonian $\mathbf{H}(\vec{\xi})$ becomes an integral operator with a kernel invariant under rotations in the four-dimensional space. These rotations form a group, the group O_4. Let $g \in O_4$, then $\mathbf{H}(g\vec{\xi}) = \mathbf{H}(\vec{\xi})$. More generally, for each $g \in O_4$ let $\Psi(g^{-1}\vec{\xi}) = \mathbf{T}(g)\Psi(\vec{\xi})$, where $\mathbf{T}(g)$ is an operator in the space of the Ψ-s. This defines a mapping $g \to \mathbf{T}(g)$ *i.e.* a representation of the group, called quasiregular representation. It can be seen that $\mathbf{T}(g)$ commutes with $\mathbf{H}$ for each $g \in O_4$:

$$\mathbf{T}(g)\mathbf{H}(\vec{\xi})\Psi(\vec{\xi}) = \mathbf{H}(g^{-1}\vec{\xi})\Psi(g^{-1}\vec{\xi}) = \mathbf{H}(\vec{\xi})\mathbf{T}(g)\Psi(\vec{\xi}).$$

To find the possible energy levels, we have to decompose our representation $\mathbf{T}(g)$ into a direct sum of irreducible components.

The four-dimensional homogeneous harmonic polynomials of degree k ($k=0, 1, \ldots$) form a complete set on the four-dimensional unit sphere. They are of the form

$$h_4^k(\vec{x}) = \sum_{\alpha_1+\alpha_2+\alpha_3+\alpha_4=k} c_{\alpha_1\alpha_2\alpha_3\alpha_4} x_1^{\alpha_1} x_2^{\alpha_2} x_3^{\alpha_3} x_4^{\alpha_4}$$

and

$$\sum_{i=1}^{4} \frac{\partial^2}{\partial x_i^2} h_4^k(\vec{x}) = 0.$$

The value of $h_4^k(\vec{x})$ in any point is uniquely determined by its value on the unit sphere point $\frac{\vec{x}}{|\vec{x}|}$. The functions $h_4^k(\vec{\xi})$ are the four-dimensional spherical harmonics; there exist $(k+1)^2$ linearly independent such functions for each k.

These functions span a space H_4^k of dimension $(k+1)^2$ which can be shown to be invariant and irreducible under $\mathbf{T}(g)$. This means that we have decomposed our representation $\mathbf{T}(g)$ into the irreducibles $\mathbf{T}_4^k(g)$-s which act in the subspaces H_4^k. The subspaces H_4^k are usually characterized by $k+1=n$. The dimensionality of H_4^k is then n^2, which means that each level is n^2-fold degenerate. The spherical harmonics are the eigenfunctions.

Now let us take the three-dimensional rotation group O_3, which is clearly a subset of O_4. Reducing $\mathbf{T}_4^k(g)$ into the direct sum of the irreducible representations of O_4, we find that

$$\mathbf{T}_4^k(g) = \sum_{l=0}^{k} \mathbf{T}_3^l(g), \quad g \in O_3,$$

where the $\mathbf{T}_3^l(g)$-s are the $2l+1$ dimensional representations of O_3. We see that $l=0, 1, \ldots, n-1$.

Now the fact which we want to point out is that the representations $\mathbf{T}_4^k(g)$, though infinitely many of them exist, do not exhaust all the possible irreducible representations. A general irreducible representation of O_4 is labelled by two indices [3]. Thus our representations are very special, as they are labelled only by one integer k. The characteristic feature of the $\mathbf{T}_4^k(g)$-s is that they are subrepresentations of the quasiregular representation.

In the space where $\mathbf{T}_4^k$ acts there is always a vector, namely x_4^k, which is left invariant by all $\mathbf{T}_4^k(h)$ for each $h \in O_3$, because it acts only on x_1, x_2 and x_3.

The interesting fact is that the $\mathbf{T}_4^k(g)$-s are the only irreducible representations of O_4 which have this property, *i.e.* restricting them to O_3, there exists a vector in their space, invariant under all operators of the representation [4]. In the language of physics this means that, among the representations of O_4, only the $\mathbf{T}_4^k(g)$-s possess in their representation space spherically symmetric states in the three-dimensional sense, *i.e.* s states.

The above correspondence between some of the representations of O_4 and the energy levels of hydrogen gives the possibility to make a pure group-theoretical classification of the energy levels of helium. The approximate symmetry group is here the direct product group $O_4 \otimes O_4 \otimes S_2$. S_2 is the two-element permutation group and appears because the system is invariant under the operation of interchanging the two electrons. The Coulomb interaction between the two electrons breaks the $O_4 \otimes O_4 \otimes S_2$ symmetry and the real symmetry of this system is only the $O_3 \otimes S_2$ group.

The appropriate irreducible representations of $O_4 \otimes O_4 \otimes S_2$ are the direct product representations $\mathbf{T}_4^{k_1} \otimes \mathbf{T}_4^{k_2} \otimes \mathbf{T}_s^i \equiv \mathbf{T}^{k_1 k_2 i}$ where the $\mathbf{T}_4^{k_i}$-s are the representations of O_4, and $\mathbf{T}_s^i$ is one of the two possible irreducible representations of S_2, namely $\mathbf{T}_s^+$ or $\mathbf{T}_s^-$. Their invariant subspaces are the symmetric and antisymmetric two-electron functions, respectively.

In the case when $k_1 > 0$, $k_2 > 0$, the energy levels of the doubly excited atoms fall into the continuous spectrum of the singly ionized helium atom and so they are optically unobservable. Thus we shall consider only the case $k_2 = 0$.

Now if we restrict the $T^{k_1 0^i}$ representations of $O_4 \otimes O_4 \otimes S_2$ to $O_3 \otimes S_2$, they will become reducible. After finding the irreducible components we obtain some levels, but they do not give the true multiplicities.

We must take into account the spin of the electrons, too. The one-electron spin states belong to the self-representation of SU_2 [5]. This is a double valued representation of O_3 and we write it $T_3^{1/2}$. The two-electron spin states belong to the irreducible parts of $T_3^{1/2} \otimes T_3^{1/2}$. These are the T_3^0 and T_3^1 representations of O_3. The functions that span the space of T_3^1 are symmetric, while those of T_3^0 are antisymmetric when interchanging the two electrons. T_3^0 and T_3^1 are one- and three-dimensional and the corresponding states are the singlet and triplet states, respectively. The helium states belong to those representations of $O_3 \otimes S_2$ which are irreducible parts of $T^{k0+} \otimes T_3^0$ and $T^{k0-} \otimes T_3^1$. According to the Pauli principle, the symmetric representations of $O_4 \otimes O_4 \otimes S_2$ with $+$ sign are to be coupled to T_3^0 (parahelium), those with $-$ sign to T_3^1 (orthohelium). The results of the reductions are shown in Table I for parahelium and in Table II for orthohelium, with the respective spectroscopic signs in the right hand column.

Table I

n	Decomposition of Direct Products	Spectroscopic Signs
1	$T^{00+} \otimes T_3^0 = T_3^0 \otimes T_3^0 = T_+^0$	1^1S_0
2	$T^{10+} \otimes T_3^0 = (T_3^{0+} \oplus T_3^{1+}) \otimes T_3^0 = T_+^0 \oplus T_+^1$	$2^1S_0, 2^1P_1$
3	$T^{20+} \otimes T_3^0 = (T_3^{0+} \oplus T_3^{1+} \oplus T_3^{2+}) \otimes T_3^0 = T_+^0 \oplus T_+^1 \oplus T_+^2$	$3^1S_0, 3^1P_0, 3^1D_2$

In the case of T^{k10-} when $k_1=0$, the corresponding space is the zero vector, so we must begin with $k_1=1$, $n=2$.

Table II

n	Decomposition of Direct Products	Spectroscopic Signs
2	$T^{10-} \otimes T_3^1 = (T_3^{0-} \oplus T_3^{1-}) \otimes T_3^1 = (T_3^{0-} \otimes T_3^1) \oplus (T_3^{1-} \otimes T_3^1) =$	
	$= T_-^1 \oplus$	2^3S_1
	$\oplus T_-^0 \oplus T_-^1 \oplus T_-^2$	$2^3P_0, 2^3P_1, 2^3P_2$
3	$T^{20-} \otimes T_3^1 = (T_3^{0-} \oplus T_3^{1-} \oplus T_3^{2-}) \otimes T_3^1 = (T_3^{0-} \otimes T_3^1) \oplus (T_3^{1-} \otimes T_3^1) \oplus$	
	$\oplus (T_3^{2-} \otimes T_3^1) = T_-^1 \oplus$	3^3S_1
	$\oplus T_-^0 \oplus T_-^1 \oplus T_-^2 \oplus$	$3^3P_0, 3^3P_1, 3^3P_2$
	$\oplus T_-^1 \oplus T_-^2 \oplus T_-^3$	$3^3D_1, 3^3D_2, 3^3D_3$

References

[1] *Fock, V. A.:* Z. Physik **98**, 145 (1935).
[2] *Bander, M., C. Itzykson:* Rev. Mod. Phys. **38**, 330 (1966).
[3] *Weyl, H.:* The Classical Groups, Princeton University Press, Princeton, 1946.
[4] *Виленкин, Н., Я.:* Специальные функции и теория представлений групп, Наука, Москва, 1965.
[5] *Wigner, E. P.:* Group Theory and its Applications in Quantum Mechanics of Atomic Spectra, Academic Press, New York, 1959.

ПРЕДСТАВЛЕНИЯ ГРУППЫ O_4 И СПЕКТРЫ ВОДОРОДА И ГЕЛИЯ

М. Г. Бенедикт, Ф. Й. Гилде

Снова определена связь между некоторыми представлениями группы O_4 и уровнями водорода. Показаны особенности проявляющихся представлений. Состояния гелия могут быть получены также с помощью $O_4 \otimes O_4 \otimes S_2$.

DETERMINATION OF THE DIMENSIONS OF CAPILLARIES IN POROUS MATERIAL BY DIFFUSION

By

F. J. GILDE

Institute of Theoretical Physics, Attila József University, Szeged

(Received July 24, 1973)

Starting from the exact solution of FICK's equation, the theoretical time dependence of the conductivity of an electrolyte diffusing into a capillary was determined. In capillaries of unknown cross-section and length the changes in time of the conductivity can be measured. By comparing the theoretical and measured conductivities, a method is given for determining the dimensions of the capillary.

FICK's differential equations for diffusion are nowadays considered as classical laws, despite the fact that this description proved to be only approximative in modern irreversible thermodynamics. The physical problems arising in connection with these equations are of steadily increasing importance, as their mathematical background has been well elaborated.

There are different experimental ways of investigating porous material [1]; of these, the method based on diffusion is especially important. Therefore the discussion of problems of diffusion based on exact solution and fitted to the experimental conditions is of great importance from the point of view of applications. Let us consider first the problem of diffusion.

Putting a prism of quadratical cross-section with open end faces, filled with a solvent of an electrolyte, into a vessel filled with an electrolyte of concentration c_0 and diffusion constant D, at this moment $t=0$ the electrolyte begins to diffuse into the interior of the prism trough the open end faces, and after a sufficiently long time the differences in concentration will be balanced. If the volume of the vessel is great enough compared with that of the prism then, after reaching the equilibrium, the concentration will be c_0 everywhere.

For considering first the well-known question [2] concerning the changes in electrolyte concentration in the interior of the prism as a function of time and place, let us take a system of coordinates according to Fig. 1 and solve FICK's equation

$$\frac{\partial c}{\partial t} = D\left(\frac{\partial^2 c}{\partial x^2} + \frac{\partial^2 c}{\partial y^2} + \frac{\partial^2 c}{\partial z^2}\right) \qquad (1)$$

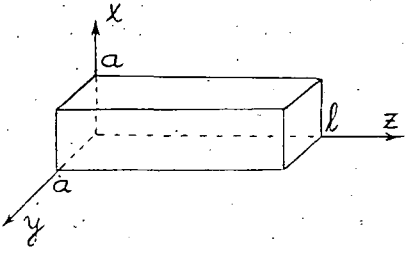

Fig. 1

with suitable conditions. We have to find a solution $c(x, y, z, t)$ with prescribed initial and boundary conditions. The initial condition is that at $t=0$ the concentration is $c=0$ in the interior of the prism and $c=c_0$ at its end faces $z=0$ and $z=l$. The boundary conditions are as follows: the concentration at the end faces $z=0$ and $z=l$ is always $c=c_0$, and at the side faces let it be always given by

$$\left(\frac{\partial c}{\partial y}\right)_{y=0,\,a} = 0, \quad \left(\frac{\partial c}{\partial x}\right)_{x=0,\,a} = 0. \tag{2}$$

These conditions, however, do not express the requirement that at $t=\infty$, $c=c_0$ everywhere. To satisfy the latter, let us consider the function

$$\vartheta = \frac{c_0 - c}{c_0} \tag{3}$$

instead of c. It is easy to see that ϑ satisfies the same differential equation as c, and the values of ϑ will be $\vartheta=1$ for $c=0$ and $\vartheta=0$ for $c=c_0$. Let ϑ be determined in the product form $T(t)X(x)Y(y)Z(z)$; in this case the differential equation will be separable. Denoting by α the separation constant, the part of the equation containing the time, and its solution will be

$$\frac{dT}{dt} = \alpha DT, \quad T(t) = e^{\alpha Dt}, \tag{4}$$

respectively. The condition $\vartheta=0$ prescibed for $t=\infty$ will be fulfilled if $\alpha<0$, therefore let be $\alpha = -k^2$. Using the decomposition $k^2 = k_x^2+k_y^2+k_z^2$ the equations

$$\frac{d^2X}{dx^2} = -k_x^2 X, \quad \frac{d^2Y}{dy^2} = -k_y^2 Y, \quad \frac{d^2Z}{dz^2} = -k_z^2 Z \tag{5}$$

will be obtained. The solution of the third of these equations, satisfying the boundary conditions $Z(0)=Z(l)=0$, is

$$B_m \sin k_z z, \quad k_z = \frac{m\pi}{l}, \quad m = 0, 1, 2, \ldots \tag{6}$$

with every B_m. The B_m-s are to be determined so as to satisfy the initial condition $\vartheta=0$ for the values $0<z<l$:

$$\sum_m B_m \sin \frac{m\pi}{l} z = 1. \tag{7}$$

From this we obtain: $B_m=0$ for even m, and $B_m = \frac{4}{m\pi}$ for odd m. Thus with $m = 2n+1$ the solution will be

$$Z(z) = \sum_{n=0}^{\infty} \frac{4}{2n+1} \sin \pi \frac{2n+1}{l} z. \tag{8}$$

Similarly, with the boundary conditions (2) in mind

$$X = 1, \quad Y = 1 \tag{9}$$

can be obtained. Returning to c, the function

$$c = c_0\left(1 - \sum_{n=0}^{\infty} \frac{4}{(2n+1)\pi} e^{-\left(\frac{2n+1}{l}\right)^2 Dt} \sin\frac{2n+1}{l}\pi z\right) \tag{10}$$

satisfies all conditions prescribed.

Let us consider Eq. (10) valid for tubes of the same cross-section q everywhere. Let two vessels of great volume, permitting to measure the conductivity, be connected by such a tube. Let us calculate with a conductivity σ, written in the form

$$\sigma = \sigma_0 \frac{c}{c_0}, \tag{11}$$

where σ_0 is the conductivity of the electrolyte of concentration c_0. At $t=0$ there is no electrolyte in the tube, therefore in this moment $\sigma=0$. To determine the function $\sigma(t)$ let the tube be divided into discs of thickness dz; than the tube can be considered as consisting of resistances in series. The total resistance R of the tube of length l will be

$$R = \int_0^l \frac{1}{\sigma}\frac{dz}{q} \tag{12}$$

i.e. using Eqs. (10) and (11)

$$R = \frac{c_0}{\sigma_0 q}\int_0^l \frac{dz}{c(z,t)} \equiv R(l,t). \tag{13}$$

If we begin to measure at a time t_0, for which

$$D\left(\frac{\pi}{l}\right)^2 t_0 \geqq 1 \tag{14}$$

than the second term of the sum in Eq. (10) will be three orders of magnitude less than the first term, thus it can be neglected. The rest can be written as

$$R(l,t) = \frac{1}{\sigma_0 q}\int_0^l \frac{dz}{1 - \frac{4}{\pi} e^{-\left(\frac{\pi}{l}\right)^2 Dt} \sin\frac{\pi}{l} z}. \tag{15}$$

With the notation

$$A = \frac{4}{\pi} e^{-\left(\frac{\pi}{l}\right)^2 Dt},$$

after integrating, we obtain the result

$$R(l,t) = \frac{4l}{\pi\sigma_0 q}\frac{1}{\sqrt{1-A^2}} \operatorname{arc\,tg}\frac{\sqrt{1-A^2}}{1-A}. \tag{16}$$

From this, for $t=\infty$, the natural value

$$R(l,\infty) = \frac{l}{\sigma_0 q} \tag{17}$$

can be obtained. The inverse of Eqs. (15) and (16) gives the conductivity.

The resistance expressed by Eq. (16) is an intricated function of time, therefore it cannot be directly used in applications, especially for studying porous materials. The quantity defined by

$$\sigma_r(t) \equiv \frac{\sigma(l, t)}{\sigma(l, \infty)} \tag{18}$$

depends on time through A, but it is independent of q. Let us introduce a new variable with the definition

$$\tau = \left(\frac{\pi}{l}\right)^2 Dt. \tag{19}$$

Some values of the function $\sigma_r(\tau)$ are listed in Table I. Finding in Table I a given value of σ_r' (e.g. about 0,8) and reading the corresponding τ', let us determine the point $\sigma_r = \sigma_r'$ of the measured σ_r curve and read the corresponding time t'. If we know the diffusion constant D of the electrolyte, l can be calculated from Eq. (19). From this, using Eq. (17), q can be obtained.

Table I

τ	σ_r	τ	σ_r
1.000	0.5795	1.709	0.8051
1.034	0.5928	1.781	0.8201
1.070	0.6094	1.858	0.8339
1.107	0.6256	1.942	0.8479
1.146	0.6416	2.033	0.8615
1.186	0.6574	2.132	0.8752
1.227	0.6731	2.244	0.8887
1.271	0.6883	2.369	0.9021
1.316	0.7037	2.512	0.9156
1.364	0.7191	2.679	0.9283
1.414	0.7338	2.880	0.9419
1.467	0.7485	3,131	0.9551
1.522	0.7630	3.468	0.9680
1.581	0.7776	3.978	0.9810
1.643	0.7918	5.077	0.9938

References

[1] *Barrer, R. M.:* J. Phys. Chem. **57**, 35 (1953). *Fatt, I.:* J. Phys. Chem. **63**, 751 (1959).
[2] *Frank, Ph., R. v. Mises:* Die Differential- und Integralgleichungen der Mechanik und Physik, II. Teil, Vieweg, Braunschweig, (1961).

ОПРЕДЕЛЕНИЕ РАЗМЕРОВ КАПИЛЛЯРОВ В ПОРИСТЫХ МАТЕРИАЛАХ ДИФФУЗИОННЫМ МЕТОДОМ

Ф. Й. Гилде

Исходя из решения уравнения диффузии Фика, мы определили временную зависимость проводимости электролита диффундирущего в узкий капилляр. В капилляре неизвестного поперечного сечения и длины временное изменение проводимости измеримо. Сравнивая теоретическую и измеряемую проводимости мы задали метод для определения размеров капилляра.

THE INFLUENCE OF VISCOSITY ON OPTICAL PROPERTIES OF DYE—DETERGENT SYSTEMS

By

J. HEVESI, E. BÁLINT and B. NÉMET

Departments of Experimental and Biophysics, József Attila University, Szeged, Hungary

(Received August 1, 1973)

The influence of glycerol on absorption and luminescence properties of dye-detergent systems containing 5.10^{-6} mole/l thionine (Th) has been studied. With increasing glycerol percentage the critical micelle concentration (c. m. c.) of these systems results to be shifted towards higher detergent concentrations. The solubilizing effect of the detergent is decreased but not fully hindered by glycerol. In solutions of the same detergent concentration the increase in luminescence intensity with increasing glycerol percentage is stronger than that of the absorption coefficient of the Th monomers. The ordered structure of water-detergent systems is found also in aqueous glycerol-detergent solutions. Accordingly, these systems can also be used as a model in studying physical processes of photosynthesis.

Introduction

For studying physical processes of photosynthesis, suitable aqueous detergent solutions (*e.g.* of sodium laurylsulphate, SLS) containing organic dyestuff were used as models [1]. In these systems, above the critical micelle concentration (c.m.c.), the cationic dyestuffs rhodamine 6G (Rh 6G), thionine (Th) and methylene blue (MB), bound to SLS micelles [2], played the role of the photosynthesizing pigments [3—5].

Earlier investigations showed, that in these systems of ordered structure, similarly as in the photosynthesizing units of plants, monomer, dimer and polymer associations (aggregates) of the dyestuffs are present and bonding (adsorption) to the detergent molecules occurs [6, 7]. It has be shown, furthermore, that the local concentration of the dyestuffs in the micelles is higher than that in the solution, *i.e.* the distribution of the dyestuffs in aqueous SLS solutions is not homogeneous [7]. Inductive resonance energy transfer, as accepted for energy migration between photosynthesizing pigments, is characteristic also in the case of the organic dyestuffs mentioned above [8—9]. The migration of the absorbed light energy occurs in the direction (Rh 6G → Th → MB), similarly as in the direction of P-700 between the photosynthesizing pigments [3, 5].

Investigations on the polarization of luminescence of chlorophyll showed that *in vivo* the molecule does not change its place during the life-time of the excited state, *i.e.* it is bound rather firmly. On the other hand, the low degree of polarization shows that the location of the molecules *in vivo* is not ordered. In the case of liquids

of low viscosity the dyestuff molecules may change their location more freely. By increasing the viscosity of the solvent it is possible to stabilize the position of the molecules in a certain degree [10].

To support this conception experimentally, we tried to influence the ordered structure of an aqueous detergent—glycerol system by changing the glycerol concentration (expressed in volume%). We studied the effect exerted on the micelle formation by the glycerol as a "foreign" solvent, and further the effect of increased concentrations of glycerol and detergent on the light absorption and emission of Th.

Materials and methods

The Th concentration was $5 \cdot 10^{-6}$ mole/l, according to [11]. The detergent (SLS) concentrations varied from $2 \cdot 10^{-3}$ mole/l to $1 \cdot 10^{-2}$ mole/l [3]. The concentrations of glycerol were 0, 15, 30, 45 and 60 volume percents. Each of the five series studied consisted of solutions of nine different SLS concentrations. Measurements were made at constant temperature (25 ± 1 °C). Changes in transport properties (viscosity, conductivity) were used to determine the c.m.c. Viscosity was determined using a Höppler viscosimeter Type U-10. The solutions were prepared, conductivity, absorption and emission spectra were measured as described in [4—6].

Experimental results and discussion

As well known, the viscosity η and conductivity τ is significantly changed by increasing the glycerol concentration. At the same SLS concentration the viscosity η increases rapidly as a function of the glycerol—water ratio [12], while the conductivity shows a less quick decrease. Therefore it is to be expected that the c.m.c. values determined from measurements of η and τ [13], respectively, will show differences. These are found in fact in the data of Table I, which gives the values of c.m.c. determined with both methods. It can be seen, however, that — irrespective of the method — the c.m.c. of the systems is shifted towards higher detergent concentrations with increasing glycerol concentration.

The increase in glycerol concentration and the consecutive increase in c.m.c. exert a significant effect on the light absorption of dyestuff—detergent systems. Fig. 1 shows the absorption spectra of Th solutions containing 30% glycerol and four different concentrations of detergent. As shown in the figure, four maxima are

Table I

	$C_{(glycerol)}$ (%)				
	0	15	30	45	60
	c.m.c.$_{(SLS)}$ 10^3 mole/l				
c.m.c. determined on the base of conductivity	3.3	4.0	4.5	5.7	7.0
c.m.c. determined on the base of viscosity	3.0	3.5	4.5	6.0	7.0

found in the spectra below the c.m.c. ($4.5 \cdot 10^{-3}$ mole/l SLS), while above the c.m.c. only two bands can be seen. Our results are in accordance with [3, 12]. The maxima at 600 nm and 565 nm can be attributed to monomer and dimer forms of the dye (bands $k_\alpha(\lambda)$ and $k_\beta(\lambda)$, respectively). The maximum observed at 460 nm may be due to Th—SLS complex salts (band $k_\gamma(\lambda)$) and the maximum at 640 nm to the light absorption of higher Th aggregates (band $k_\delta(\lambda)$).

The values of these maxima for each of the five glycerol concentrations are plotted *vs.* detergent concentration in Figs. 2 and 3. These figures show that the values of $k_\alpha(\lambda)_{max}$ and $k_\beta(\lambda)_{max}$ are significantly lower, while $k_\gamma(\lambda)_{max}$ is significantly higher

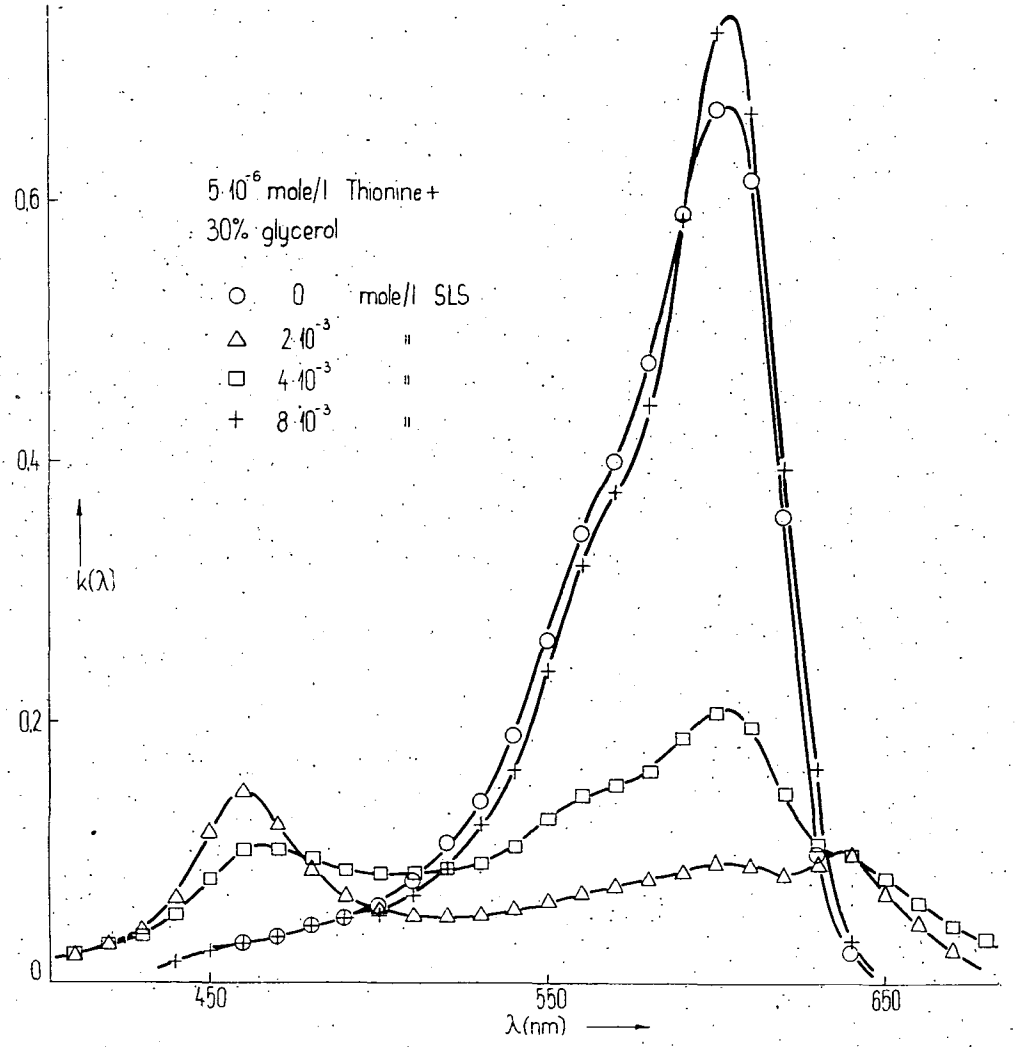

Fig. 1

Table II

glycerol % / SLS 10^3 mole/l	0		15		30		45		60	
	$k_\alpha(\lambda)_{max}$ %	$f_q(\lambda)_{max}$ %	$k_\alpha(\lambda)_{max}$ %	$f_q(\lambda)_{max}$ %	$k_\alpha(\lambda)_{max}$ %	$f_q(\lambda)_{max}$ %	$k_\alpha(\lambda)_{max}$ %	$f_q(\lambda)_{max}$ %	$k_\alpha(\lambda)_{max}$ %	$f_q(\lambda)_{max}$ %
0	100	100	100	100	100	100	100	100	100	100
2	15.3	10.1	14.1	7.1	13.4	8.3	16.2	8.8	19.4	17.8
3	35.6	29.2	25.8	13.4	19.4	10.8	18.4	12.6	21.0	19.7
4	102.0	62.8	85.0	61.3	31.2	15.9	23.1	21.0	26.0	23.7
4,5	—	—	107.0	120.0	87.0	74.0	—	—	—	—
5	114.0	128.5	111.0	126.5	107.5	105.0	31.5	24.3	28.7	28.1
6	117.0	136.0	113.0	137.0	110.0	124.0	73.0	76.0	39.4	34.3
7	—	—	—	—	—	—	114.0	135.0	52.2	46.5
8	117.5	139.0	114.0	139.0	111.0	124.5	116.5	140.0	69.5	70.0

for $2 \cdot 10^{-3}$ mole/l SLS concentration than those for pure aqueous solutions. With increasing detergent concentration the values of $k_\alpha(\lambda)_{max}$ become "saturated", the values of $k_\beta(\lambda)_{max}$ show maxima, while those of $k_\gamma(\lambda)_{max}$ decrease to reach a constant value. The changes in the values of $k_\delta(\lambda)_{max}$, not shown in our figures, are of similar character as those of $k_\gamma(\lambda)_{max}$.

The changes observed at the same glycerol concentration may be explained by the solubilizing effect of SLS [14]. Namely, the detergent dissolves, though in a less extent, the Th aggregates and Th—SLS complexes existing at low SLS concentration even below the c.m.c. Intensive solubilization occurs only with the formation of micelles, as shown by the steep increase in the $k_\alpha(\lambda)_{max}$ and $k_\beta(\lambda)_{max}$ curves and the maximum of the $k_\gamma(\lambda)_{max}$ curves. At SLS concentrations much higher than the c.m.c., first the dissolution of the dyestuff—detergent complexes comes to an end, than the decrease in the number of dimers and the resulting increase in that of monomer Th molecules ceases.

In the systems investigated, only the Th monomers show luminescence; therefore it is easier to survey the changes in the emission spectra by means of the values of $f_q(\lambda)_{max}$, than by those of the absorption spectra. In Fig. 4 $f_q(\lambda)_{max}$ is plotted for five series of solutions with different glycerol concentrations. As can be seen, the shape of the curves is similar to that of the $k_\alpha(\lambda)_{max}$ curves, with the difference that the changes in $f_q(\lambda)_{max}$, compared with pure aqueous solutions (without

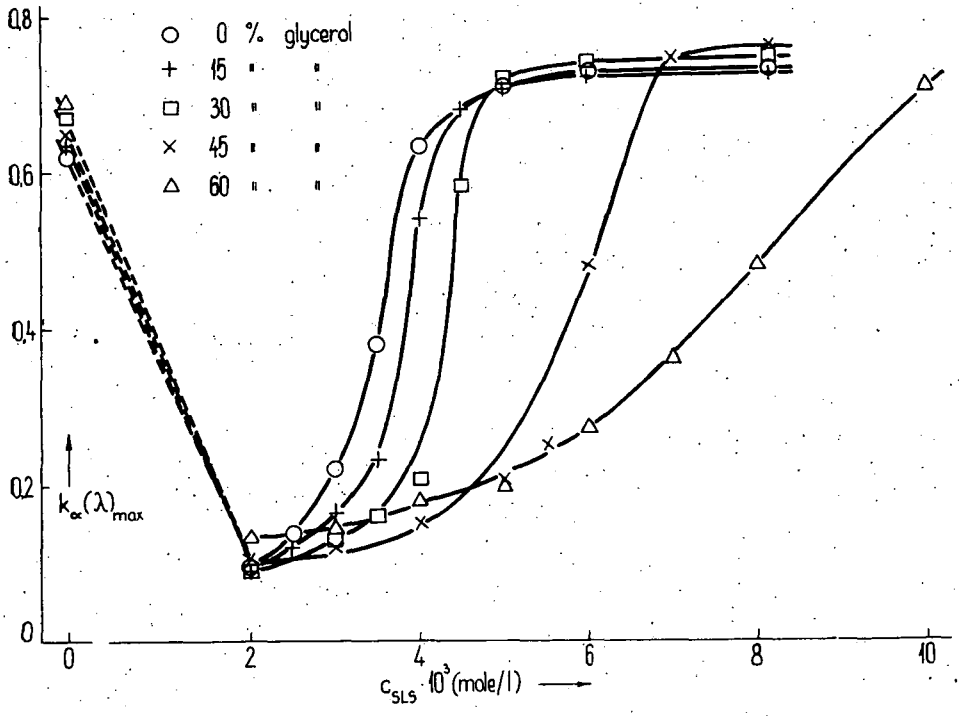

Fig. 2

glycerol), are more expressed for each glycerol concentration than in the case of $k_\alpha(\lambda)_{max}$.

The changes in intensity of emission become more conspicuous from the data of Table II, in which the changes in intensity of aqueous detergent solutions are compared with $k_\alpha(\lambda)_{max}$ and $f_q(\lambda)_{max}$ values of solutions containing no detergent. It can be seen from the table that below c.m.c. significant decreases, above c.m.c. increases in the respective values were found. Higher glycerol concentrations act against the above increase of intensity.

Fig. 2 shows that the $k_\alpha(\lambda)_{max}$ values of aqueous solutions are slightly increased with increasing glycerol concentration. This increase may be explained by a decrease of the dimer forms. This is supported by the decrease in the $k_\gamma(\lambda)_{max}$ values of aqueous solutions shown in Fig. 3. However, the increase in $k_\alpha(\lambda)_{max}$ may also be due to

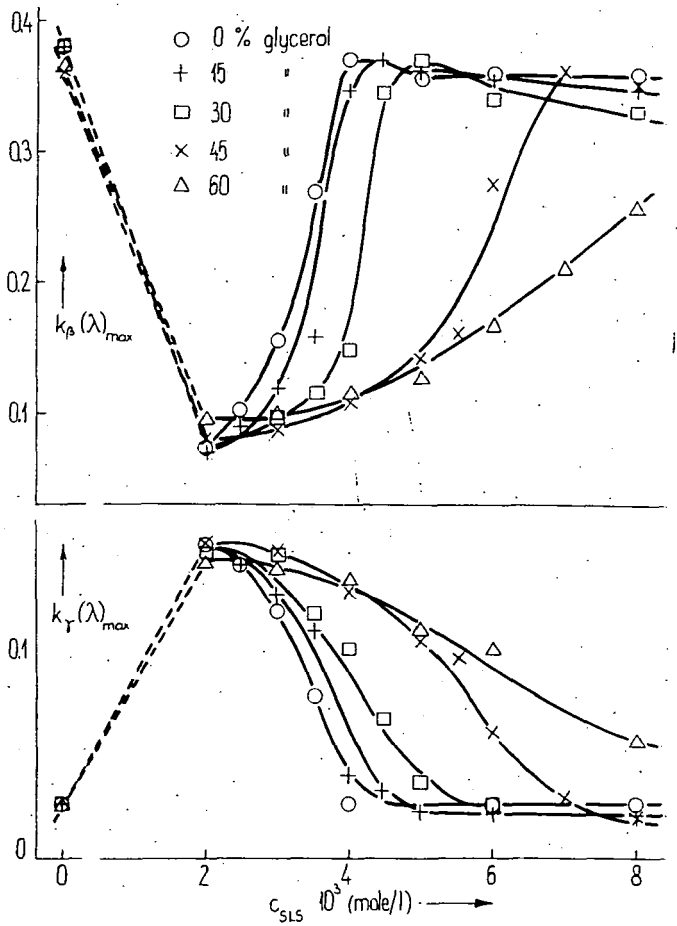

Fig. 3

dissolution caused by the glycerol of dyestuff associations of higher order, absorbing beyond the wavelength range investigated.

On the other hand, the $f_q(\lambda)_{max}$ values of aqueous solutions show greater increases owing to glycerol than the values of $k_x(\lambda)_{max}$. This may be explained as follows: with increasing glycerol concentration, the probability of extinction of excited molecules decreases, *e. g.* by the decreasing probability of kinetic collisions of molecules during the life-time of excitation. This may be caused by higher viscosity of the solvent, which shows an exponential increase as a function of glycerol concentration [12], while the emission increases linearly. Another explanation may be found in differences between macroscopic an microscopic viscosity [16].

Our results show that, by increasing the glycerol concentration in aqueous detergent solutions, the c.m.c. is shifted towards higher detergent concentrations. The solubilizing effect of the detergent is decreased, but not totally hindered by glycerol. This can be explained by the fact that, with increasing glycerol concentration, the dielectrical constants of the solutions undergo changes (the refractive index increases, the dielectric constant decreases [15]) and hereby the conditions of micelle-formation are changed. It can be stated, furthermore, that in solvent systems consisting of mixtures of water, SLS, and glycerol micelles are also formed, though at higher detergent concentrations, thus permitting the formation of ordered lamellar structures. Therefore, these systems can also be used as models for studying photosynthetizing systems.

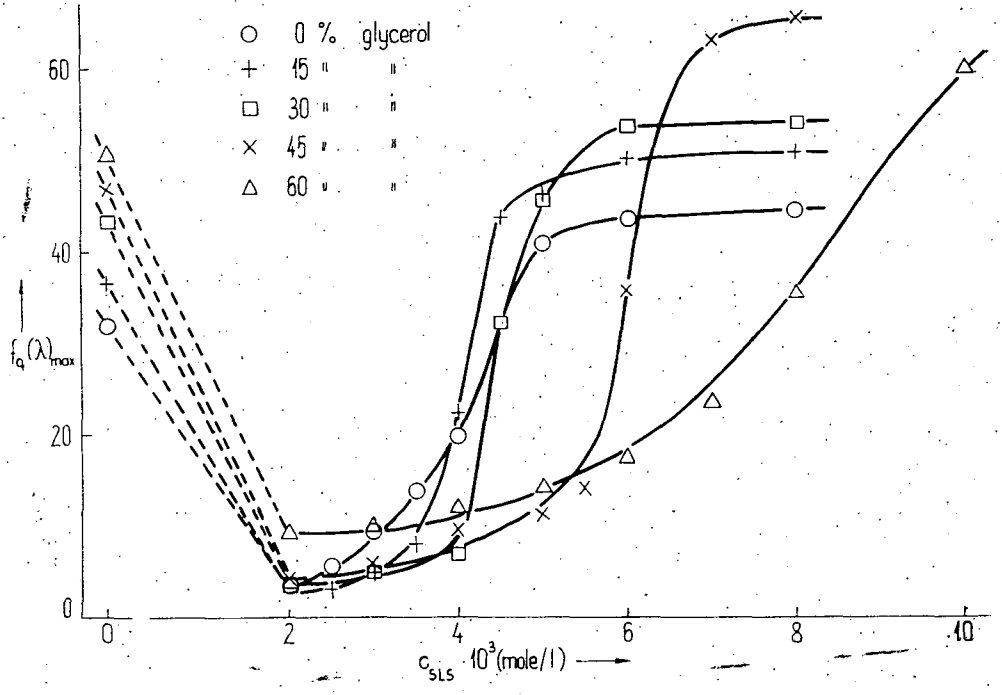

Fig. 4

References

[1] *Duysens, L. M. V.:* Progress in Biophysics, **14**, 1 (1964).
[2] *Winsor, P. A.:* Chem. Rev. **68**, 55 (1948).
[3] *Singhal, G. S., E. Rabinowitch, J. Hevesi, V. Srinivasan:* Photochem. Photobiol. **11**, 531 (1970).
[4] *Hevesi J., E. Lehoczki, E. Bálint:* Zh. Prikl. Spektr. **13**, 458 (1970).
[5] *Lehoczki E., E. Bálint, J. Hevesi:* Zh. Prikl. Spektr. **16**, 97 (1972).
[6] *Bálint E., E. Lehoczki, J. Hevesi:* Acta Phys. et Chem. Szeged **17**, 15 (1971).
[7] *Lehoczki, E., J. Hevesi:* Acta Phys. et Chem. Szeged **18**, 11 (1972).
[8] *Galanin, M. D.:* Zh. ETF **21**, 126 (1951).
[9] *Förster, Th.:* Ann. Phys. **2**, 55 (1948).
[10] *Losev, A. P., E. I. Zen'kevich:* Zh. Prikl. Spektr. **9**, 144 (1968).
[11] *Hevesi, J., Zs. Rózsa:* Acta Phys. et Chem. Szeged **17**, 127 (1971).
[12] *Erdey-Gruz T., E. Kugler:* Acta Chim. Acad. Sci. Hung. **57**, 301 (1968).
[13] *Sata, N., K. Tyuzyo:* Bull. Chem. Soc (Japan) **26**, 177 (1953).
[14] *Mukarjee, P., K. J. Mysels:* J. Amer. Chem. Soc. **77**, 2937 (1965).
[15] *Gáti, L., L. Szalay:* Acta Phys. et Chem. Szeged **5**, 87 (1958).
[16] *Frank, H. S.:* Chemical Physics of Ionic Solutions (ed. by B. E. Conway and R. G. Barradas, New York, 1966).

ВЛИЯНИЕ ВЯЗКОСТИ НА ОПТИЧЕСКИЕ СВОЙСТВА СИСТЕМ КРАСИТЕЛЬ-ДЕТЕРГЕНТ

Я. Хевеши, Э. Балинт, Б. Немет

В работе исследовалось влияние глицерина на абсорбционные и люминесцентные свойства систем краситель-детергент, содержащих $5 \cdot 10^{-6}$ моль/л тионина (Th). Критическая концентрация мицеллообразования (ККМ) с увеличением содержания глицерина смещается в сторону более высокой концентрации детергента. Солюбилизирующее действие детергента в присутствии глицерина уменьшается. В растворах, содержащих одинаковую концентрацию детергента, интенсивность люминесценции с увеличением количества глицерина сильнее возрастает, чем абсорбционный коэффициент мономерной формы тионина. В растворах вода-глицерин-детергент тоже образуется такая же упорядоченная структура как и в системах вода-детергент. Следовательно, эти системы можно использовать при исследовании физических процессов фотосинтеза в качестве модельной системы.

РАСЧЕТ СПЕКТРАЛЬНЫХ ХАРАКТЕРИСТИК ГЕНЕРАЦИИ ПРИ НАРУШЕНИИ УНИВЕРСАЛЬНОГО СООТНОШЕНИЯ СТЕПАНОВА МЕЖДУ СПЕКТРАМИ ПОГЛОЩЕНИЯ И ЛЮМИНЕСЦЕНЦИИ СЛОЖНЫХ МОЛЕКУЛ

И. КЕЧКЕМЕТИ, Л. П. ЕЖОВА, Л. КОЗМА, А. Н. РУБИНОВ

Институт экспериментальной физики Университета им. Аттилы Йожефа, Сегед;
Институт физики АН БССР, Минск

(Поступило в редакцию 25 июня 1973 г.)

Авторы исследовали совпадение лазерных параметров, полученных расчётами, используя разные аналитические выражения для спектров поглощения и люминесценции. Показано, что на основе тех формул лазерных параметров, которые содержат и спектр флуоресценции, получаются между собой хорошо совпадающие результаты.

Для расчета спектральных свойств излучения лазера на красителях необходимо знать спектр его усиления [1]:

$$K_{\text{ус}_1}(\nu) = \frac{h\nu}{v}[n_3 B_{31}(\nu) - n_1 B_{13}(\nu)] \tag{1}$$

Коэффициент усиления зависит от населенностей уровней основного и возбужденного состояний n_1 и n_3 и коэффициентов Эйнштейна для вынужденного испускания и поглощения $B_{31}(\nu)$ и $B_{13}(\nu)$. Для удобства расчетов часто используется связь между коэффициентами Эйнштейна

$$\frac{B_{13}(\nu)}{B_{31}(\nu)} = e^{-\frac{h(\nu_{\text{эл}}-\nu)}{kT}} \tag{2}$$

по существу представляющая собой видоизмененное по форме универсальное соотношение Степанова между спектрами поглощения и испускания сложных молекул [2].

Подставляя (2) в (1) можно получить две формулы для коэффициента усиления:

$$K_{\text{ус}_2}(\nu) = \frac{h\nu}{v} B_{31}(\nu)[n_3 - n_1 e^{-\frac{h(\nu_{\text{эл}}-\nu)}{kT}}] \tag{3}$$

$$K_{\text{ус}_3}(\nu) = \frac{h\nu}{v} B_{13}(\nu)[n_3 e^{\frac{h(\nu_{\text{эл}}-\nu)}{kT}} - n_1] \tag{4}$$

Для расчета по первой из них необходимо знать спектральный контур $B_{31}(\nu)$,

который определяется из спектра люминесценции вещества, а для расчета по второй — контур $B_{13}(\nu)$, однозначно определяемый из спектра поглощения.

Если универсальное соотношение Степанова выполняется строго, то результаты расчета по формулам (3) и (4), разумеется, совпадают. Однако в ряде работ показано, что универсальное соотношение может в большей или меньшей степени нарушаться [3—6] в таких случаях остается неясным, можно ли для анализа и численных расчетов характеристик генерации красителей пользоваться формулами (3) и (4) и в какой мере результаты этих расчетов будут отличаться от результатов расчетов по формуле (1).

В данной работе этот вопрос рассматривается на примере широко распространенного лазерного красителя — родамина Б. Спектры $B_{13}(\nu)$ и $B_{31}(\nu)$ этого красителя задавались аналитически.

В литературе имеется несколько способов аналитического описания кривых люминесценции и поглощения. В большинстве своем они громоздки и содержат множество параметров, которые нужно определять независимо друг от друга из различных экспериментов. Мы воспользовались аналитическими зависимостями для спектров поглощения и люминесценции, предложенными в работах [7, 8]. Эти формулы достаточно просты и хорошо согласуются с экспериментальными данными. Согласно этим работам спектральный контур коэффициентов Эйнштейна для поглощения и вынужденного испускания можно представить в виде

$$B_{31}(\nu) = Be^{-b_1\nu}\,\mathrm{sech}\,[a_1(\nu-\nu_{01})] \tag{5}$$

$$B_{13}(\nu) = Ae^{b_2\nu}\,\mathrm{sech}\,[a_2(\nu_{02}-\nu)] \tag{6}$$

где $b_i \approx \dfrac{h}{2kT}$, — характеризует ширину полос и определяется из условий эксперимента, A и B-эмпирические постоянные. Универсальное соотношение Степанова выполняется только в том случае, когда $b_1=b_2$, $a_1=a_2$, $\nu_{01}=\nu_{02}$. Однако, выражения (5) и (6) хорошо совпадают с соответствующими экспериментальными функциями лишь при $b_1 \neq b_2$, $a_1 \neq a_2$, $\nu_{01} \neq \nu_{02}$. В частности, для родамина Б необходимо использовать величины $b_1 = 7{,}59 \cdot 10^{-14}$ *сек*, $b_2 = 8{,}05 \cdot 10^{-14}$ *сек*, $a_1 = 10{,}37 \cdot 10^{-14}$ *сек*, $a_2 = 12{,}6 \cdot 10^{-14}$ *сек*, $\nu_{01} = 5{,}29 \cdot 10^{14}$ *гц*, $\nu_{02} = 5{,}33 \cdot 10^{14}$ *гц*. При этом условии результаты расчетов по формулам (1), (3) и (4) различаются. На рис. 1 приведены спектры усиления, вычисленные при разных величинах n_3/n_1 всеми тремя способами. Из рисунка видно, что расчеты по формулам (1) и (3) дают справнительно близкие результаты, особенно на длинноволновом участке полосы усиления. Существенное различие наблюдается лишь в коротковолновой части спектра. Расчёт же по формуле (4) приводит к резкому искажению спектра усиления как по величине, так и по форме и расположению полосы в шкале частот.

Формулы (1), (3), (4) обычно используются для расчета частоты генерируемого излучения. В квазистационарном приближении без учета поглощения из метастабильного состояния частота генерации $\nu_г$ может быть найдена из системы уравнений [9]:

$$\frac{\partial(K_{ус}(\nu)-K_{пот}(\nu)}{\partial\nu} = 0 \tag{7}$$

$$K_{ус}(\nu) = K_{пот}(\nu)$$

Результаты расчета $\nu_г$ различаются в зависимости от того, какое из выражений (1), (3), (4) подставляется в (7). Зависимости частоты генерации от концентрации молекул и коэффициента потерь резонатора представлены на рис. 2. и 3. Из рисунков видно, что при использовании вместо (1) формулы (3) и особенно формулы (4) получаемые значения частот и характер зависимостей

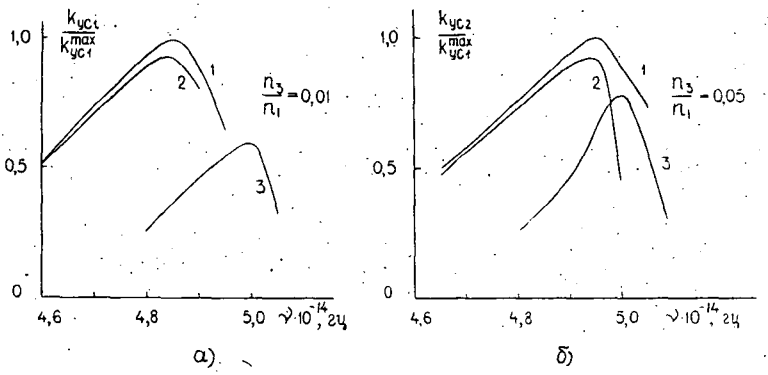

Рис. 1а, б Зависимость коэффициента усиления $K_{ус}$ растворв родамина Б от частоты при различных отношениях $\frac{n_3}{n_1}$:

а) $\frac{n_3}{n_1} = 0{,}01$; *б)* $\frac{n_3}{n_1} = 0{,}05$.

Кривая 1 рассчитана по формуле (3);
кривая 2 рассчитана по формуле (1);
кривая 3 рассчитана по формуле (4);

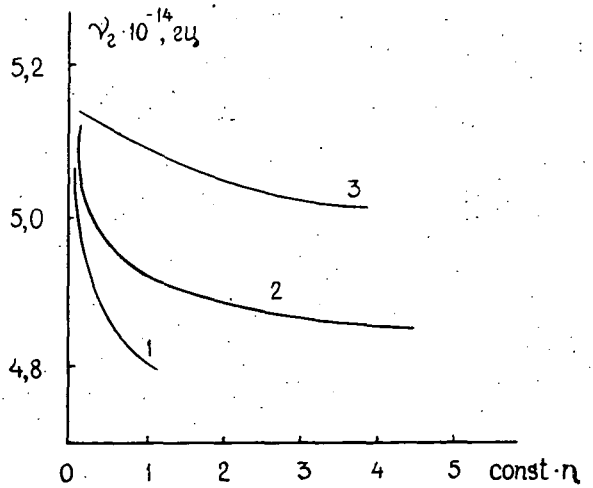

Рис. 2. Зависимость частоты генерации $\nu_{ген}$ от концентрации молекул родамина Б. Кривая 1 рассчитана по формуле (3); кривая 2 рассчитана по формуле (1); кривая 3 рассчитана по формуле (4).

существенно искажаются. Это обстоятельство надо иметь в виду при сопоставлении экспериментальных и расчетных данных особенно при определении тех или иных параметров лазера по характеристикам его генерации. Так, например, если находить коэффициент потерь лазера по частоте генерации, то использование кривой 3 вместо кривой 1 на рис. 3 может дать значение $K_{пот}$, более чем в 5 раз превышающее истинное.

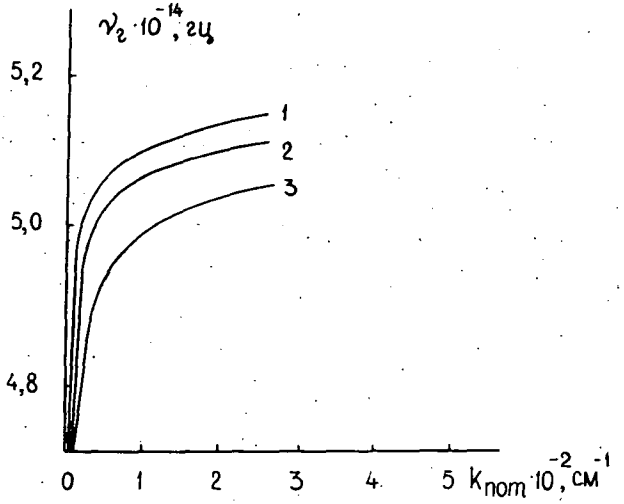

Рис. 3. Зависимость частоты генерации $\nu_{ген}$ от коэффициента потерь $K_{пот}$.
Кривая 1 рассчитана по формуле (3);
кривая 2 рассчитана по формуле (1);
кривая 3 рассчитана по формуле (4).

Литература

[1] *Степанов Б. И., Рубинов А. Н.:* УФН, вып. 1, 1968.
[2] *Степанов Б. И., Казаченко Л. П.:* ДАН СССР, **112**, 1027, 1957.
[3] *Бахшиев Н. Г., Питерская И. В., Алтайская А. В.:* Опт. и спектр. 1970, 28, № 5.
[4] *Гладченко Л. Ф., Пикулик Л. Г.:* ЖПС, 1970, 12, П 3.
[5] *Бахшиев Н. Г., Питерская И. В., Студенов В. И.:* Опт. и спектр. 1969, 27, № 2.
[6] *Степанов Б. И., Казаченко Л. П.:* ЖПС, 14, № 5.
[7] *Dombi J., Ketskeméty I., Kozma L.:* Acta Phys. et Chem. **10.** 1 (1964).
[8] *Кечкемети И., Козма Л., Хевеши Я.:* Acta Phys. et Chem. **12.** 3 (1966).
[9] „Методы расчёта оптических квантових генераторов" под редакцией Б. И. Степанова, т. 1, Минск, „Наука и техника", 1966.

CALCULATION OF THE SPECTRAL CHARACTERISTICS OF LASERS IN CASE OF DEVIATION FROM STEPANOV'S UNIVERSAL RELATION BETWEEN ABSORPTION AND LUMINESCENCE SPECTRA OF COMPLICATED MOLECULES

I. Ketskeméty, L. P. Ezhova, L. Kozma, A. N. Rubinov

The authors studied the problem as to how much the laser parameters obtained by calculation in different ways are in agreement with each other. It results that the formulas containing also emission spectrum give results wich are in good accordance.

О РАСЧЕТЕ ЧАСТОТЫ ГЕНЕРАЦИИ ЛАЗЕРОВ НА КРАСИТЕЛЯХ В КВАЗИСТАЦИОНАРНОМ РЕЖИМЕ

И. КЕЧКЕМЕТИ, Л. КОЗМА

Институт экспериментальной физики Университета им. Аттилы Йожефа, Сегед

(Поступило в редакцию 20 июня 1973 г.)

В докладе используется формула авторов для порога генерации, которой определяется частота генерации на основе экспериментальных данных флуоресценции. Вычисленные длины волны при перестройки генерации хорошо совпадают с экспериментальными данными.

Ряд работ (см. [1], [2]) посвящено теоретическому изучению процессов, протекающих в лазерах на растворах органических красителей. Самой обширной работой считается [1], в которой показано, что в квазистационарном режиме все параметры генерации определяются люминесцентными характеристиками активного вещества и параметрами резонатора. Однако формулы, описывающие связь между параметрами генерации и люминесценции, громоздкие и содержат ряд параметров, средих них таких, которые нужно определять отделными экспериментами и дополнительными расчётами. Так кажется, что по этой причине сравнительно мало таких исследований при которых вычисленные данные генерации, полученные на основе теоретических формул сравнивались бы с измеренными.

На основе общеизвестного трёхуровненного моделя генерирующего вещества нам удалось получить более простые формулы, которые содержат легко определяемые величины [3]. В работах [4] и [5] мы исследовали перестройки генерации родаминовых красителей путём изменения концентрации активного вещества и изменения селективных потерь резонатора. В другом эксперименте в резонаторе помещалась стандартная кювета с растворами (родамин Б, бриллиантовый зелёный), вызывающими селективные потери в области генерации родамина 6Ж. Конструкция резонатора позволила накачивать только активное вещество, а перестраивающий раствор облучался всего лазерным лучом. Обеими методами получился широкий диапазон длины волн перестройки, и экспериментальные данные довольно хорошо согласовались с расчётными данными, которые определялись по местам минимума функции порога генерации, полученным в [1]. При этих расчётах предполагалось, что генерация происходит на тех длиннах волн, где порог минимальный.

Цель настоящей работы, получить частоты генерации на основе нашей более простой формулы, используя экспериментальные флуоресцентные дан-

ные. В [3] для порога генерации получено соотношение

$$\tau_0 \eta_M U_H^n(\nu) = \frac{k(\nu)+\varrho}{n\dfrac{\nu^2}{8\pi\tau_0}\dfrac{f_q(\nu)}{\nu^2} - \dfrac{\varrho+[1-\eta(\nu)]k(\nu)}{P}} \qquad (1)$$

где $k(\nu)$ — коэффициент поглощения, $fq(\nu)$ — спектр флуоресценции, τ_0 — естественное время затухании, $\eta(\nu)$ — спектр квантового выхода, η_M — максимальное значение квантового выхода, v — скорость света в активной среде, ϱ — коэффициент потерь резонатора, P_{ik} — вероятность безизлучательного перехода с i-того на k-тый уровень, $\frac{1}{P} = 1 + P_{32}/P_{21}$, n-концентрация молекул активного вещества.

При расчёте перестройки частоты генерации коэффициент ϱ взят из [4], а другие величины, зависящие от концентрации, определили обычными методами. В [3] показано, что для родаминов $P=1$. На рис. 1 приведены измеренные и вычисленные длинны волн генерации родамина Б (а) и родамина 6Ж (б) при разных концентрациях.

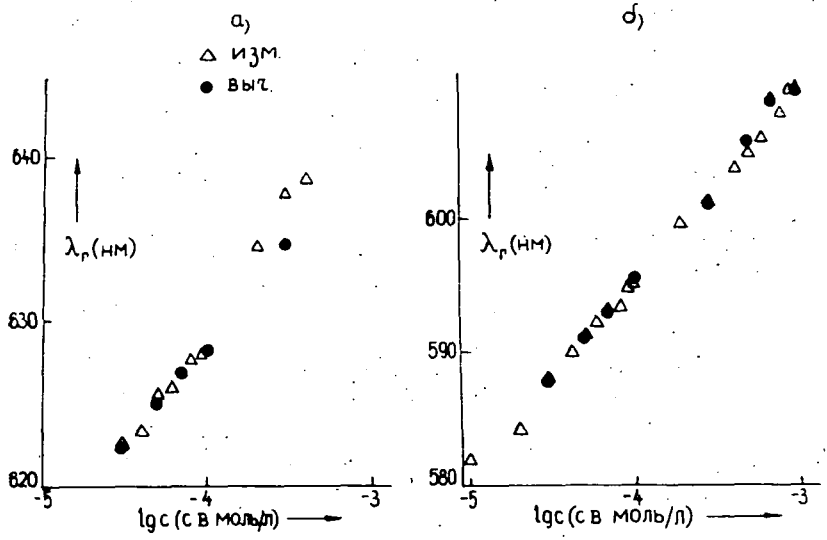

Рис. 1

Во втором методе перестраивающий раствор селективно увеличивает потери вследствие поглощения и это надо учитывать в (1) так, что вместо ϱ необходимо взять $\varrho + k_1(\nu)$, где $k_1(\nu)$ коэффициент поглощения перестраивающих растворов (родамин Б и бриллиантовый зелёный в этиловом спирте при разых концентрациях), относящийся к единичной толщине активного вещества. Все другие величины в (1) характеризуют активный раствор (родамин 6Ж в этиловом сиирте при концентрации 7.10^{-5} моль/л).

Кривые порога изображены на рис. 2. Вещества, находящиеся в перестраивающей кювете и их концентрация приведены возле кривых. Видно, что оба вещества постепенно увеличивают порог, и так родамин Б силнее поглощает в коротковолновой области генерации родамина 6Ж, бриллиантовый зелёный, наоборот, в длинноволновой, с ростом концентрации этих веществ гене-

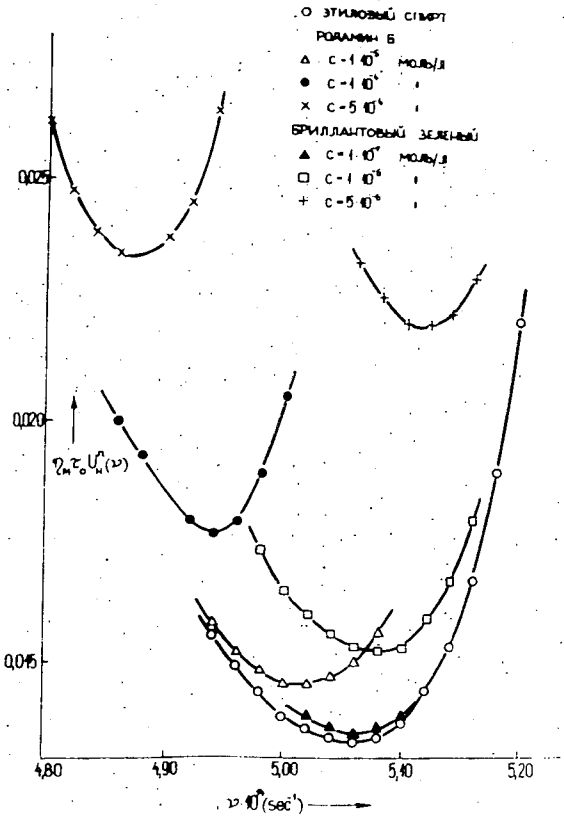

Рис. 2

рация перестраивается противоположно. Хорошее совпадение экспериментальных и теоретических данных видно из рис. 3 где приведена зависимость длины волны генерации от концентрации перестраивающего раствора. По оси ординат кружки обозначают длину волны генерации в том случае, когда в перестраивающей кювете находится этиловой спирт. Совпадение теоретических данных с экспериментальными намного лучше, чем полученных на основе других формул.

Приведенные резултаты свидетельсвуют о том, что формулы, выведенные нами, хорошо применимы для описания процессов, протекающих в лазерах на красителях.

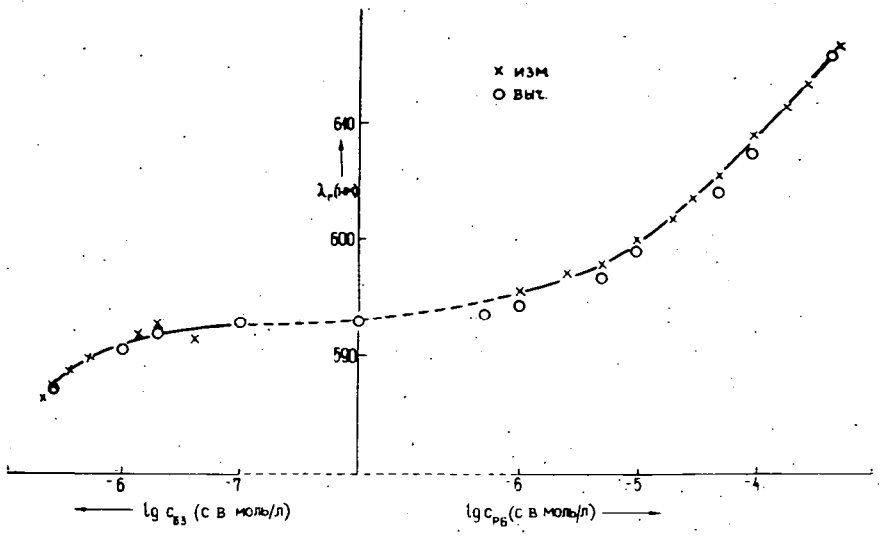

Рис. 3

Литература

[1] *Б. И. Степанов, А. Н. Рубинов:* Успехи физ. наук, **95**, 45 (1968): *Б. И. Степанов:* Методы расчёта оптических квантовых генераторов на органических красителях при монокроматическим возбуждения. Препринт. Минск, Институт физики АН БССР.

[2] *B. B. Snavely:* Proceedings of the IEEE, **57**, 1374 (1969).

[3] *Ketskeméty I., L. Kozma:* Z. Naturforsch, **27a**, 1685 (1972) Acta Phys. Hung. (В печати).

[4] *И. Кечкемети, Л. Козма, И. Салма, Б. Рац, З. Хун:* Журнал Прикладной Спектроскопии, **14**, 1000 (1971).

[5] *И. Кечкемети, Б. Рац, И. Салма, Э. Хун, Л. Козма:* Acta Phys. et Chem. Szeged **17**, 9 (1971)

CALCULATION OF THE FREQUENCY OF GENERATION OF DYE LASERS IN QUASISTATIONARY REGIME

I. Ketskeméty and L. Kozma

A formula of the authors concerning the threshold of generation is discussed. This formula permits to calculate the frequency of generation from the experimental characteristics of fluorescence. The frequencies calculated for tuning of the laser are in good agreement with experimental results.

CHEMISTRY IN LASERS: QUANTUM STATES IN DYE LASERS

By

C. P. KESZTHELYI

Department of Chemistry, The University of Texas, Austin, Texas 78 712, U.S.A.[1]

(Received July 20, 1973)

In a dye laser the quantum states of the optically active molecules comprise a photon density dependent time-oriented sequence, requiring a two-dimensional *eigenvalue spectrum matrix*, rather than the usual one dimensional array used in spontaneous fluorescence. The mathematical representation of the time-oriented sequence of quantum states is a countable finite Markov chain, and a holomorphic map containing the eigenvalues includes both the tardyon and tachyon solutions, the tardyon-Hermitian matrix being a special case. Because different quantum states dominate the spontaneous and the laser emitter particles, altered chemical properties and reactions are predicted for an optical resonant cavity.

In a previous paper dealing with chemistry in lasers [1] the fluorescence excitation and emission spectrum of a molecule in solution showing a Stokes 0—0 loss[2] [2, 3] was compared to a 3-level and 4-level laser. The comparison revealed a close similarity between the fluorescence spectrum and a 4-level laser. Information on 3-level and 4-level lasers, including the advanteges of the latter, is available in standard texts [4, 5], and in the present paper the role and significance of an optical resonant cavity is limited to the alteration of the effective radiative lifetime of the

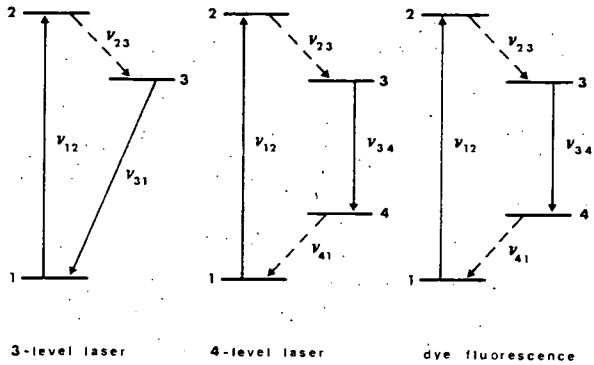

Fig. 1. Comparison of the energy levels of a fluorescor showing a Stokes 0—0 loss with 3-level and 4-level lasers (cf. text and references therein for details).

[1] Address after July 1973: Department of Chemistry, Louisiana State University, Baton Rouge, Louisiana 70803, U.S.A.

[2] The separation of the 0—0 excitation and the 0—0 emission bands, where the vibrational energy levels are being identified by "0—0".

fluorescors; other consequences of laser action on chemistry [6] are discussed in a continuation paper [7].

To summarize the earlier conclusions [1], we note (Fig. 1) that in the system characterized by a Stokes 0—0 loss, absorption of a photon by a relaxed ground state molecule $({}^1R_0(l_1))$ results in a metastable electronically excited singlet $({}^1R^*(l_2))$ that will undergo a molecular relaxation to a state labelled ${}^1R^*_{fc}(l_3)$ (the Franck—Condon relaxed excited state). Emission of a photon having energy $E_{l_3}-E_{l_4}$ from ${}^1R^*_{fc}$ results in a metastable ground state molecule $({}^1R_0(l_4))$ that will undergo a molecular relaxation to ${}^1R_0(l_1)$. An attempt to represent this simple process in terms of two potential energy surfaces (one for the excited and one for the ground state), a representation that is very common in the literature [8] as having been derived from the 'Harmonic Oscillator' model in the manner found in standard texts on physical chemistry [9], is futile: the Stokes 0—0 loss cannot be represented by only two potential energy surfaces (cf. Fig. 2). An examination of the molecular relaxation taking place between levels 2 and 3, and 4 and 1, in Fig. 1, indicates that a series of quantum states must be dealt with. The changes in the solvent cage, on the one hand, result in a shift of the *zero-point energy* [9] of the potential energy surfaces of Fig. 2; on the other hand, the solute-solvent interaction and geometric changes of the dye molecule are closely related to a time-evolution process that affects the *molecular force constants* themselves. In effect, during the relaxation process that takes the molecule from level 2 to level 3, the quantum state appropriate to describe ${}^1R^*_{fc}$ cannot be used, instead, a representation appropriate to the time-evolving sequence of *precursor states* is required. There is no single quantum mechanical operator available to generate the entire time evolving sequence of precursor states in a useful manner[3], hence we have to consider some form of a discontinuous representation of the Stokes

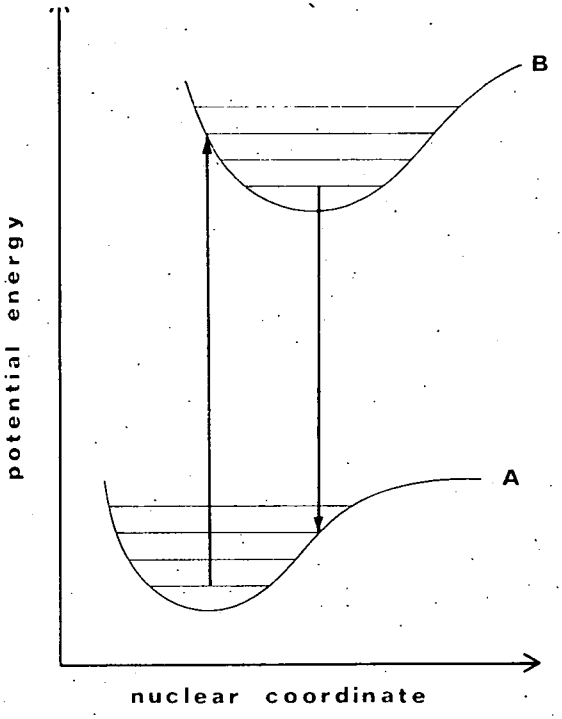

Fig. 2. Usual hypersurface representation of optical excitation and emission. It should be noted that a separation of the 0—0 excitation and 0—0 emission bands is not possible here, hence this model is unsuitable for compounds whose luminescence is characterized by a Stokes 0—0 loss.

[3] We consider the empty formalism of writing a time-dependent Schrödinger equation for large solvated dye molecules as less than useful.

0—0 loss, in the manner of Fig. 3. By taking the time-scale of the creation and annihilation of a photon as 'instantaneous', there are corresponding excited and ground states, between which dipole radiative processes occur (cf. levels i and j in the R_0 and R^* brackets in Fig. 3). For each pair of states such as $R_0(i)$ and $R^*(i)$ there exists an eigenvalue spectrum that can be considered as a one-dimensional matrix. Taking into account all the quantum states in the R_0 and R^* brackets, the full eigenvalue spectrum of the evolving sequence of states is a two-dimensional matrix. From a mathematical standpoint it is of great significance that the sequence of states is "time-oriented", for one may use a transition matrix function $P(t)$, $t>0$, in mapping a continuous time Markov process [10] based on a finite number N of states. To obtain a countable finite Markov chain [11], it is necessary to observe the process at unit intervals of time; regarding these elements as defining points in the holomorphic map R^{N^2}, where R^{N^2} has coordinates x_{ij} $(i, j=1, 2, \ldots, N)$, and letting X be the matrix (x_{ij}), if

$$f(z) = \sum_{n=0}^{\infty} f_n z^n$$

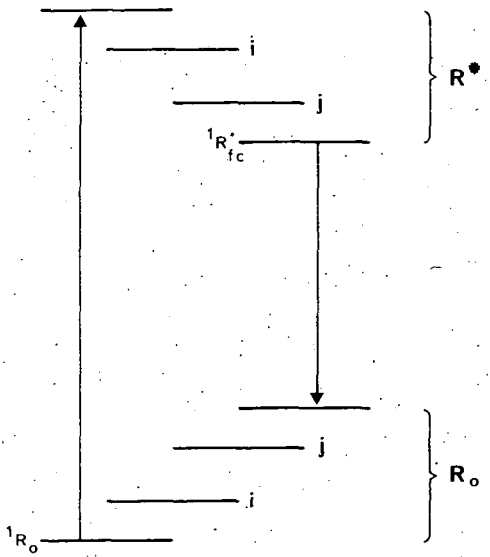

Fig. 3. Time-oriented sequence of potential energy hypersurfaces; emission of a photon results from transitions between excited and ground state manifolds having the same time coordinate (cf. levels i and j in figure for example).

is any power series with real coefficients and convergent for all z, we can define a differentiable map $F: R^{N^2} \to R^{N^2}$ by

$$F_{x_{ij}} = y_{ij},$$

where

$$y = fx = \sum_{n=0}^{\infty} f_n x^n;$$

then the Jacobian matrix of F has eigenvalues

$$\mu_{ij} = \frac{f(\lambda_i) - f(\lambda_j)}{\lambda_i - \lambda_j}$$

where λ_i are eigenvalues of X, and the expression is taken to be equal to $f'(\lambda)_i$. The *map* defined by $X \to exp\, X$ is locally homeomorphic except possibly when X has a pair of eigenvalues differing by a non-zero multiple of $2\pi i$[4].

As can be seen from the foregoing discussion and figures, to represent the

[4] As has been shown by Sudarshan [13—15] the existence of tachyons is well expected; by the exchange of a Hermitian matrix pertaining to tardyons to a Hermitian matrix pertaining to like tachyons, a difference of $-2\pi i$ vs. $2\pi i$ in the eigenvalues is predicted.

fluorescence of a compound showing a Stokes 0—0 loss in a rigorous manner, one must take into account a sequence of quantum states, and the mathematical representation involves a *countable finite Markov chain* [11]. What remains unanswered is a practical question: what is the error introduced in terms of "measurables" when the rigorous representation is forsaken in favour of the more simple one indicated by Fig. 2: In spontaneous fluorescence, if the fluorescence lifetime τ_f of R^* (τ_f defined by $I/I_0 = exp(-t/\tau_f)$ in the usual manner) is one nanosecond, then most of the excited molecules emitting photons will be characterized by R^*_{fc}, the Franck—Condon relaxed state. Accordingly, in case of spontaneous fluorescence the process may be represented, from a pragmatic standpoint, in terms of the simplified representation of Fig. 2. This empirically justifiable treatment has been adopted in the literature to treat quantum states in dye lasers also [12]. This extension is unjustifiable; it serves to illustrate how pragmatic considerations, in the absence of recourse to fundamental principles, can lead to erroneous conclusions.

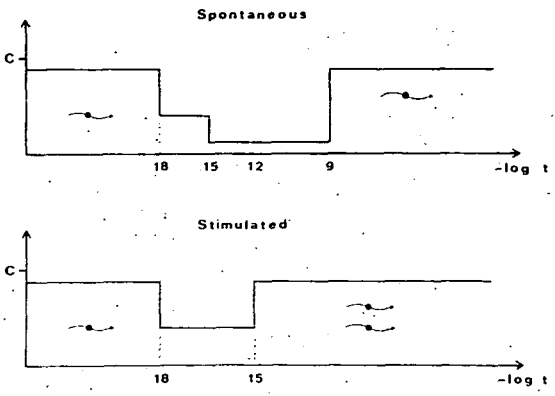

Fig. 4. A comparison of the time evolution of electronically excited states under spontaneous and stimulated emission conditions, revealing the predominance of 'early' time elements in the latter case. Ordinates represent the velocity of the highest velocity particle in the interaction sphere, abscissae represent time. This figure illustrates the extreme situation where, at a very high photon density, the stimulated emission process will occur before the excitation energy is substantially delocalized from the electric dipole vector of the molecule

As Fig. 4 indicates, under spontaneous emission conditions the simplified representation totally breaks down, for at high photon densities the lifetime of R^* will be quite different from τ_f, and the principal emitter will be a 'precursor' of the Franck—Condon relaxed state. Whenever different quantum states are required to describe an assembly of atoms or molecules, by definition it is expected that chemical and physical properties of the ensemble will also change. From this fundamental principle we may categorically state that chemistry in lasers is expected to yield results that do not coincide with the behavior of the same compounds under ordinary conditions. Detailed considerations and specific examples of chemical anomalies in a laser cavity will be discussed subsequently.

* * *

The comments and criticisms of Professors A. J. BARD, LEON ROSENFELD, and E. C. G. SUDARSHAN, pertaining to various sections of this paper, are gratefully acknowledged.

This material was presented in paper No. 87 at the 141st National Meeting of The Electrochemical Society, May 7—11, 1972, Houston, Texas.

References

[1] *Keszthelyi, C. P.:* Submitted to Spectroscopy Letters, 1973.
[2] *Stokes, G. G.:* Phil. Trans. Roy. Soc. (London) **142**, 463 (1852).
[3] See for example *Turro, N. J.:* „Molecular Photochemistry", W. A. Benjamin, Inc., New York, 1967; figure 4—1, p. 45.
[4] *Van Uitert, L. G.:* „Luminescence of Inorganic Solids", edited by P. G. Goldberg, Academic Press, 1966, Chapter 9.
[5] *Yariv, A.:* „Quantum Electronics", John Wiley and Sons, New York, 1967.
[6] *Keszthelyi, C. P.:* Submitted to Spectroscopy Letters, 1973, sequence to [1].
[7] *Keszthelyi. C. P.:* „Anomalous Material Transport in a Laser Cavity", manuscript, submitted to Analytical Chem. 1973.
[8] See for example, *Berlman, I. B.:* „Handbook of Fluorescence Spectra of Organic Molecules", Academic Press, New York, 1965; p. 35.
[9] See for example, *Pilar, F. L.:* „Elementary Quantum Chemistry", McGraw—Hill, New York, 1968, Chapter IV.
[10] *Elfwing, G.:* Acta Soc. Sci. Fennicae, Ser. **A2**, No. 8 (1937).
[11] *Chung, K. L.:* „Markov Chains With Stationary Transition Probabilities", Springer,-Heidelberg, 1960.
[12] See for example, *Sorokin, P. P., Lankard, J. R., Moruzzi, V. L., Hammond, E. C.:* J. Chem. Phys. **48**, 4741—4776 (1968).
[13] *Dhar, J., Sudarshan, E. C. G.:* Phys. Rev. **174**, 1808 (1968).
[14] *Bilaniuk, O. M., Sudarshan, E. C. G.:* Physics Today **22**, 43 (1969).
[15] *Sudarshan, E. C. G.:* Arkiv Fysik **39**, 585 (1969).

ХИМИЯ ЛАЗЕРОВ: КВАНТОВЫЕ СОСТОЯНИЯ ЛАЗЕРОВ НА КРАСИТЕЛЯХ

Ч. П. Кестхели

Квантовые состояния оптически активных молекул лазеров на красителях представляют собой ориентированную во времени последовательность, зависящую от плотности фотонов, описание которых требует применения двухдимензионной матрицы спектра собственных значений, вместо обычно применяемых для описания спонтанной флюоресценции однодимензионной матрицы. Математическое представление ориентированных во времени квантовых состояний представляет собой исчисляемый конечный ряд Маркова и голоморфное изображение, содержащее собственные значения, в котором содержатся как тардионные, так и тахионные решения; тардионная матрица Гермита представляет собой особый случай. Вследствие того, что при спонтанной эмиссии и по лазерному механизму в частицах преобладают различные квантовые состояния, в оптическом резонаторе можно ожидать изменения химических свойств и реакций.

INVESTIGATION OF THE THERMAL DECOMPOSITION OF ACETALDEHYDE

By

I. BÁRDI and F. MÁRTA

Gas Kinetics Research Group of the Hungarian Academy of Sciences, Szeged and Institute of General and Physical Chemistry, Attila József University, Szeged

(Received July 21, 1973)

The pyrolysis of acetaldehyde has been investigated at temperatures between 495 and 540 °C and at initial pressures of 25—200 torr. The reaction was followed by pressure measurements and by G.C. analysis. 3/2 order rate constants were calculated from the measured rate of formation of major products and from pressure measurement data. Arrhenius parameters are given for the overall decomposition and for the initiation step. Among the minor products, the rates of formation of hydrogen, ethane, ethylene, and acetone were measured. The routes of their formation are discussed and a simple mechanism for the decomposition of acetaldehyde is proposed.

Introduction

Among the thermal decomposition reactions, one of the most investigated model compounds is the acetaldehyde. According to STEACIE [1] this intense and permanent interest may be explained by the circumstance that "The acetaldehyde decomposition is remarkable for the lack of agreement of both mechanism and the experimental fact, and the complications involved". This statement is valid even after two decades. In consequence of this fact, a few years ago we have started to investigate the thermal decomposition of acetaldehyde and the same circumstances offer reasons to summarize the main data on the kinetics and mechanism of the decomposition.

The primary aim of our investigation was to study the overall kinetics of reaction to give some data in connection with the formation of minor products and to establish the route of their formation during the decomposition.

The acetaldehyde decomposes at 450—600°C and at medium pressures (30—300 torr) with a well measurable rate; the major products of decomposition are CO and CH_4, which form in equal amount. Besides the main products, hydrogen, acetone, ethylene, and propionaldehyde form in small amounts. The stoichiometric equation of decomposition is

$$CH_3CHO \rightarrow CH_4 + CO.$$

During the decomposition the change in mole number is 2, so the reaction can easily be followed manometrically. The relationship between the changes in mole number and pressure is verified by different authors [2, 20]. In seasoned vessel the decomposition is homogeneous, but in some percent heterogeneous reactions were observed, too [3, 5, 10].

At very low pressures the kinetics of decomposition and the composition of products change significantly. According to COLLIN and DELPLACE [6], at pressures of 0.1 torr the main products of the decomposition are acetylene, ethylene and water.

Though the stoichiometry of decomposition is simple and homogeneous, however, regarding the problem of reaction mechanism, contradictionary opinions were formed and are found in different reviews [7—9].

Order of the reaction

According to KASSEL's opinion [11] the reaction is 3/2 in order and the mechanism of the decomposition is complex. LETORT [12, 24], on the basis of very detailed investigations, distinguished two orders of the reaction, one as function of initial rates (n_0) and one as a function of conversion. The value of $n_0 = 1.5$, while n changes between 1.65—2.3. The existence of these two orders is due to the inhibiting effect of reaction products. The n_0 value, calculated on the basis of initial rates is proved by several authors [3, 13, 15—19].

The Arrhenius parameters determined from the temperature dependence of the 3/2 order rate constants in the temperature range 429—521°C are the following [20]:

$$k_0 = 4 \cdot 10^{12} \exp(-48.00/RT)\ 1^{1/2}\ \text{mole}^{-1/2}\ \text{min}^{-1}.$$

Reaction mechanism

The first mechanism of the decomposition was described by RICE and HERZFELD [21] in 1934.

$$CH_3CHO \rightarrow CH_3 + CHO \quad (1)$$

$$CHO \rightarrow CO + H \quad (2)$$

$$H + CH_3CHO \rightarrow H_2 + CH_3CO \quad (3)$$

$$CH_3CO \rightarrow CH_3 + CO \quad (4)$$

$$CH_3 + CH_3CHO \rightarrow CH_4 + CH_3CO \quad (5)$$

$$2\,CH_3 \rightarrow C_2H_6 \quad (6)$$

$$CH_3 + CH_3CO \rightarrow CH_3COCH_3 \quad (7)$$

$$2\,CH_3CO \rightarrow (CH_3CO)_2 \quad (8)$$

Among the three termination steps, the most important was considered to be (6), the ethane-producing reaction, and it was possible to interpret the experimentally observed 3/2 order of reaction.

On the basis of new experimental results, this mechanism has to be revised and extended. According to the original RICE—HERZFELD mechanism, besides the major products only ethane and hydrogen formation take place. At 500 °C a lot of other products were detected by several authors [17, 18, 22]. On the basis

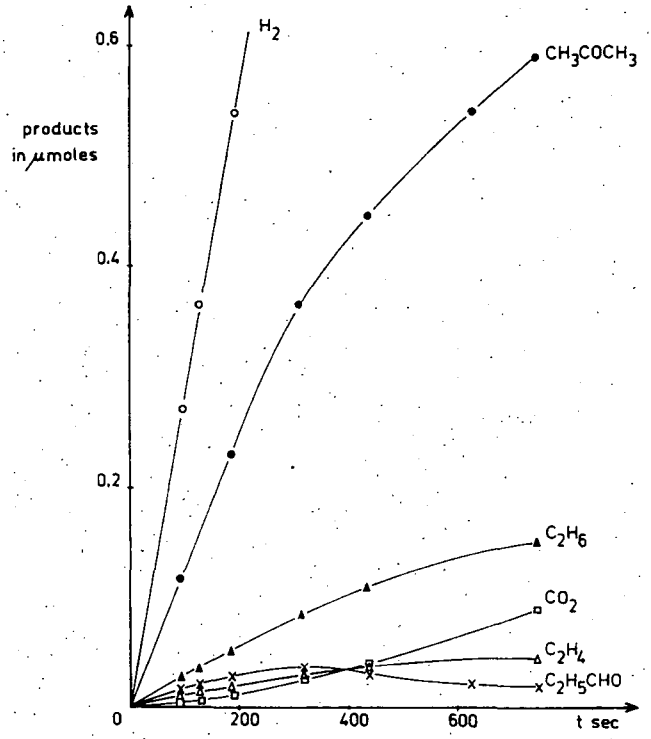

Fig. 1. Products of pyrolysis at 523°C, $p_{ald} = 117$ torr

of the original RICE—HERZFELD mechanism, the existence of this products cannot be explained.

In Fig. 1 we have shown a product distribution curve, using the analytical data of LAIDLER and LIU. In the curve the major products are not plotted.

Table I

The products of acetaldehyde pyrolysis according to literature

Major products	Minor products	Products in trace amounts	Compounds which were not obtained during pyrolysis (according to [22])
	H_2	CH_2CO[18]	HCHO
	CH_3COCH_3	C_3H_6[4, 6, 22, 28]	CH_2CO
	C_2H_6	H_2O[6, 28]	$CH_3OCH{=}CH_2$
CO	C_2H_4[4, 13, 17, 18, 22, 23]	C_2H_2[6]	$(CH_3CO)_2$
CH_4	C_2H_5CHO[17, 18, 22]	C_2H_5OH[17]	CH_3OH
	CO_2[4, 17, 18, 22, 23]	$CH_3CH{=}CHCHO$[22]	C_2H_5OH
		$CH_3COOC_2H_3$[22]	$(CH_3)_2CHOH$
			H_2O

In Table I we collected the products which were detected by several authors during the pyrolysis of acetaldehyde. In the first column of Table I the major products are shown, in the second the minor products, in the third the products formed in trace amounts (which are not always detectable). The fourth column lists the compounds (according to SCHUCHMAN and LAIDLER [22]), which could be formed, but have not been detected so far among the products of pyrolysis.

The problem of formation of minor products

H_2. According to the original Rice—Herzfeld scheme the rate of formation of hydrogen is the measure of the rate of the initiation step. However, detailed investigations did not confirm this fact. TRENWITH [5] observed an induction period for hydrogen production at 502—536 °C and in the pressure range 100—300 torr, where the order of hydrogen production was found to be 2. Investigations with specially purified acetaldehyde [18, 19, 23] did not confirm these results, no induction period was found and the order of hydrogen formation was 1.4 and 1.35. It is presumable, that the induction period observed by TRENWITH is due to the contaminations of acetaldehyde. To explain the experimental results, other hydrogen producing steps have to be supposed.

Acetone. It is an easily detectable product during the pyrolysis, its formation is described in the Rice—Herzfeld scheme, with the combination of methyl and acetyl radicals. According to the analytical measurements, the amount of acetone formed during the pyrolysis is several times higher than that of the ethane. On the basis of this fact, DEXTER and TRENWITH [17] assumed that the main termination step is the methyl+acetyl radical reaction. This assumption can easily confuted. At 500 °C the acetyl radical is thermally unstable and quite easily decomposes, therefore, its concentration is low in the system (biacetyl could not be detected during the pyrolysis). If the assumption of DEXTER—TRENWITH is accepted, then the 3/2 order is valid only in the case when the initiation step is of second order. This contradicts the experimental facts, because the order of the initiation step is close to 1. According to EUSUF and LAIDLER [16] the acetone is formed in the

$$CH_3+CH_3CHO \rightarrow CH_3COCH_3+H$$

reaction. The order of acetone production is 3/2.

Ethane. Easily detectable termination product of decomposition. The order of its production (using carefully purified acetaldehyde) at higher pressures is about 1 (1.1 [18], 1.2 [23]) and below 80 torr a significant fall off was observed, which points to the pressure dependence of the termination step.

Propionaldehyde. WALL and MOORE [35] suggested it to be a termination product during the copyrolysis of acetaldehyde and acetaldehyde-d_4. Its formation was described by the following steps:

$$CH_3+CH_3CHO \rightarrow CH_4+CH_2CHO$$

$$CH_2CHO+CH_3 \rightarrow CH_3CH_2CHO.$$

The propionaldehyde was detected first by TRENWITH [5] and its existence was confirmed by other authors [18, 22], too.

Other minor products. A number of authors have detected ethylene and CO_2 [4, 13, 17, 18, 22, 23]. There are some differences in the interpretation of the experimental data in the literature. TRENWITH assumes ethylene as a primary product of the decomposition and for its formation he considers the decomposition of CH_2CHO radical and the dimerization of CH_2 biradical into ethylene. (This assumption can hardly be accepted). LIU and LAIDLER measured a much lower rate of ethylene production, but they confirmed that ethylene is a primary product. The order of its formation at 540 °C is 1.5 and its formation can be described by the following steps:

$$CH_3+CH_3CHO \rightleftharpoons CH_3—O—CH—CH_3$$

$$CH_3—O—CH—CH_3 \rightarrow CH_3O+C_2H_4.$$

In a recent paper, LAIDLER and SCHUCHMAN [22] suggested the following steps for the ethylene formation

$$H+CH_2=CHOH \rightleftharpoons CH_2CH_2OH \rightarrow C_2H_4+OH.$$

In this step they assume the vinyl alcohol form of aldehyde, however this assumption has no experimental evidence.

Similar problems arise in connection with the CO_2 formation. TRENWITH considers the CO_2 to be a secondary product which forms in the

$$2\,CO \rightarrow CO_2+C$$

reaction step.

According to LAIDLER and LIU the CO_2 is a primary product; for its formation they mention several assumptions, for example the oxidation of CO to CO_2, the wall reaction of acetaldehyde to propylene and water. In connection with TRENWITH's assumption, LAIDLER points out that this reaction does not take place around 500 °C.

It can be seen from Table I that there are some other minor products, which were detected during the pyrolysis by several authors. However, this products were formed in a very small (often in trace) amount, their existence was not always confirmed by more recent investigations, the formation of some products (*e.g.* ketene) was even excluded. The existence of minor products and their rate of formation is strongly influenced by the contaminations of the starting aldehyde, as LAIDLER and LIU have pointed out [4]. In order to describe the formation of these products in the mechanism, sometimes very speculative steps have to be used. As an illustration, we have shown the mechanism of acetaldehyde decomposition suggested by SCHUCHMAN and LAIDLER [22] which is an extended Rice—Herzfeld scheme. Applying this mechanism the authors are able to explain the formation of all products detected by them during the pyrolysis. Steps (1)—(6) are those assumed in the Rice—Herzfeld mechanism.

$$H+CH_3CHO \rightarrow H_2+CH_2CHO \tag{7}$$

$$CH_3+CH_3CHO \rightarrow CH_4+CH_2CHO \tag{8}$$

$$CH_2CHO+CH_3CHO \rightleftharpoons CH_3\underset{\displaystyle O—}{\underset{|}{C}}HCH_2CHO \rightarrow CH_3COCH=CHOH+H \tag{9}$$

$$CH_2CHO + CH_3CHO \rightarrow CH_3CHO + CH_3CO \quad (10)$$

$$CH_2CHO + CH_3CHO \rightarrow CH_3\underset{\underset{O-}{|}}{C}HOCH=CH_2 \rightarrow CH_3COOCH=CH_2 + H \quad (11)$$

$$CH_3 + CH_3CHO \rightarrow CH_3COCH_3 + H \quad (12)$$

$$H + CH_2=CHOH \rightleftharpoons CH_2CH_2OH \rightarrow C_2H_4 + OH \quad (13)$$

$$CH_3 + CH_2=CHOH \rightleftharpoons CH_2CH(CH_3)OH \rightarrow C_3H_6 + OH \quad (14)$$

$$OH + CH_3CHO \rightarrow H_2O + CH_3CO \quad (15)$$

$$CH_3 + CH_2CHO \rightarrow C_2H_5CHO \quad (16)$$

$$CH_3CHO + CH_3CHO \xrightarrow{wall} C_3H_6 + CO + H_2O \quad (17)$$

$$CH_3CHO + CH_3CHO \xrightarrow{wall} C_3H_6 + CO_2 + H_2 \quad (18)$$

$$CH_3CHO + CH_3CHO \xrightarrow{wall} CH_3CH=CHCHO + H_2O \quad (19)$$

Experimental

The decomposition was carried out in a conventional static system. The cylindrical Supremax reaction vessel of 250 cc capacity was enclosed in an electrically heated furnace. The temperature of the vessel was controlled within ± 0.5 °C. The reaction was followed by pressure measurements and by G.C. analysis. The apparatus used and the procedure was described in detail previously [27].

After decomposition, the reaction mixture was led into a series of traps at the temperature of liquid air, the non-considerable fraction was then collected and measured by a Toepler gauge. The G.C. analysis was carried out using a Carlo Erba Fractovap Model C ATC/f apparatus, equipped with a hot wire detector. The non-condensables were analyzed on a 2.5 m, 60—80 mesh silicagel column ($\varnothing = 0.5$ cm) maintained at 50 °C. For the condensables we used 1.6 m long column of 20% β,β'-oxydipropionitrile on Chromosorb P, silanized (60—80 mesh) at 50 °C. Hydrogen was used as carrier gas in both cases at a flow rate of 60 ml/min. The hydrogen was analyzed on a 2.5 m Molecular Sieve 5A column (60—80 mesh) maintained at 50 °C, using nitrogen as carrier gas (60 ml/min). The analysis of minor products (*e.g.* C_2H_6, C_2H_4, etc.) was done on a chromatograph Carlo Erba Fractovap Mod. C type AID/f, equipped with FID, using 2.5 m silicagel column (60—80 mesh) at 80 °C, using nitrogen as carrier gas ($v = 30$ ml/min). In some runs, we made mass spectrometrical analysis, using a Finnigan mass spectrometer type 1016 S/L (quadrupole system). The energy of ion source was 70 eV, m/e range 1—100.

Materials. Acetaldehyde, obtained from Fluka, was purified by a number of bulb to bulb distillations at -78 °C, in vacuo. The middle fraction was collected and stored in the absence of air and light at room temperature. No trace impurity was revealed by G.C. Methane, hydrogen and nitrogen (high purity) were taken from cylinders and, after the usual purification processes, were led into the storing vessels. The carbon monoxyde was prepared by dropping sulfuric acid on sodium formate, dried by passing through traps at -180 °C.

Results

According to our measurements, the acetaldehyde starts to decompose in a measurable extent at 460 °C; above 550 °C the decomposition will be extremely fast. Therefore, we carried out our experiments at 495.5, 512, 527.5 and 539.5 °C at initial pressures of 25, 50, 80, 100, 150 torr and at different conversions (5—70%). During the reaction, we measured the pressure increase and at the end of the reaction we determined the amount of major products (CO, CH_4), the unreacted aldehyde, and some of the minor products (H_2, C_2H_6, CH_3COCH_3, etc.) by G.C.

The kinetics of formation of major products. Some typical concentration—time plots for CO and CH_4 formation are shown in Fig. 2. The shape of the curves agrees

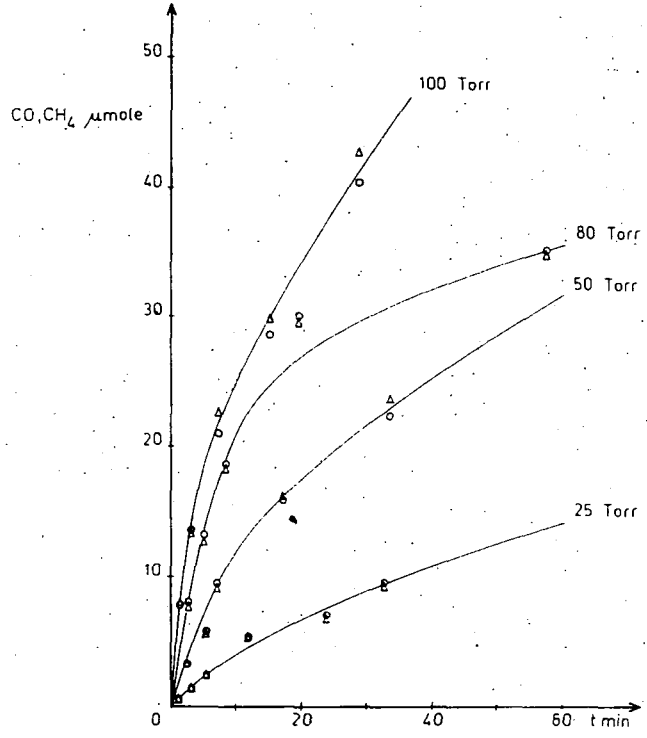

Fig 2. Major products *vs.* time curves at 527.5 °C, ○ CH_4; △ CO

well in the case of CO and CH_4 and the amounts of major products are equal during the reaction, as it can be seen from Fig. 2. The shape of the curves remains similar if the pressure increase is plotted as a function of time. It can be established, from the plots that there is no induction period in the formation of major products and their rate of formation is proportional to the initial concentration of acetaldehyde. Due to the equal amount of major products during the pyrolysis, further we used only one data.

Mass Balance. Making a mass balance for the major products and the starting material, we may establish that, from the decomposing aldehyde, CH_4 and CO form in a proportional amount, as it can be seen in Fig. 3, where the results of a series of experiments ($p_0 = 100$ torr and $t = 527.5$ °C) are shown. This mass balance is not disturbed by the minor products, because their concentrations are not comparable with those of the major products.

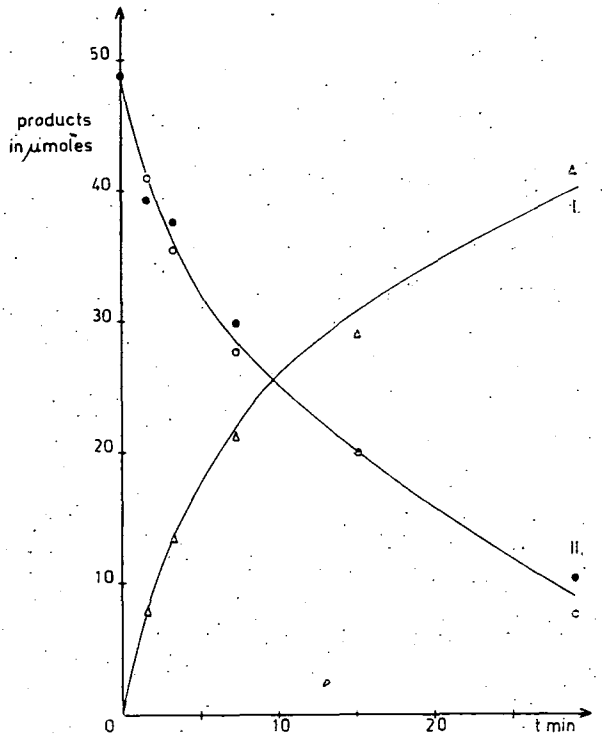

Fig. 3. Mass balance curve at 527.5 °C, $p_{ald.} = 100$ torr

In Fig. 3, curve I shows the pressure increase, while △ symbols denote the analytically determined CH_4 amounts. The two curves fit well and this fact means that the pressure increase is proportional to the amounts of major products formed. This fact also gives the possibility to use the pressure—time data in some cases to elucidate the kinetics of this decomposition. On curve II the decrease of the concentration of acetaldehyde (○ determined analytically, ● determined manometrically) is plotted. The agreement of both curves shows the fitting of the analytical data obtained from two different sources.

Determination of the overall order of reaction. With the aid of the initial rates (w_0), determined from the product—time curves the overall order (n_0) was determined. From the same experiments, the overall order n can be calculated as a function of CH_4 formed. These orders were calculated from our data obtained from both

Table II

The overall order of reaction as a function of time and temperature

t °C	Analytical data						Pressure measurement data					
	at the formation of						at the formation of					
	n / n_0	1	2	4	7	10	n / n_0	1	2	4	7	10
	n_0	μmole CH_4					n_0	μmole CH_4				
495.5	1.43 ±0.16	1.40	1.42	1.37	1.38	1.40	–	—	—	—	—	—
512	1.57 ±0.23	1.52	1.48	1.38	1.33	1.39	1.49 ±0.02	1.54	1.55	1.57	1.56	1.65
527.5	1.57 ±0.15	1.56	1.55	1.52	1.46	1.33	1.49 ±0.02	1.50	1.52	1.53	1.56	1.62
539.5	1.64 ±0.13	1.64	1.60	1.53	1.39	1.30	1.53 ±0.02	1.56	1.60	1.65	1.74	—
550.5	—	—	—	—	—	–	1.54 ±0.02	1.57	1.63	1.67	1.72	1.44
Mean value:	1.55						1.51					

pressure—time measurements as well as analytically, and the results are listed in Table II.

In both cases the initial rates are derived from curve-fitting data obtained by computer and the error limits are given by standard deviations, calculated with linear least square methods. It can be seen from Table II that the n_0 values increase slightly with increasing temperature (this increase is smaller in the case of pressure—time data). The mean value of n_0 data, calculated from pressure measurements is very close to 1.5 and is in excellent agreement with the data given in the literature. However, the analytically determined n_0 values show a significant deviation from 1.5. This is probably due to errors in analytical determination.

As it can be seen from Table II — in contrary with LETORT's results — big increase of order with time could not be observed in our experiments and the value of n never exceeds 1.8.

Determination of Arrhenius parameters. The $n_0=3/2$ order is demonstrable with the following simple method. As known, the rate constant for 3/2 order reactions is described by the following equation:

$$k = \frac{2}{t}(c^{-1/2} - c_0^{-1/2})$$

where c_0=initial concentration, c=concentration at time t. Introducing the symbols $c/c_0=x$ and $c_0^{1/2}t=\tau$, the result will be

$$x^{-1/2} = 1 + \frac{1}{2}k\tau .$$

Table III

3/2 *Order overall rate constants,* $k \cdot 10^{-2}$ *(in* $l^{1/2}$ $mole^{-1/2}$ sec^{-1}*), calculated from the analytical results at different temperatures and initial aldehyde pressures*

p_{ald} → / t °C	25	50	80	100	150 torr	Mean value
495.5	5.61 ±2.12	3.89 ±0.94	4.55 ±0.47	4.17 ±0.35	3.73 ±0.49	4.39±0.84
512	—	6.74 ±0.73	7.76 ±0.69	6.84 ±0.52	7.29 ±1.31	7.16±0.81
527.5	12.30 ±1.64	12.68 ±0.85	14.56 ±0.92	12.86 ±0.80	14.01 ±0.70	13.23±0.98
539.5	17.89 ±0.72	21.37 ±1.86	25.05 ±1.39	—	21.18 ±1.39	21.37±1.35

If the 3/2 order is valid for the decomposition, then plotting $x^{-1/2}$ *vs.* τ, we obtain a straight line of slope $k/2$ and the intercept will be 1. In Fig. 4 the results of a series of typical experiments at 512 °C, calculated from the methane analysis data can be seen. The initial pressure of aldehyde changed between 50—150 torrs. Within the limits of experimental error a straight line was obtained. Using this method we calculated the overall rate constants from the analytical data (by means of least square methods) as it can be seen in Table III.

From the temperature dependence of these rate constants (see Fig. 5) we calculated $E_a = 47.09 \pm 1.32$ kcal/mole for the activation energy of the decomposition,

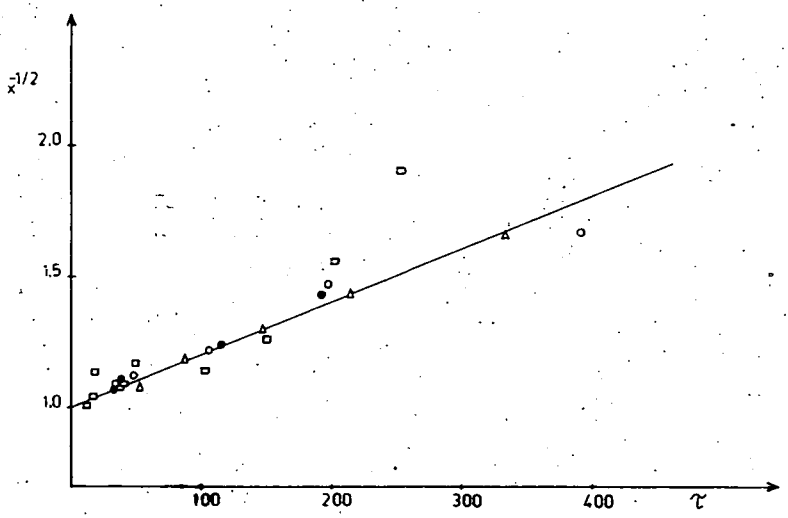

Fig. 4. Relation between $1/x^{1/2}$ and $c_0^{1/2}t$ at 512 °C. The data are calculated on the basis of methane analysis. $p_{ald.}$ = □ 50 torr; ○ 80 torr; △ 100 torr; ● 150 torr

Table IV

3/2 *Order overall rate constants,* $k \cdot 10^{-2}$ *(in* $l^{1/2}$ $mole^{-1/2}$ sec^{-1}*), calculated from pressure-time measurements, at different temperatures and initial aldehyde pressures*

p_{ald} / t °C	50	100	200 torr
495.5	—	—	0.99±0.06
512	2.10±0.07	2.20±0.03	1.91±0.05
527.5	3.80±0.04	3.96±0.05	4.07±0.04
539.5	6.34±0.05	6.30±0.04	—
544.8	7.13±0.09	7.39±0.04	7.41±0.05
550.5	9.49	—	—
561.5	12.94±0.12	13.47±0.05	—

and $A = 5.36 \pm 2.13 \cdot 10^{12}$, for the A value which agree satisfactorily with earlier data. The overall rate constants may be given by

$$k = 5.36 \cdot 10^{12} \exp(-47.09/RT)\ l^{1/2}\ mole^{-1/2}\ sec^{-1}$$

in the temperature range 495—550 °C.

Table IV contains the mean values of overall rate constants, calculated from pressure measurements with the aid of the following expression:

$$k = \frac{2}{t}(c^{-1/2} - c_0^{-1/2})$$

From these data, we obtained the Arrhenius parameters $E_a = 49.52 \pm 1.26$ kcal/mole,

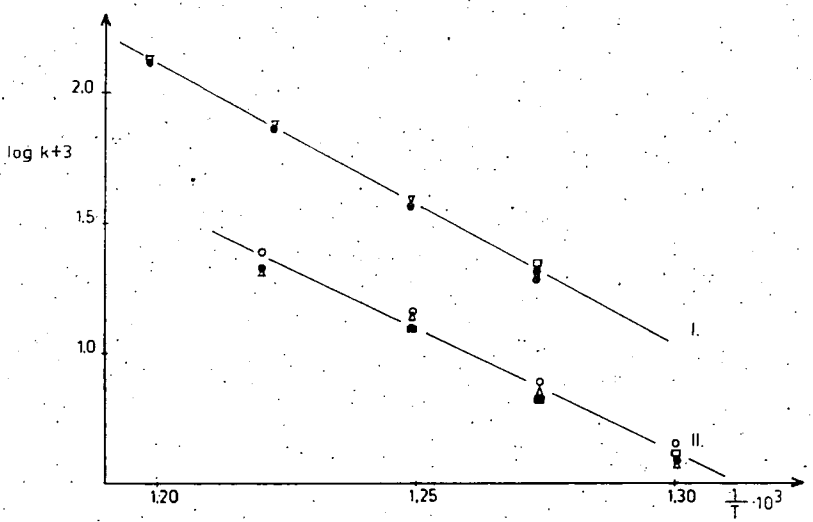

Fig. 5. Arrhenius plot of the 3/2 order overall rate constants. Initial aldehyde pressures: ● 50 torr; ○ 80 torr; □ 100 torr; △ 150 torr; ▽ 200 torr. Curve I is calculated from pressure—time measurements; Curve II from analytical measurements

$A = 2.36 \pm 1.77 \cdot 10^{12}$, and the overall rate constant is

$$k = 2.36 \cdot 10^{12} \exp(-49.52/RT)\ l^{1/2}\ \text{mole}^{-1/2}\ \text{sec}^{-1}$$

The agreement of E_a and A values, calculated from analytical and pressure measurements is quite satisfactory.

Measurement of minor products

H_2. Among the minor products, hydrogen forms in the greatest amount. A typical H_2 yield-time curve is shown in Fig. 6. As it can be seen from Fig. 6, the curves are similar to the yield—time curves of major products and there is no sign of induction period, in contrary with TRENWITH [5]. The order of hydrogen production was determined from the initial slopes of these curves. The order is 1.36, which agrees well with the value 1.4, determined by LAIDLER [4] and COME [23, 29]. This shows that the simple Rice—Herzfeld mechanism is not valid for the decomposition, because in this case the rate of formation of hydrogen would be a measure of the rate of the initiation step.

Acetone. The product quite easily detectable with hot-wire detector if the initial aldehyde concentration is above 80 torr. The amount of acetone was always

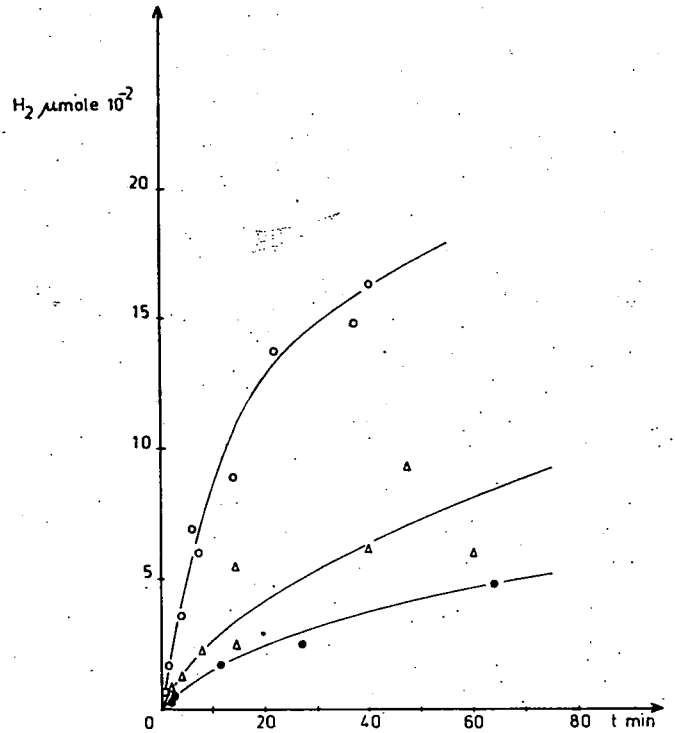

Fig. 6. Typical yield *vs.* time plot for hydrogen formation at 527.5 °C. $p_{ald.}$ = ● 25 torr; △ 50 torr; ○ 100 torr

less than the amount of hydrogen. The shapes of yield—time curves were similar to the curves of major products and no induction period existed in this case either.

Ethane. One of the termination products of decomposition. It was produced in smaller amounts than the former ones. No induction period was observable and the yield curves of ethane production as a function of conversion and concentration showed a similar shape as those of major products.

Ethylene. The amount of this product is comparable with, though smaller than that of ethane. The characteristics of the yield—time curves are the same as in the case of ethane.

Propionaldehyde. According to the literature mentioned earlier, this compound is the other termination product besides ethane. During our investigations it could be detected only in a trace amount by mass spectroscopy, therefore we did not make detailed experiments concerning its formation.

Carbon dioxide. It could be detected in trace amount only; no quantitative measurements were made.

Other products. During the analysis of decomposition products we could not find propylene, ethanol, higher aldehydes [22] and water. These informations were very useful for suggesting the mechanism given below.

In Fig. 7 we present the analytical data obtained by the decomposition of 80 torr acetaldehyde at 482 °C. The ratio of the products is easily comparable in the figure.

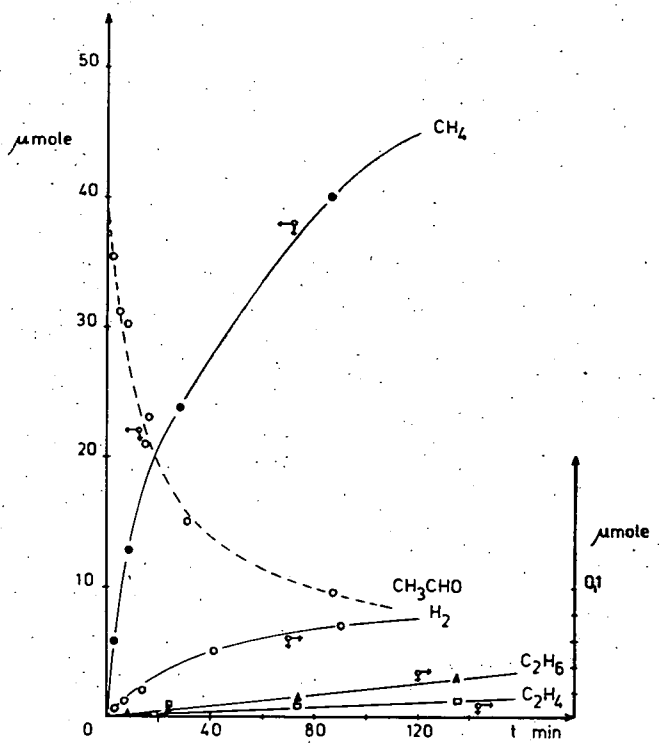

Fig. 7. Products of pyrolysis at 482 °C. $p_{ald.} = 80$ torr

Discussion

As mentioned in the introduction, the simple Rice—Herzfeld scheme is not suitable for describing the mechanism of the thermal decomposition of acetaldehyde, especially the production of minor products. On the basis of the literature and our experimental data we suggest the following mechanism, which is an extended Rice—Herzfeld scheme.

The initiation step is the unimolecular decomposition of acetaldehyde

$$CH_3CHO \rightarrow CH_3 + CHO \qquad (1)$$

In the pressure range used in our experiments the reaction is in its first order region. This step is followed by the chain propagation step

$$CHO \rightarrow CO + H. \qquad (2)$$

The H atoms react with the aldehyde molecule

$$H + CH_3CHO \rightarrow H_2 + CH_3CO \qquad (3)$$

and

$$H + CH_3CHO \rightarrow H_2 + CH_2CHO. \qquad (7)$$

In consequence of the higher reactivity of formyl hydrogen, step (3) occurs more frequently than step (7) requiring a higher activation energy: $[D(H—CH_2CHO)] \sim \sim 102$ kcal/mole, while $[D(CH_3CO—H)] \sim 87$ kcal/mole [34]. The reaction steps proposed by LAMBERT *et. al.* [37]

$$H + CH_3CHO \rightarrow CH_4 + CHO$$

and

$$CHO + CH_3CHO \rightarrow CO + H_2 + CH_2CHO$$

have no experimental evidence.

Methyl radicals, forming in the initiation step, have two possibilities to react with the acetaldehyde in a H abstraction reaction,

$$CH_3 + CH_3CHO \rightarrow CH_4 + CH_3CO \qquad (5)$$

$$CH_3 + CH_3CHO \rightarrow CH_4 + CH_2CHO. \qquad (8)$$

The direct determination of the relationship of these two reactions was carried out first by AUSLOOS and STEACIE [25]. According to these authors, reaction (8) is negligible in comparison with reaction (5). The rate constant of step (5) was determined by BRINTON and VOLMAN [32] and the Arrhenius parameters of reaction (8) were estimated by LAIDLER and LIU [18] and SCHUCHMAN and LAIDLER [22]. The estimation is based on similar abstraction reactions of methyl radicals. At 500 °C the k_8/k_5 ratio $=0.116$ [22], but in the literature published earlier by the same authors the values 10^{-4} [18] and 10^{-2} [4] are found. According to our current investigations, the highest value is the most probable.

The acetyl radical arising from the reaction (5) at about 500 °C decomposes rapidly

$$CH_3CO \rightarrow CH_3 + CO \qquad (4)$$

so further reactions of this radical do not exist. Since we did not detect ketene as

reaction product, the reaction

$$CH_3CHO + H \rightarrow CH_2CO + H_2$$

must be excluded from the mechanism [36]. The fate of CH_2CHO radicals arising from reactions (7) and (8) may be as follows:

1. Decomposition according to the equation

$$CH_2CHO \rightarrow CH_2CO + H.$$

Ketene was not found as reaction product, though it is stable under these experimental conditions (450—525 °C) [22]; thus this step has to be rejected.

2. Reaction with the acetaldehyde molecule

$$CH_2CHO + CH_3CHO \rightarrow CH_3CHO + CH_3CO. \qquad (10)$$

The estimated value of k_7 according to LAIDLER is $10^{7.4}$ cc · mole^{-1} · sec^{-1}, the concentration of CH_2CHO radicals $\approx 10^{11.6}$ mole · cc^{-1}, exceeds the concentration of methyl radicals in the system, therefore this radical is of great importance in the mechanism of decomposition. According to BENSON [33], the reactivity of CH_2CHO radicals is similar to that of methyl radicals (in contrary LAIDLER assumes the reactivity to be similar to that of allyl radicals) and its concentration is lower than estimated by LAIDLER.

3. Isomerization to acetyl radicals

$$CH_2CHO \rightarrow CH_3CO.$$

The activation energy of this step is about 47 kcal/mole, which is negligible compared with reaction (7); the estimated ratio of the two reactions is $v_i/v_7 \sim 10^{-2}$.

4. The most probable reaction is the propionaldehyde production, which can be expressed by the following equation

$$CH_3 + CH_2CHO \rightarrow CH_3CH_2CHO. \qquad (16)$$

The fact that propionaldehyde was detected as a product of pyrolysis verifies the existence of this step as termination step, though it has smaller importance than the methyl recombination step.

The methyl radicals reacting with the starting material in a hydrogen rearrangement reaction

$$CH_3 + CH_3CHO \rightarrow CH_3COCH_3 + H \qquad (12)$$

give acetone.

According to LAIDLER's estimation the ratio of the concentrations of acetyl and methyl radicals is $10^{-2}-10^{-3}$, which shows that the most important termination step is the methyl recombination

$$CH_3 + CH_3 \rightarrow C_2H_6. \qquad (6)$$

The formation of easily detectable ethylene may be explained for instance in the following way (by radical isomerization and decomposition)

$$H + CH_3CHO \rightarrow CH_3CH_2O \rightarrow C_2H_4 + OH. \qquad (7a)$$

CO_2 was detected in trace amount, its formation, according to LAIDLER, is the following:

$$2\,CH_3CHO \xrightarrow{\text{wall}} C_3H_6 + CO_2 + H_2. \qquad (17)$$

This step explains at the same time the formation of propylene, which we did not find in our case, though its existence seems to be proved from literature.

On the basis of our experiments and literature data, the thermal decomposition of acetaldehyde may be described by the reaction steps (1)—(17) given above.

Since the rate of formation of major products is three orders higher than that of the other products, the aldehyde decomposition can be well approached by the original Rice—Herzfeld scheme. On the basis of this scheme, the equation of decomposition is the following:

$$-\frac{d[CH_3CHO]}{dt} = 2k_1[CH_3CHO] + k_5\left(\frac{k_1}{k_6}\right)^{1/2}[CH_3CHO]^{3/2}.$$

Assuming the consumption of aldehyde to be negligible in the initiation step, this expression can be simplified as follows:

$$-\frac{d[CH_3CHO]}{dt} = +\frac{d[CH_4]}{dt} = k_5\left(\frac{k_1}{k_6}\right)^{1/2}[CH_3CHO]^{3/2}.$$

The value of k_1 may be calculated from the known k_5 [26] and k_6 [30] values. With the aid of k_1 we can determine the Arrhenius parameters of the initiation step.

In Fig. 8, the $\log k_1 - 1/T$ curves, calculated from analytical and pressure—time measurement data, are shown. From these curves the following value of activation energies for the initiation step are obtained:

$E_1 = 81.49 \pm 3.25$ kcal/mole (from pressure—time data)

$E_1 = 79.69 \pm 1.38$ kcal/mole (from analytical data).

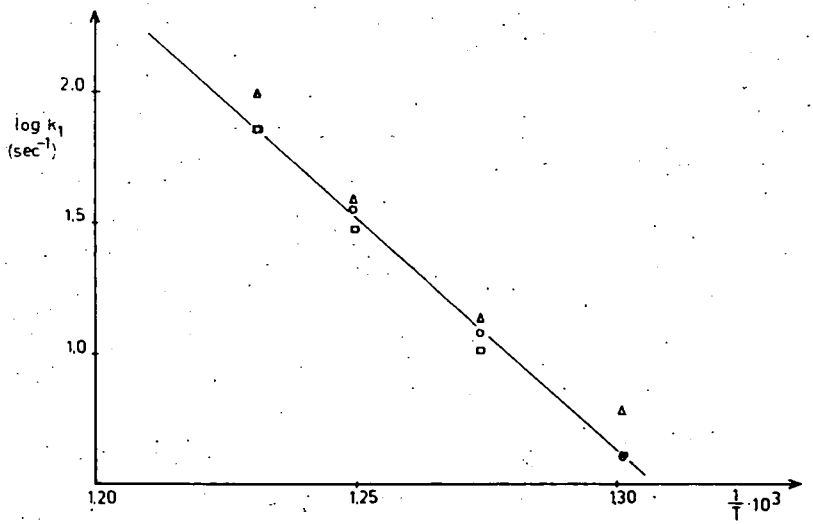

Fig. 8a. Arrhenius plot of the first order rate constants (k_1), calculated from the analytical data. $p_{ald.}$ = □ 50 torr; △ 80 torr; ○ 150 torr

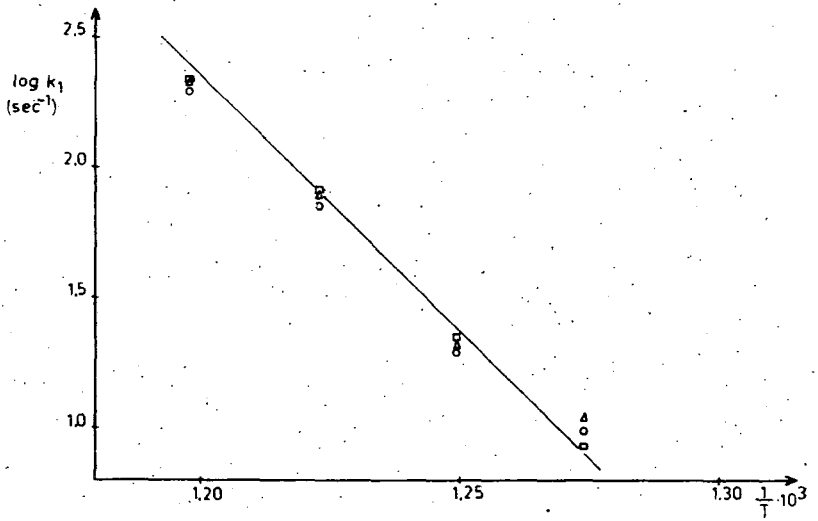

Fig. 8b. Arrhenius plot of the first order rate constants (k_1), calculated from pressure—time measurements. $p_{ald.}$ = ○ 50 torr; △ 100 torr □ 200 torr

while the A values are:

$A_1 = 8.87 \pm 4.42 \cdot 10^{16}$ (from pressure measurement)

$A_1 = 3.88 \pm 2.94 \cdot 10^{16}$ (from analytical data).

These values agree well with the values of other authors, because E_1 varies between 79—82 kcal/mole [23, 4, 14, 31] and $A_1 = 10^{16}$ [23].

The chain length (ν) may be given as the ratio of the overall rate of acetaldehyde decomposition and the rate of chain initiation:

$$\nu = \frac{W_{\text{overall}}}{W_{\text{initiation}}}$$

Table V

Chain lengths as functions of pressure and temperature

p_{ald} / t °C	80	100	200
495.5	—	17000	35950
512	12400	15000	17000
527.5	6200	9300	10700
539.5	4400	—	8600

Using the k_1 value derived from analytical data, the values given in Table V are obtained.

The chain lengths calculated from pressure measurement data are similar.

* * *

The authors are grateful to Prof. Z. G. SZABÓ for initiation the investigations and helpful suggestions at the initial stages of this work, to Dr. T. BÉRCES for valuable discussions, to Dr. I. SZILÁGYI for mass spectrometric analyses, to Dr. L. ZALOTAI for computer calculations and to I. TRITZ for technical assistance.

References

[1] *Steacie, E. W. R.:* Atomic and free radical reactions, Reinhold Publ. Corp., New York, 1954.
[2] *Leifer, E., H. C. Urey:* J. Am. Chem. Soc. **64**, 944 (1942).
[3] *Ho, S. K.:* Proc. Roy. Soc. **A276**, 278 (1963).
[4] *Liu, M. T. H., K. J. Laidler:* Can. J. Chem. **46**, 479 (1968).
[5] *Trenwith, A. B.:* J. Chem. Soc. **1963** 4426.
[6] *Collin, J. E., A. Delplace:* Bull. Soc. Chim. Belges **75**, 304 (1966).
[7] *Laidler, K. J.:* Chemical Kinetics, 2nd Ed., McGraw Hill Book Co., New York, 1965.
[8] *Benson, S. W.:* The Foundation of Chemical Kinetics, McGraw Hill Book Co., New York, 1960.
[9] *Bérces, T.:* The Decomposition of Aldehydes and Ketones, In: Comprehensive Chemical Kinetics (Ed.: Bamford, C. H., C. F. Tipper) Vol. 5. p. 234. Elsevier, Amsterdam, 1972.
[10] *Hinshelwood, C. N., W. K. Hutchinson:* Proc. Roy. Soc. **A111**, 380 (1926).
[11] *Kassel, L. S.:* J. Phys. Chem. **34**, 1166 (1930).
[12] *Letort, M.:* Compt. rend. **199**, 351 (1934), *ibid.* **119**, 1617 (1934).
[13] *Freeman, G. R., C. J. Danby, C. N. Hinshelwood:* Proc. Roy. Soc. **A245**, 456 (1958).
[14] *Setser, D. W.:* J. Phys. Chem. **70**, 826 (1966).
[15] *Imai, N., Y. Yoshida, O. Toyama:* Bull. Chem. Soc. Japan **35**, 752 (1962).
[16] *Eusuf, M., K. J. Laidler:* Can. J. Chem. **42**, 1851 (1964).
[17] *Dexter, R. W., A. B. Trenwith:* J. Chem. Soc. **1964** 5459.
[18] *Laidler, K. J., M. T. H. Liu:* Proc. Roy. Soc. **A297**, 365 (1967).
[19] *Come, G. M., M. Dzierzynski, R. Martin, M. Niclause:* Compt. rend. Ser. **C264**, 548 (1967).
[20] *Boyer, A., M. Niclause, M. Letort:* J. Chim. Phys. **49**, 345 (1952).
[21] *Rice, F. O., K. F. Herzfeld:* J. Am. Chem. Soc. **56**, 284 (1934).
[22] *Schuchmann, H. P., K. J. Laidler:* Can. J. Chem. **48**, 2315 (1970).
[23] *Come, G. M., M. Dzierzynski, R. Martin, M. Niclause:* Rev. Inst. Franc. Petrole **23**, 1365 (1968).
[24] *Letort, M.:* J. Chim. Phys. **34**, 265 (1937).
[25] *Ausloos, P., E. W. R. Steacie:* Can. J. Chem. **33**, 31 (1955).
[26] *Dodd, R. E.:* Can. J. Chem. **33**, 699 (1955).
[27] *Márta, F.:* Magy. Kém. Foly. **67**, 216 (1961).
[28] *Seddon, R. W., M. V. Travers:* Proc. Roy. Soc. **A149**, 355 (1935).
[29] *Come, G. M.:* Theses I. Nancy, 1968.
[30] *Shepp, A. J.:* J. Chem. Phys. **24**, 939 (1956).
[31] *Benson, S. W.:* J. Chem. Phys. **40**, 105 (1964).
[32] *Brinton, R. K., D. H. Volman:* J. Chem. Phys. **20**, 1053 (1952).
[33] *Benson, S. W.:* Thermochemical Kinetics, John Wiley, New York, 1968.
[34] *McKnight, Ch., H. Niki, B. Weinstock:* J. Chem. Phys. **42**, 5219 (1967).
[35] *Wall, L. A., W. J. Moore:* J. Phys. Chem. **55**, 965 (1951).
[36] *Avery, H. E., R. J. Cvetanovic:* J. Chem. Phys. **43**, 3727 (1965).
[37] *Lambert, R. M., M. I. Christie, J. W. Linnett:* Chem. Comm. **1967**, 388.

ИЗУЧЕНИЕ ТЕРМИЧЕСКОГО РАСПАДА АЦЕТАЛЬДЕГИДА

И. Бárди, Ф. Марта

Изучен термический распад ацетальдегида в области температур 495—540 °C при исходных давлениях 25—200 торр. За ходом реакции следили по изменениям давления и газохроматографическим методом анализа. С применением обеих методов были рассчитаны константы скорости, которые независимо от метода, для образования основных продуктов получались соответствующими 3/2 порядку реакции. Для общей реакции и реакции инициирования были определены Аррениусовые параметры. Обсуждены реакции образования побочных продуктов и предложен простой механизм распада ацетальдегида.

TETRAGONALLY DISTORTED TETRAHEDRAL ML_4-COMPLEXES, IV

Splitting of the d^5-Configuration in Strong Ligand Field of D_{2d}-Symmetry

By

M. I. BÁN

Institute of General and Physical Chemistry, Attila József University, Szeged

(Received September 10, 1973)

The energies of spectroscopic terms arising from the splitting, in ligand field of D_{2d}-symmetry, of d^5 strong field configurations have been given in expressions of the electronic repulsion parameters B and C, the three ligand field parameters K, L and M and the distortion angle β.

By using the procedure described in the previous papers [1—3] of this series, energy matrices[1] including the terms of electronic repulsions and electron-ligand interactions of five d-electrons in strong ligand field of D_{2d}-symmetry have been given as follows:

$$^6A_1[a_1b_1b_2e^2]:0 \tag{1}$$

$^4A_1$	$[a_1b_1b_2e^2]$	$[a_1b_1b_2e^2]$	$[a_1b_1b_2e^2]$
$[a_1b_1b_2e^2]$	$\frac{35}{3}B+5C$	$\sqrt{\frac{20}{9}}B$	$-\sqrt{\frac{60}{9}}B$
$[a_1b_1b_2e^2]$		$\frac{34}{3}B+5C$	$-\sqrt{\frac{48}{9}}B$
$[a_1b_1b_2e^2]$			$14B+5C$

(2)

$^4A_2$	$[a_1b_1^2e^2]$	$[a_1b_2^2e^2]$	$[a_1b_1b_2e^2]$
$[a_1b_1^2e^2]$	$10B+6C-12L$	C	$\sqrt{18}B$
$[a_1b_2^2e^2]$		$10B+6C+12L$	$\sqrt{18}B$
$[a_1b_1b_2e^2]$			$19B+7C$

(3)

[1] The matrices are symmetrical, thus the indication of the off-diagonal elements above the diagonals is sufficient.

$^2A_1$	$[a_1e^4]$	$[a_1b_1^2b_2^2]$	$[a_1b_1^2e^2]$	$[a_1b_2^2e^2]$	$[a_1^2b_1e^2]$	$[a_1^2b_2e^2]$	$[b_1b_2^2e^2]$	$[b_1^2b_2e^2]$	$[a_1b_1b_2e^2]$	$[a_1b_1b_2e^2]$	$[a_1b_1b_2e^2]$
$[a_1e^4]$	$35B+10C-12K+6M$	0	$\sqrt{2}(3B+C)$	$\sqrt{2}(3B+C)$	$-\sqrt{6}B$	$\sqrt{6}B$	0	0	$3B$	$-\sqrt{27}B$	$\sqrt{72}B$
$[a_1b_1^2b_2^2]$		$35B+10C+12K-6M$	$\sqrt{2}(3B+C)$	$\sqrt{2}(3B+C)$	0	0	$\sqrt{6}B$	$-\sqrt{6}B$	$3B$	$-\sqrt{27}B$	$\sqrt{72}B$
$[a_1b_1^2e^2]$			$23B+11C-12L$	C	$-\sqrt{75}B$	0	0	$-\sqrt{75}B$	$\sqrt{\frac{9}{2}}B$	$-\sqrt{\frac{27}{2}}B$	$6B$
$[a_1b_2^2e^2]$				$23B+11C+12L$	0	$\sqrt{75}B$	$\sqrt{75}B$	0	$\sqrt{\frac{9}{2}}B$	$-\sqrt{\frac{27}{2}}B$	$6B$
$[a_1^2b_1e^2]$					$27B+9C+6K-6L+4M$	$-3B$	$4B+C$	0	$\sqrt{6}B$	0	$-\sqrt{12}B$
$[a_1^2b^2e^2]$						$27B+9C+6K+6L+4M$	0	$4B+C$	$\sqrt{\frac{3}{2}}B$	$\sqrt{\frac{9}{2}}B$	$\sqrt{12}B$
$[b_1b_2^2e^2]$							$27B+9C-6K+6L-4M$	$-3B$	$-\sqrt{6}B$	0	$\sqrt{12}B$
$[b_1^2b_2e^2]$								$27B+9C-6K-6L-4M$	$-\sqrt{\frac{3}{2}}B$	$-\sqrt{\frac{9}{2}}B$	$-\sqrt{12}B$
$[a_1b_1b_2e^2]$									$\frac{49}{3}B+8C$	$-\sqrt{\frac{100}{3}}B$	$\sqrt{\frac{8}{9}}B$
$[a_1b_1b_2e^2]$										$23B+8C$	$-\sqrt{\frac{8}{3}}B$
$[a_1b_1b_2e^2]$											$\frac{56}{3}B+8C$

(7)

$^2A_2$	$[a_1b_1^2e^2]$	$[a_1b_2^2e^2]$	$[a_1^2b_1e^2]$	$[a_1^2b_2e^2]$	$[b_1b_2^2e^2]$	$[b_1^2b_2e^2]$	$[a_1b_1b_2e^2]$	$[a_1b_1b_2e^2]$
$[a_1b_1^2e^2]$	$13B+9C-$ $-12L$	C	$-3B$	0	0	$-3B$	$-\sqrt{\frac{9}{2}}B$	$\sqrt{\frac{27}{2}}B$
$[a_1b_2^2e^2]$		$13B+9C+$ $+12L$	0	$-3B$	$-3B$	0	$-\sqrt{\frac{9}{2}}B$	$\sqrt{\frac{27}{2}}B$
$[a_1^2b_1e^2]$			$27B+9C+6K-$ $-6L+4M$	$3B$	$4B+C$	0	0	$-\sqrt{150}B$
$[a_1^2b_2e^2]$				$27B+9C+6K+$ $+6L+4M$	0	$4B+C$	$\sqrt{\frac{225}{2}}B$	$-\sqrt{\frac{75}{2}}B$
$[b_1b_2^2e^2]$					$27B+9C-6K+$ $+6L-4M$	$3B$	0	$-\sqrt{150}B$
$[b_1^2b_2e^2]$						$27B+9C-6K-$ $-6L-4M$	$\sqrt{\frac{225}{2}}B$	$-\sqrt{\frac{75}{2}}B$
$[a_1b_1b_2e^2]$							$25B+10C$	$-\sqrt{12}B$
$[a_1b_1b_2e^2]$								$29B+10C$

(8)

$^2B_1$	$[b_1e^4]$	$[a_1^2b_1b_2^2]$	$[a_1b_1^2e^2]$	$[a_1b_2^2e^2]$	$[a_1^2b_1e^2]$	$[a_1^2b_2e^2]$	$[b_1b_2^2e^2]$	$[b_1^2b_2e^2]$	$[a_1b_1b_2e^2]$	$[a_1b_1b_2e^2]$
$[b_1e^4]$	$15B+10C-18K-$ $-6L+2M$	0	$-\sqrt{6}B$	0	$\sqrt{2}(B+C)$	0	$\sqrt{2}(3B+C)$	$\sqrt{54}B$	0	$-\sqrt{12}B$
$[a_1^2b_1b_2^2]$		$15B+10C+18K+$ $+6L-2M$	0	$\sqrt{6}B$	$\sqrt{2}(3B+C)$	$-\sqrt{54}B$	$\sqrt{2}(B+C)$	0	0	$-\sqrt{12}B$
$[a_1b_1^2e^2]$			$17B+9C-$ $-12L$	C	$-\sqrt{75}B$	0	0	$-3B$	$\sqrt{\frac{27}{2}}B$	$\sqrt{\frac{9}{2}}B$
$[a_1b_2^2e^2]$				$17B+9C+$ $+12L$	0	$-3B$	$\sqrt{75}B$	0	$-\sqrt{\frac{27}{2}}B$	$-\sqrt{\frac{9}{2}}B$
$[a_1^2b_1e^2]$					$33B+11C+6K-$ $-6L+4M$	$-\sqrt{27}B$	$4B+C$	0	0	$-\sqrt{150}B$
$[a_1^2b_2e^2]$						$27B+9C+6K+$ $+6L+4M$	0	$4B+C$	$\sqrt{\frac{3}{2}}B$	$\sqrt{\frac{9}{2}}B$
$[b_1b_2^2e^2]$							$33B+11C-6K+$ $+6L-4M$	$\sqrt{27}B$	0	$-\sqrt{150}B$
$[b_1^2b_2e^2]$								$27B+9C-6K-$ $-6L-4M$	$-\sqrt{\frac{3}{2}}B$	$-\sqrt{\frac{9}{2}}B$
$[a_1b_1b_2e^2]$									$19B+8C$	$-\sqrt{12}B$
$[a_1b_1b_2e^2]$										$23B+8C$

(9)

$^2B_2$	$[b_2e^3]$	$[a_1^2b_1^2b_2]$	$[a_1b_1^2e^2]$	$[a_1b_2^2e^2]$	$[a_1^2b_1e^2]$	$[a_1^2b_2e^2]$	$[b_1b_2^2e^2]$	$[b_1^2b_2e^2]$	$[a_1b_1b_2e^2]$	$[a_1b_1b_2e^2]$
$[b_2e^4]$	$15B+10C-18K+$ $+6L+2M$	0	0	$\sqrt{6}B$	0	$\sqrt{2}(B+C)$	$-\sqrt{54}B$	$\sqrt{2}(3B+C)$	$3B$	$-\sqrt{3}B$
$[a_1^2b_1^2b_2]$		$15B+10C+18K-$ $-6L-2M$	$-\sqrt{6}B$	0	$\sqrt{54}B$	$\sqrt{2}(3B+C)$	0	$\sqrt{2}(B+C)$	$3B$	$-\sqrt{3}B$
$[a_1b_1^2e^2]$			$17B+9C-$ $-12L$	C	$-3B$	0	0	$-\sqrt{75}B$	$-\sqrt{\frac{27}{2}}B$	$-\sqrt{\frac{9}{2}}B$
$[a_1b_2^2e^2]$				$17B+9C+$ $+12L$	0	$\sqrt{75}B$	$-3B$	0	$\sqrt{\frac{27}{2}}B$	$\sqrt{\frac{9}{2}}B$
$[a_1^2b_1e^2]$					$27B+9C+6K-$ $-6L+4M$	$\sqrt{27}B$	$4B+C$	0	$\sqrt{6}B$	0
$[a_1^2b_2e^2]$						$33B+11C+6K+$ $+6L+4M$	0	$4B+C$	$\sqrt{\frac{225}{2}}B$	$-\sqrt{\frac{75}{2}}B$
$[b_1b_2^2e^2]$							$27B+9C-6K+$ $+6L-4M$	$-\sqrt{27}B$	$-\sqrt{6}B$	0
$[b_1^2b_2e^2]$								$33B+11C-6K-$ $-6L-4M$	$\sqrt{\frac{225}{2}}B$	$-\sqrt{\frac{75}{2}}B$
$[a_1b_1b_2e^2]$									$19B+8C$	$-\sqrt{12}B$
$[a_1b_1b_2e^2]$										$23B+8C$

(10)

^4E	$[a_1^3e^3]$	$[b_1^3e^3]$	$[b_2^3e^3]$	$[a_1b_1e^3]$	$[a_1b_1e^3]$	$[a_1b_2e^3]$	$[a_1b_2e^3]$	$[b_1b_2e^3]$	$[b_1b_2e^3]$ ...
$[a_1^3e^3]$	$45B+10C+7M$	$4B+C$	$4B+C$	$-\sqrt{\frac{75}{2}}B$	$-\sqrt{\frac{9}{2}}B$	$\sqrt{\frac{75}{2}}B$	$-\sqrt{\frac{9}{2}}B$	0	0
$[b_1^3e^3]$		$15B+10C-12K-12L-M$	C	$-\sqrt{\frac{75}{2}}B$	$\sqrt{\frac{9}{2}}B$	0	0	$-\sqrt{\frac{9}{2}}B$	$\sqrt{\frac{27}{2}}B$
$[b_2^3e^3]$			$15B+10C-12K+12L-M$	0	0	$\sqrt{\frac{75}{2}}B$	$\sqrt{\frac{9}{2}}B$	$\sqrt{\frac{9}{2}}B$	$\sqrt{\frac{27}{2}}B$
$[a_1b_1e^3]$				$26B+9C-6K-6L+3M$	$\sqrt{3}B$	$-\frac{3}{2}B$	$\sqrt{\frac{27}{4}}B$	$\sqrt{\frac{75}{4}}B$	$-\frac{3}{2}B$
$[a_1b_1e^3]$					$22B+9C-6K-6L+3M$	$-\sqrt{\frac{9}{2}}B$	$\frac{9}{2}B$	$\frac{3}{2}B$	$\sqrt{\frac{147}{4}}B$ (11a)
$[a_1b_2e^3]$						$26B+9C-6K+6L+3M$	$-\sqrt{3}B$	$\sqrt{\frac{75}{4}}B$	$\frac{3}{2}B$
$[a_1b_2e^3]$							$22B+9C-6K+6L+3M$	$-\frac{3}{2}B$	$\sqrt{\frac{147}{4}}B$
$[b_1b_2e^3]$								$15B+9C-12K-M$	0
$[b_1b_2e^3]$ ...									$21B+9C-12K-M$

(11b) (cont.)

^3E	... $[a_1^2b_1^2e]$	$[a_1^2b_2^2e]$	$[b_1^2b_2^2e]$	$[a_1b_1b_2^2e]$	$[a_1b_1b_2^2e]$	$[a_1b_1^2b_2e]$	$[a_1b_1^2b_2e]$	$[a_1^2b_1b_2e]$	$[a_1^2b_1b_2e]$
$[a_1^2e^3]$	$3B+C$	$3B+C$	0	0	0	0	0	$-\sqrt{\frac{81}{2}}B$	$-\sqrt{\frac{27}{2}}B$
$[b_1^2e^3]$	$B+C$	0	$3B+C$	0	0	$\sqrt{\frac{3}{2}}B$	$-\sqrt{\frac{9}{2}}B$	0	0
$[b_2^2e^3]$	0	$B+C$	$3B+C$	$\sqrt{6}B$	0	0	0	0	0
$[a_1b_1e^3]$	$-\sqrt{6}B$	0	0	$3B+C$	0	$\frac{9}{2}B$	$\sqrt{\frac{27}{4}}B$	$-\sqrt{\frac{3}{4}}B$	$\frac{3}{2}B$
$[a_1b_1e^3]$	0	0	0	0	$3B+C$	$\sqrt{\frac{243}{4}}B$	$-\frac{3}{2}B$	$\frac{3}{2}B$	$\sqrt{\frac{3}{4}}B$
$[a_1b_2e^3]$	0	$\sqrt{6}B$	0	0	$-\sqrt{27}B$	$-\frac{1}{2}(3B+C)$	$\sqrt{\frac{3}{4}}(3B+C)$	$-\sqrt{\frac{3}{4}}B$	$\frac{3}{2}B$
$[a_1b_2e^3]$	0	0	0	$\sqrt{27}B$	$6B$	$\sqrt{\frac{3}{4}}(3B+C)$	$\frac{1}{2}(3B+C)$	$\frac{3}{2}B$	$\sqrt{\frac{3}{4}}B$
$[b_1b_2e^3]$	0	0	0	$\sqrt{3}B$	0	$-\sqrt{\frac{3}{4}}B$	$\frac{3}{2}B$	$-\frac{1}{2}(B+C)$	$\sqrt{\frac{3}{4}}(B+C)$
$[b_1b_2e^3]$	0	0	$\sqrt{54}B$	0	$\sqrt{3}B$	$\frac{3}{2}B$	$\sqrt{\frac{3}{4}}B$	$\sqrt{\frac{3}{4}}(B+C)$	$\frac{1}{2}(B+C)$
...									

^2E	... $[a_1^2b_1^2e]$	$[a_1^2b_2^2e]$	$[b_1^2b_2^2e]$	$[a_1b_1b_2^2e]$	$[a_1b_1b_2^2e]$	$[a_1b_1^2b_2e]$	$[a_1b_1^2b_2e]$	$[a_1^2b_1b_2e]$	$[a_1^2b_1b_2e]$
...									
$[a_1^2b_1^2e]$	$15B+10C+12K-$ $-12L+M$	C	$4B+C$	0	0	$\sqrt{\frac{3}{2}}B$	$-\sqrt{\frac{81}{2}}B$	$-\sqrt{\frac{9}{2}}B$	$-\sqrt{\frac{27}{2}}B$
$[a_1^2b_2^2e]$		$15B+10C+12K+$ $+12L+M$	$4B+C$	$\sqrt{\frac{75}{2}}B$	$-\sqrt{\frac{9}{2}}B$	0	0	$-\sqrt{18}B$	0
$[b_1^2b_2^2e]$			$45B+10C-$ $-7M$	$\sqrt{\frac{75}{2}}B$	$\sqrt{\frac{9}{2}}B$	$\sqrt{24}B$	$-\sqrt{18}B$	0	0
$[a_1b_1b_2^2e]$				$26B+9C+6K+$ $+6L-3M$	$\sqrt{3}B$	$3B$	0	$-\sqrt{12}B$	$3B$
$[a_1b_1b_2^2e]$					$22B+9C+6K+$ $+6L-3M$	$\sqrt{27}B$	0	$6B$	$\sqrt{3}B$
$[a_1b_1^2b_2e]$						$\frac{49}{2}B+9C+6K-$ $-6L-3M$	$-\sqrt{\frac{27}{4}}B$	$\sqrt{\frac{75}{4}}B$	$\frac{3}{2}B$
$[a_1b_1^2b_2e]$							$\frac{47}{2}B+9C+6K-$ $-6L-3M$	$\frac{3}{2}B$	$\sqrt{\frac{147}{4}}B$
$[a_1^2b_1b_2e]$								$\frac{39}{2}B+9C+12K+$ $+M$	$\sqrt{\frac{27}{4}}B$
$[a_1^2b_1b_2e]$									$\frac{33}{2}B+9C+12K+$ $+M$

(11c) (cont.)

$^1B_1$	$[a_1^2b_2e^2]$	$[b_1^2b_2e^2]$	$[a_1b_1b_2e^2]$
$[a_1^2b_2e^2]$	$18B+6C+6K+6L+4M$	$4B+C$	$-\sqrt{6}B$
$[b_1^2b_2e^2]$		$18B+6C-6K+6L-4M$	$\sqrt{6}B$
$[a_1b_1b_2e^2]$			$13B+5C$

(4)

$^1B_2$	$[a_1^2b_1e^2]$	$[b_1b_2^2e^2]$	$[a_1b_1b_2e^2]$
$[a_1^2b_1e^2]$	$18B+6C+6K-6L+4M$	$4B+C$	$\sqrt{6}B$
$[b_1b_2^2e^2]$		$18B+6C-6K+6L-4M$	$-\sqrt{6}B$
$[a_1b_1b_2e^2]$			$13B+5C$

(5)

^4E	$[a_1b_1e^3]$	$[a_1b_2e^3]$	$[b_1b_2e^3]$	$[a_1b_1b_2^2e]$	$[a_1b_1^2b_2e]$	$[a_1^2b_1b_2e]$
$[a_1b_1e^3]$	$16B+6C-6K+6L+3M$	0	$\sqrt{12}B$	$3B+C$	$-3B$	$\sqrt{3}B$
$[a_1b_2e^3]$		$16B+6C-6K+6L+3M$	$\sqrt{12}B$	$-3B$	$3B+C$	$\sqrt{3}B$
$[b_1b_2e^3]$			$12B+6C-12K-M$	$\sqrt{3}B$	$\sqrt{3}B$	$B+C$
$[a_1b_1b_2^2e]$				$16B+6C+6K+6L-3M$	0	$\sqrt{12}B$
$[a_1b_1^2b_2e]$					$16B+6C+6K-6L-3M$	$\sqrt{12}B$
$[a_1^2b_1b_2e]$						$12B+6C+12K+M$

(6)

The energy expressions (1)—(11) find their main uses in the interpretation [4] of the spectral properties of four-coordinate transition metal complexes.

References

[1] *Bán, M. I.:* Acta Phys. et Chem. Szeged **18**, 45 (1972).
[2] *Bán, M. I.:* Acta Phys. et Chem. Szeged **18**, 185 (1972).
[3] *Bán, M. I.:* Acta Phys. et Chem. Szeged **19**, 57 (1973).
[4] e.g. *Bán, M. I., J. Császár:* Applications of the Tetragonally Distorted Tetrahedral Ligand Field Model. Theoretical Treatment of Four-coordinate Transition Metal Complexes. Paper presented at the VIII. Colloquium on Coordination Chemistry, Sopron, Hungary, May 21—23, 1973. (To be published in Magy. Kém. Folyóirat)

ТЕТРАГОНАЛЬНО ДЕФОРМИРОВАННЫЕ ТЕТРАЭДРИЧЕСКИЕ КОМПЛЕКСЫ ML_4. IV

Расщепление d^5-конфигураций в сильных полях лигандов D_{2d} симметрий

М. И. Бан

Используя приближение сильного поля, рассчитали энергетическое состояние электронов, происходящих из расщепления конфигураций создаваемых из d^5 электронных структур в лигандных полях D_{2d} (деформированные тетраэдрические) симметрии, в зависимости от параметров электростатических и лигандных полей, а также угла деформации.

KINETIC STUDIES ON THE CATALYTIC DECOMPOSITION OF AMMONIUM PERCHLORATE

By

F. SOLYMOSI

Gas Kinetics Research Group of the Hungarian Academy of Sciences, Attila József University, Szeged

(Received June 20, 1973)

The available data on the effect of different oxides and salts on the slow and fast decomposition and ignition of ammonium perchlorate are reviewed. On the basis of the effeciency of the additives the most important properties of the catalysts, playing an essential part in accelerating the decomposition of ammonium perchlorate, are pointed out.

Introduction

In an earlier publication [1] we summarized the main results of studies relating to the slow and fast decompositions, the sublimation and the explosion of pure ammonium perchlorate (AP). It is a characteristic feature of AP that its stability is extremely sensitive to the presence of various additives. Depending on their structures and chemical properties, these additives increase the rate of the slow decomposition of AP, decrease the ignition temperature and also affect the rate of combustion of AP. Considering that AP plays a key-role in solid propellants, it can be seen that from the point of view of the increase in performance of the propellant the discovery of the most suitable catalysts is of fundamental importance. Research work in this field began about 10—12 years ago, primarily in laboratories dealing with the production and development of propellants.

However, the considerable sensitivity of the stability of AP to the presence of foreign substances also aroused interest, since this property provided the possibility for the elucidation of the regularities of solid-phase catalytic processes, an area of catalytic reactions which had been completely neglected up to that time.

The present paper summarizes the main results of studies made in this field and the reaction mechanisms proposed by different authors. The effects of various salts and oxides are surveyed separately, greater stress being placed on the kinetic studies. Since, in several cases, the effect of a given substance has been examined by a number of research groups, the characteristics of the effects of additives are always reported on the basis of the first detailed kinetic study. Only the more important results and observations of other work are emphasized.

In addition to the studies published in the various technical journals, numerous special publications, research institute reports and proceedings also deal with the catalytic decomposition of AP. It was possible to obtain some of these, while knowl-

edge about others can be extracted from earlier reviews. It is clear that the greater part of the data published elsewhere than in international journals is of a fairly qualitative nature, and the restricted publication can in many respects be attributed to this and not to the special nature of the subject.

Kinetic studies

Effect of oxides on the decomposition of AP

Manganese dioxide

It was first observed by BIRCUMSHAW and NEWMAN [2] that MnO_2 exerts a very great effect on the decomposition of AP at 235 °C.

The first detailed kinetic measurement series with MnO_2 was made by GALWEY and JACOBS [3] in the range 137—212 °C. The reaction proceeded in two steps. The first stage, which had the higher rate, was a manganese dioxide catalysed process, while the second corresponded to the decomposition of pure AP.

For MnO_2 contents of 34—90% the rate constant of the catalysed reaction was independent of the composition of the sample. This result indicates that the rate of the catalytic reaction depends primarily on the extent of the contact surface between the oxide and the AP and not on the amount of the catalyst. If a powder mixture was used, the decomposition proceeded to 100%. The initial fast process, which was linear in time, was described by the equation

$$p = mkt \qquad (1)$$

and the break-down stage by

$$1-(1-\alpha)^{1/2} = kt \qquad (2)$$

(m = weight of AP).

The activation energy of the catalytic reaction was found to be 33.2 and 31.5 kcal, respectively. From studies using oxide containing ^{18}O it turned out that the oxide does not take part chemically in the process. The authors also examined the catalytic effects of manganese oxides of various compositions. MnO_2 was 5 times more effective than MnOOH and 10 times more effective than Mn_2O_3. Mn_3O_4 at 153.5 °C did not show accelerating effect. The MnO_2-catalysed decomposition of AP was also studied by HERMONI and SALMON [4]. The activation energy of the reaction in the temperature ranges 170—200, 200—240 and 249—272 °C was 28, 34 and 48 kcal, respectively. KURATANI [5] studied the catalytic effect of MnO_2 (1%) in the high temperature decomposition of AP above 310 °C, and obtained an activation energy value of 31.0 kcal. In both works the kinetic analysis was made with equation (2). The lowest temperature of explosion of AP in the presence of MnO_2 was 265 °C.

Iron(III) oxide

Iron(III) oxide proved to be a less active catalyst than manganese dioxide; this is primarily of interest because iron oxide is one of the most frequently used catalysts in AP-containing propellants.

Below 240 °C in air at atmospheric pressure the decomposition of AP was scarcely changed by iron(III) oxide, even in large amounts [6]. Its effect was observed

primarily in that the transformation during the decomposition was 40—45% instead of 30—33%

In the presence of a small amount of oxide above 240 °C, up to 25—28% conversion, the reaction had practically the same rate as in the case of the pure salt. The effect of a greater amount of iron oxide (1:1 molar ratio) was not only a higher conversion but also almost a doubling of the reaction rate, and this latter further increased with increase of the amount of iron oxide. The α *vs.* t curves had an autocatalytic character, and the τ_{max} values practically agreed for the different compositions. The values of the rate maximum w_{max} were greatest for a powder mixture containing much iron oxide. The decomposition proceeded up to 60—95%.

For the determination of the rate constants the Prout—Tompkins equation

$$\log \frac{\alpha}{1-\alpha} = kt + C \tag{3}$$

and the Avrami—Erofeyev equation

$$-[\log (1-\alpha)]^{1/3} = kt + C \tag{4}$$

proved the most suitable in the present case. Activation energies of 32 kcal and 30.5 kcal were found for the acceleration stage and the break-down stage, respectively.

In this same temperature region, SHIDLOVSKII [7] obtained a value of 41.0 kcal for the activation energy of the catalytic decomposition. The experimental conditions differred from the above in that the measurements were made in vacuum.

Under adiabatic conditions the activation energy of the reaction was found to be 34.3 kcal [8].

The effect of iron(III) oxide on the high temperature decomposition of AP was studied in the range 320—380 °C [6]. The α *vs.* t curves were divided into two sharply separated stages. The initial fast stage was completely independent of the temperature of reaction and the amount of oxide, and depended only on the quantity of AP. In this stage the reaction proceeds to about 30%. Equation (4) was found to be the most suitable for the kinetic evaluation of the second stage. Depending on the amount of catalyst, the value of the activation energy varied between 22 and 30.8 kcal.

With the differential scanning calorimetric method, WAESCHE and VENOGRAD [9] obtained an activation energy of 48.0 kcal at 300—350 °C.

The explosion of AP in the presence of iron(III) oxide occurred at a substantially lower temperature than in the pure state [10]. The lowest temperature of explosion decreased gradually with the increase of the amount of catalyst. The 1:1 molar mixture exploded at the lowest temperature, at 300 °C.

Copper(I) oxide

The effect of copper(I) oxide, primarily on the inducing of the explosion of AP, was studied by JACOBS and KUREISHY [11, 12]. In the presence of copper(I) oxide the AP exploded even at 248 °C. Two factors play a part in the occurrence of the explosion: the heat of reaction liberated during the oxidation of the oxide, and the catalytic effect of the copper(II) oxide formed.

The amounts of both AP and the catalyst exerted an effect on the occurrence

of the explosion: in the presence of a small amount of catalyst (22 mole %) the explosion took place at a higher temperature, probably because the reaction heat evolved during the oxidation of the catalyst was not sufficient for a significant increase of the rate of decomposition.

The above was confirmed with the help of a thermocouple placed in the sample. In the presence of greater amounts of catalyst a well-measurable temperature increase was observed in the sample. From a kinetic analysis of the reaction leading to explosion, an activation energy of 28 kcal was obtained, whereas from the temperature dependence of the induction periods prior to the explosion a value of 28.1 kcal was found.

The large catalytic effect of copper(I) oxide was also observed by other authors [5, 7]. Fairly large deviations were shown in the activation energy values for the catalytic reaction.

Copper(II) oxide

While the decomposition of pure AP is immeasurably slow below 200 °C, in the presence of copper(II) oxide it already begins at 180 °C after an induction period of about 10—15 hours [13]. The reaction was followed in air by measuring the amount of gas. The induction period varies on increase of the amount of copper oxide. The shortest induction period was found with a 16:1 molar mixture. The catalytic effect of copper oxide could be observed even when present in only 0.5 weight%. The reaction has an autocatalytic nature. The conversion was 50—60%. The mathematical approximations for the α *vs.* t curves were made with the Prout—Tompkins and Avrami—Erofeyev equations. The activation energy values for the catalytic reaction were 28.9—32.9 kcal. At 200—240 °C the decomposition of AP proceeded at a higher rate than the previous up to 80—90%, but with a considerably larger activation energy of 40—42 kcal.

With a further increase of the temperature range for the reaction, to 240—289 °C, the activation energy for the decomposition increases to 47.7 [14] and 53.5 kcal [7]. This result is certainly connected with a change in the mechanism of the catalytic reaction. It seems also probable that in this temperature interval the reaction is already very fast, and so it is fairly difficult to ensure isothermal conditions.

In addition to the large increase in the rate of decomposition, it is relevant that above 250 °C in the presence of a sufficient amount of oxide the AP exploded after an induction period of only 2—3 minutes [13]. On addition of 0.15 weight% copper oxide, the explosion occurred already at 270 °C. The induction period was the shortest in the 16:1 molar mixture and this composition exploded at the lowest temperature, 251 °C. If a larger amount of catalyst was used (1:5 molar ratio), merely a degenerate explosion occurred. From the temperature dependence of the induction periods, activation energy values of 29—31 kcal were obtained for the explosion of mixtures of different compositions [13, 5]; these values are substantially smaller than those obtained for the catalytic decomposition process in the same temperature range. It is presumably of importance for the different activation energy values that up to the occurrence of the explosion (during the induction period) only 20—26% of the AP decomposed. This activation energy value agrees essentially with that determined for the slow decomposition at 180—200 °C, and hence it was assumed that in both cases the same decomposition mechanism is dominant [13].

Considering that the activation energies of the decomposition of AP catalysed by MnO_2 [3], Fe_2O_3 [6] and CuO [13], especially at lower temperatures, were practically the same as the activation energy of the electron transfer process in the decomposition of AP, it was rightly possible to assume that the oxides accelerate the decomposition of AP by an electron transfer process, and the role of the oxides consists in promoting the electron transfer from the perchlorate anion to the ammonium cation, and in the inhibition of the back reaction [3]. On this basis it was expected that the effectivity of an oxide would depend sensitively on its electronic structure, and that the rate of the catalytic reaction would change with the concentrations of electrons and defect-electrons on the oxide, or in other words with the electron acceptor ability. CuO appeared particularly suitable to check this working hypothesis since its electrical conductivity can be increased and decreased by the incorporation of small amounts of ions of different valencies. With this aim, CuO was doped with 1 mole% Li_2O and with 1 mole% Cr_2O_3 [13]. With the copper oxide doped with lithium oxide, at 170—200 °C the decomposition of AP began sooner and the reaction proceeded much more quickly than in the presence of the pure oxide. In contrast, the chromic oxide doping increased the induction period and slightly decreased the reaction rate. The activation energies were essentially unaffected by the doping of the copper oxide and were 29—32 kcal.

The effects of the doping are presented in Fig. 1.

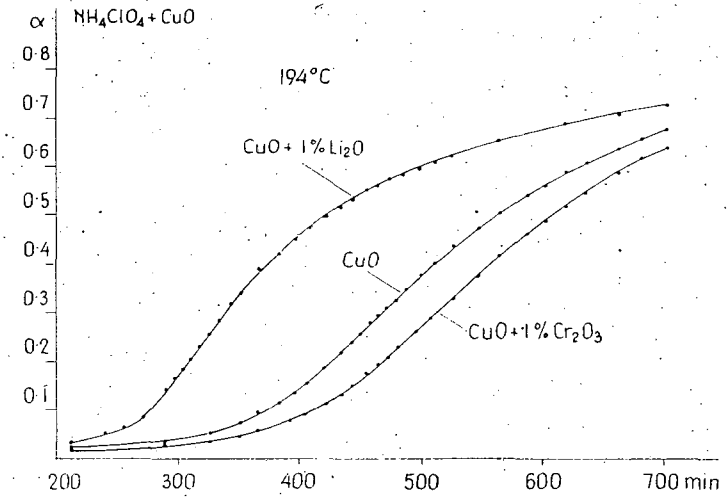

Fig. 1. Effect of doping with CuO on the catalytic decomposition of AP

At 200—240 °C the doping of the copper oxide with foreign ions did not produce a clear-cut change; this was explained, on the basis of the activation energy increase observed in this temperature interval, by the fact that the catalysed reaction in this stage no longer proceeds by the electron transfer mechanism. However, the effect of doping the catalyst could be observed in the course of the copper oxide initiated explosion of AP. The AP exploded at the lowest temperature in the presence of

the copper oxide doped with lithium oxide, and at the highest temperature with the chromic oxide doped catalyst. Nevertheless, at the temperature where all three mixtures exploded, there was scarcely any difference in the induction periods (Fig. 2). The activation energy values were 29—31 kcal in these cases, too.

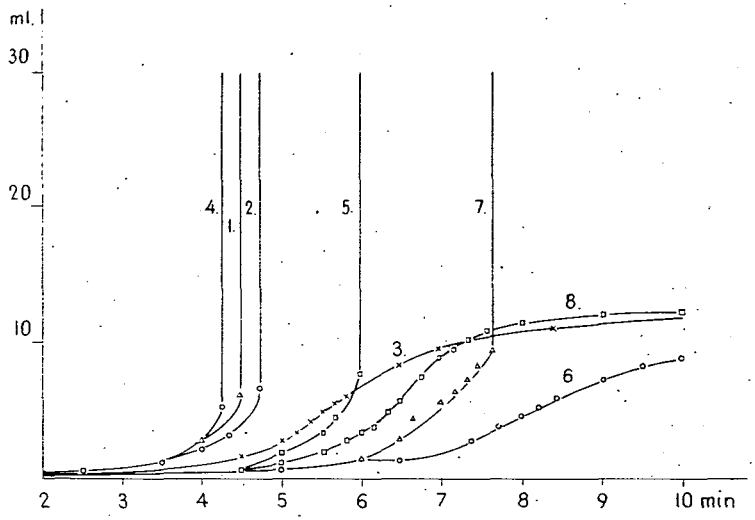

Fig. 2. Effect of doping with CuO on the ignition of AP. AP:CuO mole ratio 5:1 CuO + 1% Cr_2O_3: 1. 269.6 °C; 2. 266.5 °C; 3. 264.0 °C; CuO + 1% Li_2O: 4. 269.7 °C; 5. 262.2 °C; 6. 257.2 °C; 7. 260.0 °C; 8. pure CuO. 264.0 °C

Nickel(II) oxide

The effect of nickel on the stability of AP was first studied in detail by HERMONI and SALMON [4] by measuring the weight losses and the pressures of permanent gases at 200—260 °C. If powder mixtures were used, almost complete decomposition of the AP was observed. The final pressure of non-condensing gases varied with the quantity and quality of the oxide. The evaluation of the α *vs.* t curves was carried out with equation (3). A decomposition consisting of two sections was obtained, the rate in the first stage being the greater; however, this was not evaluated kinetically.

The activation energies of the catalytic reaction at 170—200°C and at 210—240°C were 33 and 43 kcal, respectively. The increase of the value of the activation energy is explained by a change of mechanism. The kinetic studies by SHIDLOVSKII [7] led to essentially the same results.

The effect of NiO, similarly to that of CuO, depended on the electrical properties [15]. It began first below 200°C in the presence of nickel oxide doped with lithium oxide. Incorporation of chromic oxide into the nickel oxide decreased the extent of catalysis significantly. The effect of doping the nickel oxide showed up, in general, in the initial section of the decomposition (the induction period, the stage of acceleration). Below 200 °C the decomposition proceeded to about 55%. The Prout—Tompkins equation proved most suitable in the evaluation of the α *vs.* t curves, but the Avrami—Erofeyev equation also gave satisfactory results. The value of the

activation energy was 30—35 kcal. Apart from the doping, the effect of the nickel oxide catalyst also changed with the temperature of pre-treatment [15]. With the increase of the ignition temperature of the oxide, in the range 500—1000 °C, the catalytic effect decreased considerably. Such a large effect of the temperature of pre-treating the oxide was not observed in the case of any other catalyst. A part may be played in the decrease of the catalytic effect not only by changes in the extent of the surface of the catalyst but also by a significant modification of the defect and the electronic structure of the nickel oxide.

In experiments with nickel oxide, BOLDYREV *et. al.* [16], however, showed that its catalytic effect at 250—300 °C depends on the extent of the BET surface of the oxide.

Chromic oxide

HERMONI and SALMON [4] also investigated the effect of Cr_2O_3 in the manner reported above. The characteristics of the catalytic reaction were the same as in the presence of NiO. The activation energies at 210—230 °C and at 250—275 °C were 26.7 and 37.7 kcal, respectively. An outstandingly large value of the activation energy, 68 kcal, was obtained by the adiabatic method [8].

Interesting results were produced by studying the effect of the electrical structure of the Cr_2O_3 [17]. The latter was doped with zinc(II), nickel(II) and titanium(IV) ions. The incorporation of the foreign ions was promoted by firing of the samples at 1100 °C. The high temperature treatment resulted in a considerable decrease of the effectiveness of the chromic oxide. The course of the slow decomposition of AP at 230 °C up to about 30% transformation was almost the same in the case of both pure and doped chromic oxide. A noticeable difference appeared only

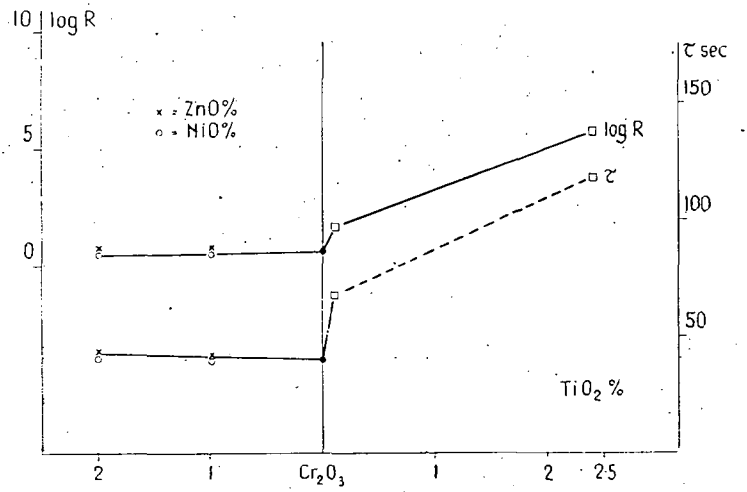

Fig. 3. Effect of doping on the electric resistivity of Cr_2O_3 and on the induction period for the ignition of AP

in the subsequent stage, where the slowest decomposition occurred in the presence of chromic oxide doped with 2.5% titanium dioxide.

At higher temperatures, the AP exploded even in the presence of a small amount of chromic oxide (100:1 molar ratio) at 295 °C. The explosion temperature decreased with increase of the amount of chromic oxide and then reached a limiting value. The lowest explosion temperature was 251 °C (AP:Cr_2O_3 molar ratio 1:1); while with a 10:1 molar mixture it was 275 °C. The incorporation of zinc and nickel oxides into the chromic oxide practically did not affect the behaviour of the latter. However, doping with titanium dioxide produced a significant change; compared with the effect of pure chromic oxide, it increased both the explosion temperature of the AP and the time till the explosion. The activation energy values calculated from a temperature analysis of the induction periods were 29—31 kcal in these cases, too. The effect of doping the chromic oxide on the induction period of the explosion of AP is shown in Fig. 3.

Cobalt(II, III) oxides

Cobalt oxide is likewise an effective catalyst of the decomposition of AP. Using the method reported above, HERMONI and SALMON [4] obtained an activation energy of 33 kcal for the catalytic decomposition at 170—200 °C. At 210—230 °C they obtained a value of 42 kcal, and SHIDLOVSKII [7] one of 38.3 kcal.

In the presence of cobalt oxide AP exploded at 241 °C. The activation energy value was 45.8 kcal. The value of the induction period preceding the explosion decreased with increase of the gas pressure.

Carbon and copper chromite

It is practical to consider studies of the effects of carbon and copper chromite together, for in many cases the two substances are applied jointly. Copper chromite (together with or without carbon) is the catalyst most generally used in the composite propellant based on AP to increase the rate of ignition. In spite of this, it is surprising that relatively few studies have been carried out in connection with its effects on the slow decomposition of AP.

The decomposition of AP below 240 °C was practically not affected by active carbon [18]. After the reaction, the carbon remained in an unchanged state. Between 240 and 260 °C the decomposition began without an incubation stage and the breakdown section was substantially longer than in the case of the pure salt. Above 260 °C the decomposition accelerated and a mild explosion was produced. From the temperature dependence of the times up to explosion an activation energy of 40 kcal was calculated. Experiments were also made to determine the critical temperature of explosion and the critical amount of AP.

With an adiabatic method they determined an activation energy of 52.5 kcal for the decomposition catalysed by carbon [8].

At 216—277 °C copper chromite (Harshaw, 0202P product) increased the rate of decomposition of AP altogether by 50%. The value of the activation energy was the same as in the decomposition of pure AP, 31 kcal [14]. A substantially greater effect on the high temperature (280—340 °C) decomposition of AP, was

exerted by copper chromite. Increase of the amount of catalyst in the range 0.5—5 weight% increased the rate constant of decomposition, but the addition of carbon to the copper chromite hardly affected it. The α *vs.* t curves obtained from gravimetric measurements were of a break-down nature; their mathematical analyses were carried out with equation (2) ($n=2$). The value of the activation energy was 48 kcal. A similar activation energy was also obtained in this temperature region for the decomposition of pure AP.

The explosion of the AP occurred first at 290 °C (5% catalyst). From the temperature dependence of the induction periods at 290—440 °C surprisingly low activation energies of 12—14 kcal were obtained.

With the adiabatic method, using different amounts of copper chromite, activation energies of 40—46 kcal were determined [8]. In agreement with the above, it was found that in the presence of catalyst the autocatalytic nature of the decomposition is lost.

Zinc oxide

Similarly to the above, a surprisingly large acceleration of the reaction occurred in the presence of zinc oxide; this approximated, and in some respects exceeded the effects of the most effective transition-metal oxide [19, 20].

On the admixture of only small amounts of zinc oxide (50:1 molar ratio), the decomposition of AP retained its autocatalytic nature but proceeded not to 30% but, instead, to about 75—80%. The zinc oxide decreased the value of the induction period (τ_0), the effect being more pronounced with increase of the amount of zinc oxide. The measurements were evaluated using the Prout—Tompkins and the contracting cube equations. The activation energy values at 200—240 °C for the various compositions were around 30 kcal.

Above 240 °C the catalytic reaction proceeded extremely violently and, after a fairly long induction period of 10—25 minutes, the AP exploded. The induction period increased slightly with increase of the amount of zinc oxide up to a 1:1 molar ratio. The activation energy values were prectically the same as above [19, 20, 5].

The lowest temperature of explosion of AP in the presence of zinc oxide was 233 °C (100:1 and 50:1 molar ratios). This means that the zinc oxide decreased the temperature of explosion of the AP by more than 200 °C.

Detailed studies were also carried out with doped zinc oxide samples. The AP:oxide molar ratio was 16:1. On the incorporation of 1 mole% aluminium oxide the catalysed decomposition began sooner and the reaction itself proceeded more quickly. Doping the zinc oxide with lithium oxide increased the induction period and decreased the reaction rate. However, in these cases the decomposition of AP proceeded to 85—95%. The value of the activation energy in the presence of the doped catalysts did not change. On the other hand, doping of the zinc oxide did alter the induction period of the explosion of AP; it decreased on the incorporation of aluminium oxide and increased on the incorporation of lithium oxide.

Investigation of the mixture during and after the reaction yield valuable data. It was observed that in the presence of zinc oxide the AP partially melted. The solid residue contained water soluble zinc salt.

The melting of the AP was interpreted by the reaction of the zinc oxide and the

AP at the temperature of decomposition:

$$ZnO + 2\ NH_4ClO_4 = Zn(ClO_4)_2 + 2\ NH_3 + H_2O,$$

the zinc perchlorate formed yielding a eutectic of lower melting point with the remaining AP.

The addition of zinc perchlorate to AP supported the above explanation; this led to the partial melting of the AP and to the increase of the decomposition rate observed in the presence of zinc oxide [20, 21].

The large catalytic effect of zinc oxide and the reaction between zinc oxide and AP were confirmed by many later studies [5, 22—24]. BOLDYREVA [25] proved the formation of zinc perchlorate by infrared spectroscopic investigation.

Cadmium oxide

Cadmium oxide also exerted a considerable accelerating influence on the decomposition of AP [26], although its effect was smaller than that of zinc oxide. The beginning of decomposition, especially in the presence of larger amounts of oxide, was preceded by an unusually long induction period. A catalytic effect was primarily shown with smaller concentrations (100:1 and 16:1 molar rations). From kinetic measurements at 200—240 °C an average activation energy of 28 kcal was obtained.

Cadmium oxide reduced the lowest temperature of explosion of AP by about 180 °C. The 10:1 molar ratio mixture exploded at 260 °C. However, here too, the induction period preceding explosion was unusually long, being 17 minutes at 270 °C (16:1 molar ratio). Since cadmium oxide contains a significant amount of excess cadmium, it was conceivable thet the cadmium excess incorporated into the oxide was responsible for the large accelerating effect. The answer to this question was provided by doping experiments.

CIMINO and MAREZIO [27] demonstrated with X-ray studies that on the incorporation of indium the number of interstitial cadmium atoms gradually decreases, and becomes zero at an indium oxide content of about 0.15 mole%. Since the behaviour of cadmium oxide prepared by the method of CIMINO and MAREZIO, and containing the critical amount of indium oxide, was essentially unchanged, the possibility of the cadmium excess being responsible for the catalytic effect of cadmium oxide was ruled out.

In experiments carried out below 240 °C it was observed that if the AP contained less cadmium oxide than a 10:1 molar ratio, then the originally greyish-black mixture began to lighten during the induction period and in the acceleration stage the colour of the cadmium oxide could already hardly be seen. The situation was similar in experiments carried out above 250 °C, too, but here melting of the substance in certain parts of the tablet could also be observed. This indicated that a reaction between the AP and the cadmium oxide took place, analogous to that in the case of zinc oxide. Before the explosion, the cadmium oxide reacted either in part or completely with the AP. Considering the extremely long induction period, it was concluded from these results that AP explodes in the presence of cadmium oxide only when the reaction between the two substances has proceeded to a definite extent. The reaction between AP and cadmium oxide was confirmed by chemical analyses [26] and IR spectroscopic studies [25].

Magnesium oxide

Among the insulating oxides, an effect increasing the reaction rate was observed [28, 29, 4] only in the case of magnesium oxide. The extent and rate of the decomposition of AP depended extremely sensitively on the temperature and the quantity of magnesium oxide. An acceleration effect occurred in the presence of small amounts of MgO. The use of much MgO (AP:MgO molar ratio 2:1) hindered the course of the AP decomposition. HERMONI and SALMON [28] found that at 170—230°C the decomposition is complete, but at 240, 250 and 280°C it proceeded only to 20, 4.81 and 23%, respectively. The rate of decomposition of the 2:1 AP:MgO mixture in the range 200—280°C was the greatest at 230 °C and the least at 240—250 °C. From kinetic measurements at 206—235°C in the presence of a little oxide, an activation energy of 29—31 kcal was obtained for the reaction [28, 29, 4]. Above 300°C even a small amount of magnesium oxide delayed the beginning of decomposition significantly [29]. After a reaction time depending on the temperature and the amount of oxide, the inhibition changed to catalysis. Also here the catalytic effect was more pronounced when a small amount of oxide was used. This is supported, among others, by the fact that while the 100:1 molar mixture exploded at 270°C, the 25:1 mixture exploded only at 336°C (Fig. 4). Evaluation of the temperature dependence of the induction period of the explosion led to an activation energy of 26—30 kcal. From a kinetic analysis of the decomposition leading to explosion using the equation

$$\log p = kt + C$$

an activation energy of 33.5 kcal was obtained.

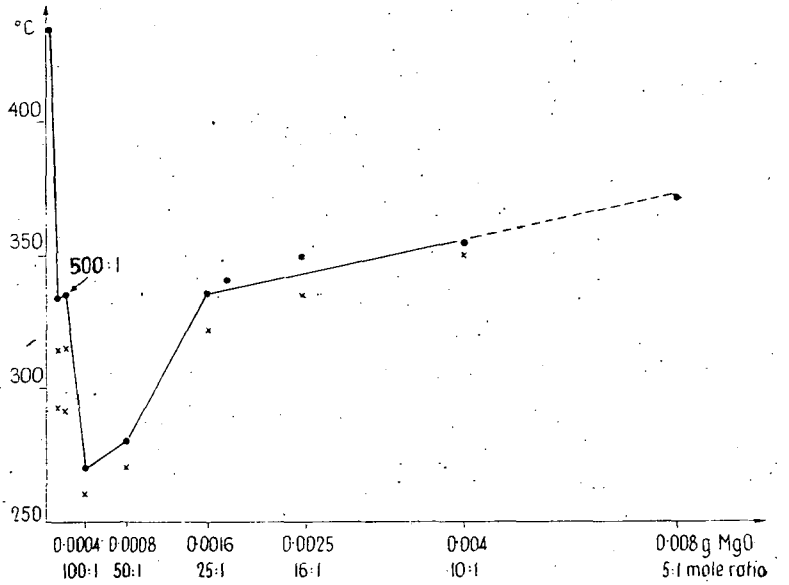

Fig. 4. The minimum ignition temperature of AP as a function of the amount of MgO

From the behaviour of the mixtures it was clear that the AP reacts with the magnesium oxide. As a result of the reaction, magnesium perchlorate is formed and the AP partially melts.

Titanium and tin dioxides

Pure titanium dioxide can be considered to be a practically inactive substance in the decomposition of AP [5, 17]; below 240 °C the decomposition of AP in the presence of titatium dioxide differs from the decomposition of pure AP only at the end of the break-down stage. The situation was similar in experiments carried out at 248.5 °C. The rate constant of the acceleration and break-down stage agreed with the rate constants of pure AP, and their temperature dependences were essentially the same, too. Activation energy values of 30 and 29.5 kcal were found [17]. The effect of titanium dioxide remained slight at 300—440°C, too, and the temperature of the explosion of AP was reduced from 436 °C only to 420—425 °C. The situation was essentially similar if 1% tungsten(VI) oxide (electron concentration increase) or 1% nickel oxide or aluminium oxide (electron concentration decrease) were incorporated into the titanium dioxide. However, an extremely large change occurred when the titanium dioxide was doped with chromic oxide. Even 0.1 mole% chromic oxide in the titanium dioxide led to a noticeable change, while on the incorporation of 1 mole% chromic oxide the explosion temperature of AP decreased by about 150 °C. The effect of the amount of chromic oxide was especially expressed in the case of mixtures containing little titanium dioxide + chromic oxide catalyst (AP:oxide molar ratio 10:1); on the incorporation of only 3.8×10^{-4} g chromic oxide into the titanium dioxide the AP exploded at 290°C. The activation energy of the process leading to the explosion varied from 29 to 32 kcal for the different compositions.

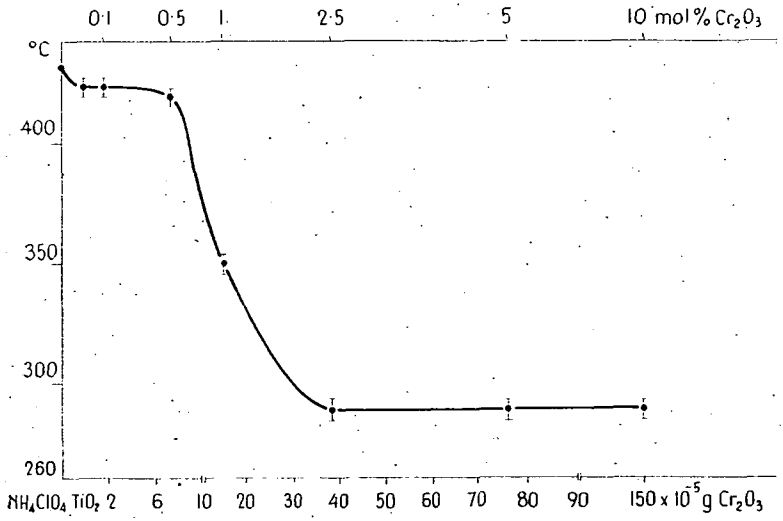

Fig. 5. The minimum ignition temperature of AP as a function of the Cr_2O_3 content of TiO_2

The effect of the amount of chromic oxide incorporated into the titanium dioxide on the lowest temperature of explosion of the AP is shown in Fig. 5.

On appraisal of the large catalytic effect of titanium dioxide doped with chromic oxide, it must be taken into consideration that the chromic oxide added to the titanium dioxide cannot be considered as "free" oxide; as a consequence of the high temperature of pre-treatment of the catalyst, the chromic oxide is incorporated into the surface layer of the titanium dioxide. Study of the mechanism of incorporation of the chromic oxide led to the result [30] that, as a consequence of the oxidation (valence inductivity) accompanying the incorporation of the chromic oxide, the chromium becomes partially tetravalent and partially pentavalent.

A study of the effect of tin dioxide led to similar results [31]. Pure tin dioxide exerted only an extremely slight effect on the decomposition of AP at various temperatures. The lowest temperature of explosion of AP was reduced in all by 40 °C. The effectiveness of the catalyst, however, improved considerably on doping it with 0.1—1 mole% chromic oxide (Fig. 6).

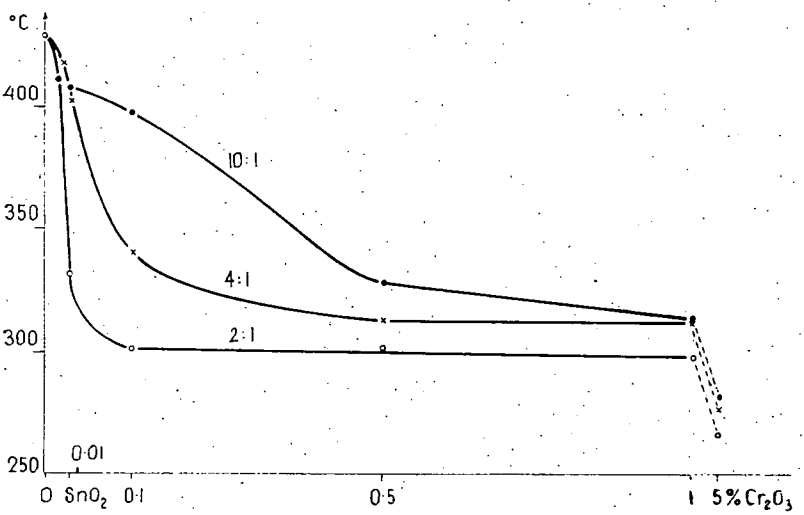

Fig. 6. The minimum ignition temperature of AP:SnO_2 mixtures of different mole ratios as a function of the Cr_2O_3 content of SnO_2

From a detailed physical and chemical investigation of the oxide mixture, it turned out that, here again, on incorporation the chromium ions were oxidized to higher valencies, which were stabilized by the tin dioxide lattice.

Other oxides

With regard to other oxides very few data can be found in the literature. According to BIRCUMSHAW [2] aluminium oxide can be considered as a practically inactive substance and calcium oxide acts as an inhibitor.

According to the most recent measurements, very slight effects on the stability of AP are exerted by tungsten(VI), molybdenum(VI) and vanadium(V) oxides [32]. All three substances belong to the group of *n*-conducting semiconductors.

Table 1

Kinetic data for the decomposition of AP catalysed by oxides

Oxides	Characteristics of AP	Amount of oxides, mole%, (mole ratio)	Temperature range °C	Methods	Kinetic equation	Validity $\alpha =$	Activation energy $\left(\frac{\text{kcal}}{\text{mole}}\right)$	Log A (min^{-1})	Ref.
MnO_2	2× cryst	34—90	137—162	*p*, vacuum	C—2		31.5		[3]
		10	177—212		$p = mkt$		33.2		
	Baker								
	1× cryst	13	170—200	*w*, vacuum	C—3	0.2—0.9	28.0	8.60	[4]
		13	200—240	*p*, vacuum	C—3	0.2—0.9	34.0		
		13	249—272	*p*, vacuum	C—3	0.2—0.9	48.0		
		5(s)	214—245	*w*, in air	A—E		33.7	12.7	[7]
	3× cryst	1	317—340	*p*,	C—2		31.0	7.76	[5]
Fe_2O_3	Merck	20	249—268	*v*, in air	P—T	0.01—0.27	35.6		[6]
		20			P—T	0.37—0.89	30.9		
		20			first order	0.09—0.83	28.2		
		50			P—T	0.01—0.22	28.5		
		50			P—T	0.41—0.92	29.0		
		50			first order	0.16—0.83			
		50:1	320—377		C—3	0.32—0.81	30.9		
		20:1				0.32—0.88	25.7		
		8:1				0.33—0.85	22.0		
		5(s)	250—296	*w*, in air	A—E		41.0	14.42	[7]
	88—124μm	4.9			adiabatic		34.3		[8]
	43—61μm	4.8					36.6		
Cu_2O	BDH	4.56	240—270	*p*, 250 torr N_2	$p = Ce^{kt}$		29.0		[11]
	3× cryst	1.0	260—280	*p*,	$\log = kt$		36.0	12.54	[5]
		5(s)	250—270	*w*, in air	A—E		45.5	17.15	[7]
CuO	Merck								
	2× cryst.	5:1	180—200	*p*, air	P—T	0.0—0.36	32.7		[13]
		5:1	180—200		A—E	0.0—0.58	32.9		
		1:1	180—200		P—T	0.0—0.36	30.0		
		1:1	180—200		A—E	0.0—0.58	28.9		
CuO		5:1	180—200		P—T		32.1		
$+1\%\ Cr_2O_3$		5:1	180—200		A—E		30.0		
CuO		5:1	180—200		P—T		29.2		
$+1\%\ Cr_2O_3$		5:1	180—200		A—E		31.7		
CuO		5:1	201—227		P—T		42.9		
		5:1	201—227		A—E		40.9		
		1:1	203—228		P—T		40.2		
		1:1	203—228		A—E		42.2		

Oxides	Characteristics of AP	Amount of oxides, mole %, (mole ratio)	Temperature range °C	Methods	Kinetic equaiton	Validity $\alpha =$	Activation energy $\left(\frac{kcal}{mole}\right)$	Log A (min^{-1})	Ref.
CuO +1% Li_2O		5:1	201—227		P—T		41.2		
CuO +1% Cr_2O_3		5:1	201—227		P—T		37.1		
Ni_2O_3	Baker	13	170—200	*w*, vacuum	C—3		33.0	12.48	[4]
	1× cryst	13	210—235	*p*, vacuum	C—3		43.0		
		13	245—265	*p*, vacuum	C—3		40.2		
		5(w)	270—296	*w*, in air	A—E		49.2	17.8	[7]
Co_2O_3 + Co_3O_4	Baker	13	170—200	*w*, vacuum	C—3		33.0	13.95	[4]
	1× crys)	13	210—230	*p*, vacuum	C—3		42.0		
		5(w)	215—245	*w*, in air	A—E		38.3	14.87	[7]
Cr_2O_3	Baker								
	1× cryst.	13	210—230	*p*, vacuum	C—3		26.7	9.00	[4]
		13	250—275	*p*, vacuum	C—3		37.7		
		5(*w*)	260—309	*w*, in air	A—E		30.1	9.90	[7]
	BDH	0.85	306—348		C—3		31.3	8.80	[14]
		4.8			adiabatic		68.0	27.3	[8]
CuO + Cr_2O_3	BDH	0.5—5	207—277	*w*, in air	A—E		31.6	11.82	[14]
		0.5—5	283—315		C—2		47.7	15.67	
		2.9			adiabatic		40.0	13.8	[8]
		4.8					43.0	16.5	
		4.8	250—308				46.0	17.7	
		0.5—5	300—350		C—2		48.0		[9]
Active carbon	2× cryst	3—17	195—240	*p*, vacuum	P—T		32.1		[18]
		2.5			adiabatic		52.5	19.9	[8]
ZnO	Merck	16:1	215—231	*v*, in air	P—T	0.0 —0.15	29.7		[19, 20]
		16:1			P—T	0.15—0.85	33.7		
		16:1			C—3	0.1 —0.8	33.3		
		50:1			P—T	0.0 —0.15	31.3		
		50:1			P—T	0.15—0.85	22.5		
		50:1			C—3	0.1 —0.8	29.5		
		100:1			P—T	0.0 —0.15	24.0		
		100:1			P—T	0.0	26.0		
		100:1			C—3	0.1 —0.8	27.9		

Oxides	Characteristics of AP	Amount of oxides mole %, (mole ratio)	Temperature range °C	Methods	Kinetic equation	Validity $\alpha =$	Activation energy $\left(\frac{\text{kcal}}{\text{mole}}\right)$	Log A (min^{-1})	Ref.
CdO	Fluka 2× cryst	16:1	206—233	p, vacuum	P—T	0.0 —0.18	26.7		[26]
MgO		13.5 (w)	215—230	p, vacuum	C—3		31.4	11.2	[28]
			215—230		P—T		29.2	10.8	
	Fluka 2× cryst	16:1	206—231	p, vacuum	P—T	0.01—0.43	30.3		[29]
					A—E	0.01—0.46	28.5		

A—E = Avrami—Erofeyev equation
P—T = Prout—Tompkins equation
C—3 = "Contracting cube" formula, $n = 3$
C—2 = "Contracting cube" formula, $n = 2$
p = pressure measurements
w = weight-loss measurements
v = volume measurements
s = weight%

Effects of various salts on the stability of AP

The decomposition of AP is catalysed not only by metal oxides but also by many metal salts. The first intensive kinetic study dealt with the effects of silver, copper and iron perchlorates [33]. Silver perchlorate proved the most effective additive; even 0.001 mole% increased the rate of decomposition of AP below 240 °C, and the effect increased with increase of the amount. The catalysed decomposition remained of an autocatalytic nature and stopped after about 40—45% transformation. The value of the activation energy was 28 kcal.

Copper(II) and iron(III) ions exerted somewhat less effects. The rate and the activation energy of the catalytic reaction depended on the preparation of the AP—perchlorate salt mixture. The reaction proceeded at a higher rate and with a lower activation energy if copper perchlorate was evaporated with the AP solution than if the solid substances were mixed together. A part in bringing about a greater lability may be played (in addition to the more homogeneous distribution of the additive) by the incorporation of the copper ion and the change in the defect structure of the AP.

In the presence of 1 mole% of the above perchlorates the explosion of AP occurred at the following temperatures:

copper perchlorate 269 °C
silver perchlorate 274 °C
iron perchlorate 276 °C.

From the temperature dependence of the times up to the explosion, a few kcal smaller activation energy values were found than for the slow catalysed decomposition. These data show convincingly that the effects of the above additives in bring-

ing about the explosion of AP approach and even exceed the effects of the most active oxides.

From later studies it turned out that zinc, cadmium and magnesium perchlorates also effectively accelerate the decomposition of AP [34, 21, 26]. From the point of view of the mechanism of decomposition of AP, this result is a very important observation, since it shows that not only ions capable of electron transfer are able to catalyse the decomposition of AP.

In the presence of any of the three substances, a large rate increase was observed even at 200—240 °C; the induction period decreased significantly and the decomposition proceeded to 100%. In the presence of the cadmium or magnesium salt the decomposition was autocatalytic, but the zinc salt brought about a change to breakdown nature.

An interesting observation was that in the AP:perchlorate salt composition range 100:1—1:1 the decomposition started in every case in the mixture containing the less additive. The acceleration stage of the decomposition, however, was shorter than in the presence of larger amounts of cadmium and magnesium perchlorates. In the 5:1, and particularly in the 1:1 mixture, the rate of decomposition was considerably lower than *e.g.* in the 100:1 molar mixture. The activation energies of the decompositions catalysed by cadmium and magnesium ions were about 28—32 kcal. A larger value, 37 kcal, was obtained in the presence of zinc perchlorate. Recent kinetic measurements on the effect of magnesium perchlorate, at 280—320 °C, resulted in higher values, 44—47 kcal/mole, for the activation energy [35]. This is presumably due to the higher temperature range.

In the optimum (100:1) molar mixture the explosion of AP occurred at the following temperatures:

zinc perchlorate	240 °C
cadmium perchlorate	260 °C
magnesium perchlorate	270 °C.

Fig. 7 characterizes the great effect of zinc perchlorate.

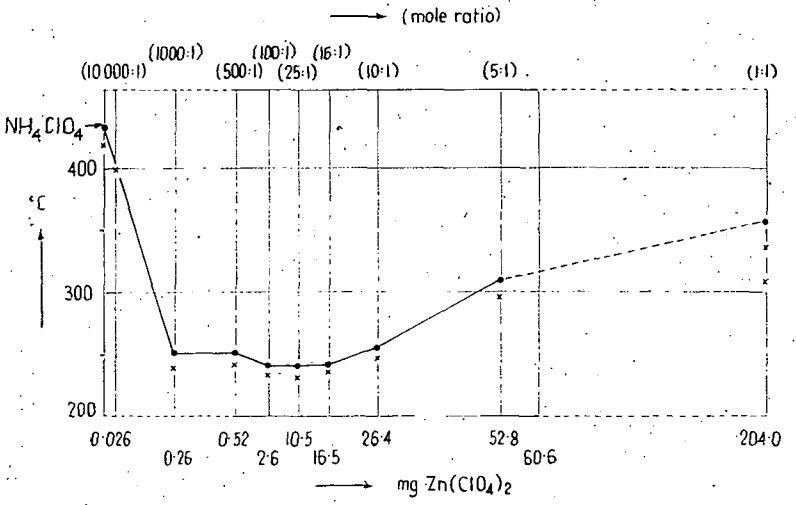

Fig. 7. The minimum ignition temperature of AP as a function of the amount of $Zn(ClO_4)_2$

On addition of even 0.1 mole% zinc perchlorate to AP, it explodes at a 190°C lower temperature than in the pure state. Increase of the amount of the perchlorate salt in all three cases proved unfavourable. At 240—290°C the activation energy of the reaction preceding the explosion was 27—32 kcal.

As regards the evaluation of the effects of the additives, it was important that in the presence of the above perchlorates the solid mixture partially melted already below 240 °C. Taking into account the melting points of the compounds concerned, this can only be explained by the formation of a melting eutectic. The effect of a salt increased in the order Mg, Cd, Zn; this corresponds to the increase in polarizing power of the metal ions.

It should be noted that the chloride salts of the metal ions in question exerted very similar effects on the stability of AP as the perchlorates. The partial melting of the AP could be observed here, too. However, the acceleration of AP decomposition did not occur with the use of zinc, cadmium and magnesium sulphates, and in their presence the AP did not melt.

The knowledge of the phase diagram of the AP+lithium perchlorate system gave the possibility of studying the thermal behaviour of AP in the molten phase. The eutectic mixture contained 35.5 mole% AP and its melting point was 182 °C [36].

Below 240 °C the rate and extent of the decomposition decreased with increasing amount of lithium perchlorate. The highest extent of decomposition (90—95%) occurred in the mixture containing 10 mole% lithium perchlorate. The eutectic mixture and mixtures containing lithium perchlorate in excess showed no noticeable decomposition up to 270 °C, even in 24 hours.

The high stability of the eutectic composition indicated that, although the lithium perchlorate brings about the melting of the AP, the formation of the eutectic also increases its stability to a large extent. It was interesting to observe that in a mixture containing excess AP as compared with the eutectic composition the amount of AP decomposed exceeded the excess amount of AP. This means that the decomposition of AP in the eutectic also began as a result of the decomposition of solid AP in the melt.

The activation energies of the decomposition of mixtures of various compositions (AP excess) agreed with the activation energy values determined for the decomposition of pure AP in the same temperature range.

The explosion of mixtures containing an AP excess was preceeded by decomposition, the extent of which decreased with increase of the amount of lithium perchlorate. The lowest temperature of explosion was 320—340 °C. The explosion of mixtures containing excess lithium perchlorate occurred at 290 °C after an unusually long induction period of 2—3 hours. The explosion was extremely violent, and was not preceded by evolution of gas. The effective catalysts of the decomposition of AP (Cu^{2+}, ClO_3^-, CuO, etc.) also decreased the stability of the eutectic considerably.

SHIDLOVSKII *et al.* [7] studied gravimetrically the effects of various salts (carbonate, chloride, oxalate) of manganese, cobalt, copper, iron, nickel and chromium on the stability of AP at atmospheric pressure. The manganese and cobalt compounds proved the most effective additives. The effects of the iron, nickel and chromium compounds appeared above 240 °C. In the case of the cobalt salts, the effect decreased in the order carbonate, oxalate, oxide, chloride. The activation energies of the catalytic reaction varied in the range 30—53 kcal. The effectiveness of a compound

was ascribed to the formation of its oxide: the more easily the oxide formed, the more effective was the compound.

Kinetic studies are also known with regard to the effects of iodide and bromide ions [33]. At 200—240 °C primarily the rate and extent of the acceleration reactions of AP are increased. The explosion of AP takes place at 260 and at 298 °C.

The lowest temperature and induction period of the explosion change sensitively with the concentration of the additive. With increase of the temperature the optimum amount of substance shifts towards lower concentrations.

Table II contains data for the decomposition of AP—salt additives. The effects of catalysts on the explosion of AP are collected in Table III.

Differential thermal analysis studies

In comparing the effects of additives, the fastest method involves thermal analysis procedures. The DTA measurements of LAND [38] refer to the effects of oxides. The order of effectiveness of oxides was the following:

Co Cu Ni Zn Mn Cd Pb Fe Ag Mg K Ba Na.

The temperature difference T_x between the crystallographic transition and the decomposition of the AP served as the basis for comparison. Since this value can be affected by numerous factors (particle size, catalyst surface, etc.), this order can only be regarded as of a qualitative nature. The development of a realistic picture is made difficult by the fact that LAND added the oxides to the AP in weight%.

RHEES and HAMMAR [39] studied the effect of modifying the AP surface, using a DTA method. Large effects were exerted by copper and magnesium oxides in particular, even in low concentration. The exothermic peaks in the decomposition of AP changed depending on the added substance.

LAND [40] studied the stability of AP in the presence of metal perchlorates and obtained the following series:

Cu Mn Zn Cd Pb Fe Mg Ag Ba K Na.

The amount of each perchlorate salt was 5 mole%. The preparation of the mixtures, however, gave a possibility for the incorporation of the metal ion into the crystal lattice of the AP and for the change of its defect structure, which likewise affect the stability of AP.

The effects of the perchlorates of transition metals (cobalt, nickel and iron) on the decomposition of AP were studied by BOLDYREV *et al.* [41] at 260—275 °C using a thermogravimetric method. The catalytic effectiveness decreased in the series cobalt, nickel, iron. The effects of the perchlorate salts were attributed to the actions of the oxides, for it was observed that before and during the decomposition of the AP the perchlorates decompose to Co_2O_3 and Ni_2O_3. The effectiveness of the above oxides practically agreed with that of the corresponding perchlorate and the above series was found again. Similarly to the earlier investigations [26, 34], the sulphates did not exhibit an acceleration effect; this was explained by their higher stabilities. The evaluation of the results is made difficult also by the fact that during the preparation of the mixture the additives might co-crystallise with the AP; and

as a result it is not possible to know what role the change of the defect structure of the AP (in this case the increase of the number of cation-free sites) plays in the awaited effect.

Using differential thermal analysis, OSADO and SAKAMOTO [42] studied the effects of various chlorides. Iron(III) and copper(II) chlorides showed the greatest

Table II

Kinetic data for the decomposition of AP catalysed by metal salts

Salts	Characteristics of AP	Amount of oxides mole %, (mole ratio)	Temperature range °C	Methods	Kinetic equation	Validity $\alpha =$	Activation energy (kcal/mole)	Log A (min^{-1})	Ref.
$AgClO_4$	p.a. 2× cryst.	0.1	209—235	v, in air	P—T	0.04—0.5	27.7		[33]
$Cu(ClO_4)_2$	p.a. 2× cryst.	1.0 5.0(*s*)	203—232 204—226	v, in air v, in air	A—E A—E	0.04—0.5	25.0 29.0		
$Fe(ClO_4)_3$	p.a. 2× cryst.	1.0 5.0	206—224 204—230	v. in air v, in air	A—E A—E		34.0 28.9		
$Zn(ClO_4)_2$	Fluka 2× cryst.	10:1	206—232 206—232	p, vacuum	first order	— 0.01—0.65	24.5 37.8		[21, 34]
$Cd(ClO_4)_2$	Fluka 2× cryst.	10:1	210—231	p, vacuum	A—T $\log p = kt$	— 0.0—0.22 0.0—0.2	28.7 29.3 33.0		[26, 34]
$Mg(ClO_4)_2$	Fluka 2× cryst.	10:1	201—231	p, vacuum	τ_0 P—T	 0.01—0.6 0.6—0.95 0.4—0.85 0.01—0.28	31.9 30.2 25.0 26.6 32.4		[34]
	Fisher	1.75	291—343	w, 740 torr N_2	C—2	0.1 —0.8	43.4		[35]
		6.6	286—318	w, 740 torr N_2	first order	0.27—0.89	45.2		
$LiClO_4$		10 30 50	210—240 210—240 210—240	v, in air v, in air v, in air	first order	0.1 —0.7 0.1 —0.7 0.1 —0.7	29.3 32.0 28.2		
NH_4I	p.a. 2× cryst.	0.1	206—235	v, in air	A—E	0.05—0.6	35.5		[34]
NH_4Br	p.a. 2× cryst.	0.1	206—235	v, in air	A—E	0.05—0.6	27.5		
$K_2Cr_2O_7$		1.67	312—339	w	C—2		47.7		[14]
$KMnO_4$		2.00	215—290			0.3	20.0		[46]
$CaCrO_4$			245—265				16.0		[46]

effects but calcium, magnesium and, to a smaller extent, sodium and potassium chlorides also shifted the second large exothermic peak, characteristic of the decomposition of AP, towards lower temperatures. The authors assumed that chemical reaction between the AP and the chlorides takes place with the formation of perchlorate salts which are effective with regard to the decomposition of AP. It should

Table III

Ignition of AP in the presence of additives

Additive	Characteristics of AP	Amount of additive mole %, (mole ratio)	AP mg	Minimum ignition temperature °C	Temperature range °C	Activation energy kcal/mole	Ref.
MnO_2	3× cryst	1.0	100	336		33.5	[5]
	1× cryst	5.0	150	265			[7]
	Baker 1× cryst	16(s)	100	310	310—335	34.3	[4]
Fe_2O_3		1:1	100	300			[10]
Cu_2O	BDH						
		6.7	30	248		28.1	[11]
		50.0	30	253		31	
	3× cryst	1.0	100	269		38.1	[5]
CuO	Merck	16:1	50	259	270—286	29.9	[13]
	2× cryst	16:1	100	270	265—286	31.2	
+1% Li_2O		16:1	100	260	260—286	30.0	
+1% Cr_2O_3		16:1	100	266.5	266.5—287	31.0	
		16:1	200	251	251—276	29.8	
	3× cryst	1.0	100	258		31.0	[5]
Ni_2O_3	Merck	1:1	100	253.2	255—275	29.1	[15]
Co_2O_3—Co_3O_4	Baker 1× cryst	30(s)	100	241	240—260	45.8	[4]
Cr_2O_3	BDH	1:1	100	251			[17]
	1× cryst	10:1	100	257	257—292	27.9	
+1% NiO		10:1	100	259	259—299	26.3	
+1% ZnO		10:1	100	270	270—312	20.6	
+0.5% TiO_2		10:1	100	294	294—329	23.6	
+2.5% TiO_2		10:1	100	314	314—341	29.4	
$CuO.Cr_2O_3$	BDH	0.5	40	300	300—410	12.2	[14]
		2.5	40	287	290—395	13.8	
		5.0	40	290	290—460	14.0	
ZnO	Merck	200:1	200			27.9	[20]
		100:1	200			29.5	
		50:1	100			31.6	
		25:1	200			27.0	
		16:1	100			28.3	
		10:1	200			27.6	
		5:1	200			29.6	
		16:1	200	224	224—242	34.0	
	3× cryst	1.0	100	247		29.5	[5]

Additive	Characteristics of AP	Amount of additive mole %, (mole ratio)	AP mg	Minimum ignition temperature °C	Temperature range °C	Activation energy kcal/mole	Ref.
CdO	Fluka	100:1	100	300	300—328	22.2	[26, 29]
	2× cryst	16:1	100	265	265—295	22.5	
		10:1	100	260			
		16:1	100	256	256—291	24.2	
MgO	Fluka	100:1	100	270.5	270.5—324	26.8	[29]
	2× cryst	50:1	100	280.0	280—324	31.8	
	3× cryst	1.0	100	330		43.5	[5]
TiO_2	BDH	2:1	100	420			[17]
$+0.1\ Cr_2O_3$	1× cryst	2:1	100	416			
$+0.5\ Cr_2O_3$		2:1	100	370			
$+1.0\ Cr_2O_3$		2:1	100	290	290—320	29.0	
$+2.5\ Cr_2O_3$		2:1	100	285	285—315	30.0	
SnO_2	BDH	2:1	100	410			[31]
	2× cryst						
$+0.01\ Cr_2O_3$		2:1	100	330	330—360	17.0	
$+0.1\ Cr_2O_3$		2:1	100	300	300—325	16.5	
$+1.0\ Cr_2O_3$		2:1	100	300	300—325	18.0	
Active carbon	2× cryst	20	16	260	260—290	40.0	[18]
$AgClO_4$	2× cryst	0.5	100	277.6	278—306	15.9	[33]
		1.0	100	277	277—306	19.2	
$Cu(ClO_4)_2$	2× cryst	1.0	100	269	269—283	22.6	[33]
$Fe(ClO_4)_3$	2× cryst	1.0	100	276	276—295	29.6	[33]
$Zn(ClO_4)_2$	Fluka	100:1	100	240	240—265	29.8	[21, 34]
	2× cryst	10:1	100	240	240—265	22.7	
$Cd(ClO_4)_2$	Fluka	100:1	100	257	257—280	31.0	[26, 34]
	2× cryst	10:1	100	260	260—285	26.0	
$Mg(ClO_4)_2$	Fluka	100:1	100	273	273—300	27.0	[34]
	2× cryst	10:1	100	270	270—300	32.0	
$LiClO_4$		69	50	290			[37]
NH_4I	2× cryst	1.0	100	248	248—281	22.5	[34]
NH_4Br	2× cryst	0.01	100	302	302—338	21.8	
		0.1	100	297	297—338	22.6	
		0.5	100	297	297—338	24.2	

be mentioned that calcium, sodium and potassium perchlorates do not exert any accelerating effect at all.

The effects of silver and copper perchlorates and of ammonium iodide on the DTA behaviour of AP were studied by FREEMAN *et al.* [43]. They showed that the above ions decrease the stability of AP. It was interesting that in their presence the

effects of γ and X-radiations also increased; *e.g.* 1 mole% silver perchlorate caused a 100-fold increase.

The thermal stability of AP is decreased significantly by the chlorate ion [44]. According to DTA studies, the effect of chlorate appears only after a crystal transformations; nevertheless the effect of even 0.001 mole% $KClO_3$ can be detected. In the presence of 0.1% $KClO_3$ the exothermic peak for the complete decomposition of AP occurred at a 150 °C temperature lower. From measurements under isothermal conditions, it turned out that chlorate ions also accelerate the decomposition of AP below 240 °C [45]. The explosion of the AP took place at 260—280 °C. Bromate and iodate ions also act similarly [45].

Interesting results were obtained by SCHMIDT [46] from the investigation of the effects of various organometallic compounds. Ferrocene and copper acetylacetonate give especially reactive compounds on interaction with the ammonium ion, and as a result of this the exothermic peak of AP at 475 °C occurs instead at 260—360 °C.

Using the DTA method under isothermal conditions at 250 °C, BOLDYREV *et al.* [47] studied the effects of various copper salts (sulphate, dichromate, benzoate, oxalate, lactate and nitrate) on the thermal decomposition of AP. They showed that the effectiveness of the additives depended on the course of their thermal decomposition. Salts which are stable at the temperature of the decomposition of AP did not exert a catalytic effect (sulphate and dichromate). An acceleration effect was found, however, in the presence of benzoate, the decomposition of which occurred parallel with that of the AP. Even greater effects were observed in the case of other salts. In the evaluation of the results it was assumed that the decomposition of AP is affected not only by the oxides formed in the decomposition of the salts but also by the gases which also evolved.

References

[1] *Solymosi, F.:* Kémiai Közlemények, in press.
[2] *Bircumshaw, L. L., B. H. Newman.:* Proc. Roy. Soc. **A227**, 115 (1954).
[3] *Galwey, A. K., P. W. M. Jacobs:* Trans. Faraday Soc. **55**, 1165 (1959).
[4] *Hermoni, A., A. Salmon:* Eighth Symposium (International) on Combustion, Williams and Wilkins Co., Baltimore, p. 656, 1962.
[5] *Kuratani, K.:* Rept. Aeronaut. Res. Inst. No. 372. 79 (1962).
[6] *Шоймоши, Ф., Л. Ревес:* Кин. и Кат. **4**, 88 (1963).
[7] *Шидловский, А. А., Л. Ф. Шмагин, В. В. Буланова:* Изв. Выс. Учеб. Зав., Хим. и Хим. Технол. **8**, 533 (1965).
[8] *Inami, S. H., W. A. Rosser, H. Wise:* Combust. Flame **12**, 41 (1968).
[9] *Waesche, R. H. W., J. Venograd:* The Combustion Institute Western States Section Meeting Nr. 8. (1967).
[10] *Solymosi, F.:* Unpublished results.
[11] *Jacobs, P. W. M., A. R. T. Kureishy:* „Eighth Symposium (International) on Combustion" The Williams and Wilkins Co., Baltimore, Md., 1962, pp. 672—677.
[12] *Jacobs, P. W. M., A. R. T. Kureishy:* J. Chem. Soc. 556 (1962).
[13] *Solymosi, F., E. Krix:* J. Catalysis **1**, 468 (1962).
[14] *Jacobs, P. W. M., A. Russel—Jones:* „Eleventh Symposium (International) on Combustion", The Combustion Institute, Pittsburgh, Pa., 1967, pp. 457—462.
[15] *Krix, E.:* Thesis, Szeged, 1961.
[16] *Болдырева, А. В., Б. Н. Безруков, В. В. Болдырев:* Кин. и Кат. **8**, 29 (1967).
[17] *Solymosi, F.:* Combustion and Flame **9**, 141 (1965).
[18] *Galwey, A. K., P. W. M. Jacobs:* Trans. Faraday Soc. **56**, 581 (1960).

[19] *Solymosi, F., L. Révész:* Nature **192**, 64 (1961).
[20] *Solymosi, F., L. Révész:* Z. anorg. Chem. **322**, 86 (1963).
[21] *Solymosi, F., J. Raskó:* Z. phys. Chem. N. F. **67**, 76 (1969).
[22] *Stammler, M., W. G. Schmidt:* 21st Interagency Solid Propulsion Meeting, 1965. Vol. I. p. 71.
[23] *Шмагин, Л. Ф., А. А. Шидловский:* Иссл. в Обл. Хим. и Технол. Минер. Солей и Окислов, АН СССР, Сб. Статей 112—114 (1965).
[24] *Pellett, G. L., A. R. Saunders:* AIAA Sixth Aerospace Sciences Meeting, New York, N. Y., AIAA Preprint 68—149, (1968).
[25] *Болдырева, А. В., В. Н. Мозхова:* Кин. и Кат. **7**, 734 (1966).
[26] *Solymosi, F., K. Fónagy:* „Eleventh Symposium (International) on Combustion", The Combustion Institute, Pittsburgh, Pa., 1967, pp. 429—437.
[27] *Cimino, A., M. Merezio:* J. Phys. Chem. Solids. **17**, 57 (1960).
[28] *Hermoni, A., A. Salmon:* Bull. Res. Counc. of Israel **9**, 206 (1960).
[29] *Solymosi, F.:* Magy. Kém. Foly. **73**, 358 (1967).
[30] *Szabó, Z. G., F. Solymosi:* Acta Chim. Hung. **25**, 145 (1960).
[31] *Solymosi, F., T. Bánsági:* Proceedings of the 2nd International Conference on Space Engineering, D. Reidel Publ., Dordrecht 1970, p. 145.
[32] *Bór, P.:* Thesis, Szeged, 1970.
[33] *Solymosi, F., K. Dobó:* "Fifth Internationa Symposium on the Reactivity of Solids", Elsevier Publishing Co., Amsterdam, 1965.
[34] *Solymosi, F.:* Magy. Kém. Foly. **73**, 366 (1967).
[35] *Acheson, R. J., P. W. M. Jacobs:* J. Phys. Chem. **74**, 281 (1970).
[36] *Markovitz, M. M., R. F. Harris:* J. Phys. Chem. **63**, 1519 (1959).
[37] *Solymosi, F., M. Ránics:* Combust. Flame **10**, 398 (1960).
[38] *Pittman, Ch. U.:* Report No. RK—TR—66—13. Propulsion Laboratory, Redstone Arsenal, Alabama. Ref. 27.
[39] *Rhees, R. C., H. N. Hammer:* „Effect of Surface Modification on the Properties of Ammonium Perchlorate", American Potash and Chemical Corp., Whittier, Calif., July 1966.
[40] See: [38] Ref. 66.
[41] *Гарева, Е. Х., В. В. Болдырев:* Кин. и Кат. **9**, 425 (1968).
[42] *Osada, H., E. Sakamoto:* Kogyo Kayaku Kyokaishi **24**, 236 (1963).
[43] *Freeman, E. S., D. S. Anderson, J. J. Campisi:* J. Phys. Chem. **64**, 1727 (1960).
[44] *Petricciani, J. C., S. E. Wiberley, W. H. Bauer, T. W. Clapper:* J. Phys. Chem. **64**, 1309 (1960).
[45] *Solymosi, F.:* to be published.
[46] *Schmidt, W. G.:* Report, NASA CR-66457 (1967) Aerojet-General Corp. Sacramento.
[47] *Плюсин, И. Б., А. В. Болдырева, В. В. Болдырев:* Кин. и Кат. **10**, 761 (1969).

КИНЕТИКА КАТАЛИТИЧЕСКОГО РАЗЛОЖЕНИЯ ПЕРХЛОРАТА АММОНИЯ

Ф. Шоймоши

В работе автор подытоживает важнейшие результаты, достигнутые в области кинетического изучения распада перхлората аммония, катализированного разными окислами металлов и солями. Автор рассматривает влияние добавок на взрыв перхлората аммония и устанавливает те свойства солей металлов, которые играют основную роль в катализе распада перхлората аммония.

OXYTOCIN-SYNTHESE AN FESTER PHASE

Von

P. PALLAI, K. KOVÁCS UND B. PENKE

Insitut für Organische Chemie der Attila-József-Universität, Szeged

(Eingegangen am 1. Juni, 1973)

Zur Untersuchung der Peptidsynthese an fester Phase wurde Oxytocin mit drei verschiedenen Methoden synthetisiert. Es wurde festgestellt, daß reines Oxytocin sich mit ausschließlicher Anwendung von NPS-Aminosäuren nicht herstellen läßt. Infolge von Transpeptidations-Nebenprodukten ist auch der nachträgliche Ausbau der Amidgruppen des Asparagins und Glutamins durch Ammonolyse der entsprechenden Ester nicht durchführbar. Zur Kontrolle der Kopplungsreaktion wurde eine neue Hydrolysemethode ausgearbeitet, die die quantitative Bestimmung aller Aminosäuren durch Ionenaustausch-Chromatographie ermöglicht.

Die von MERRIFIELD [1] in 1962 eingeführte Peptidsynthese an fester Phase ist bis heute ein viel diskutiertes Problem der Peptidchemie. Zahlreiche biologisch aktive Peptide wurden mit dieser Methode hergestellt. YAMASHIRO u.a. [2] berichteten in der letzten Zeit über die erfolgreiche Synthese des Human-ACTH. Das Hauptproblem der Peptidsynthese an fester Phase ist die Bildung von Fehlsequenzen mit falscher Aminosäurenfolge. Mehrere Forschergruppen beschäftigten sich mit der Beseitigung dieses „Geburtsfehlers", doch konnte das Problem bis heute nicht volkommen gelöst werden. Auch in unserem Institute befaßten wir uns seit Jahren mit der Lösung dieses Problems und der Weiterentwicklung der Methode der Peptidsynthese an fester Phase. Als Modellverbindung wurde das Oxytocin gewählt, da es in mancher Hinsicht (wegen der leichten Herstellbarkeit, der enthaltenen trifunktionellen Aminosäuren und der bequemen Meßbarkeit der biologischen Wirkung) für das Studium der Kontrolle der Peptidsynthese-Methoden am besten geeignet erscheint.

Mehrere Synthesen des Oxytocins an fester Phase sind bekannt [3—8]. Die verschiedenen Darstellungsmethoden unterscheiden sich vor allem in der Wahl der angewandten Schutzgruppen, der Reinigungsverfahren und dem Typ der festen Träger. IVES [3] benutzte die leicht herstellbaren NPS-Aminosäuren zur Synthese des Oxytocins, die Seitenketten des Cysteins und Tyrosins mit Benzylgruppen schützend. Mit dieser Schutzgruppenkombination gelang es ihm, Oxytocin von verhältnismäßig guter Aktivität zu synthetisieren, das, entsprechend gereinigt, ein Produkt von voller biologischer Aktivität ergab, obwohl die Ausbeute ziemlich klein war. Infolge der Billigkeit der Nitrophenylsulfenyl-Aminosäuren erschien ihre Anwendung wirtschaftlich gerechtfertigt, deshalb versuchten wir auch das Oxytocin nach der IVESschen Methode herzustellen. Nach unseren Erfahrungen kann das C-terminale Tetrapeptid des Oxytocins mit Verwendung der NPS-Aminosäuren an fester Phase wirklich gut erhalten werden. Da aber die aktivierten Ester des

NSP-Asparagins und NPS-Glutamins rein, kristallin nicht herstellbar sind, ist diese Schutzgruppenkombination zur Synthese des reinen Oxytocins nicht geeignet. Die gesteigerte Säurelabilität der NPS-Schutzgruppe würde zwar sowohl in diesem als auch in anderen Fällen eine schonende Peptidsynthese ermöglichen, doch ist die Anwendung von NPS-Aminosäuren in der Form von DCHA-Salzen mit Nachteilen verbunden, indem während der Befreiung der Salze viel Aminosäure verloren geht. Dabei können bei der Abspaltung der NPS-Schutzgruppe Nebenreaktionen auftreten [9]. Infolge der erwähnten Nachteile erscheint die NPS-Gruppe nach unseren Erfahrungen nur für die Merrifield-Synthese kürzerer Peptidketten geeignet.

Der empfindlichste Punkt der Oxytocin-Synthese an fester Phase ist der Einbau des Asparagins und Glutamins ins Molekül, da in diesen Fällen die Dicyclohexylcarbodiimid-Kondensation infolge der Nitrilbildung [10, 11] nicht anwendbar ist. Durch die Anwendung aktivierter Ester läßt sich diese Nebenreaktion umgehen. Eine weitere, aus der Literatur [12, 13] bekannte Möglichkeit, nämlich der nachträgliche Ausbau der erwähnten Amidgruppen aus entsprechenden ω-Estern wurde von INUKAI u.A. [8] zur Synthese von Oxytocin verwendet. Der Vorteil dieser Methode besteht darin, daß sie die weit wirksamere DCC-Kopplung ermöglicht. Deshalb versuchten wir diese Methode bei der Oxytocin-Synthese zu verwenden, obwohl wir dabei auch mit der Bildung von Isoasparagin und Isoglutamin enthaltenden Sequenzteilen zu rechnen hatten [14, 15]. Das durch Abspaltung des geschützten Oxytocin-Nonapeptids vom Träger erhaltene Produkt erwies sich tatsächlich nicht einheitlich; der größte Teil bestand aus Isoasparaginyl- und Isoglutaminyl-Peptiden. Wir zogen zwar ihre Bildung in Betracht, doch rechneten wir auf Grund der Angaben von INUKAI u.A. [8] damit, daß im Falle des Oxytocins die Transpeptidation infolge der ungünstigen sterischen Wirkung [16] nicht bevorzugt sein wird. Das Oxytocin läßt sich von den chemisch sehr ähnlichen, aber biologisch inaktiven Verunreinigungen mit den in der Peptidchemie üblichen Methoden nicht befreien; deren Gegenwart ist aber durch Dünnschichtchromatographie, Elektrophorese und die niedrige biologische Aktivität des Produktes nachweisbar. Da die Menge der inaktiven Nonapeptide im gereinigten Endprodukt 60% erreicht, ist der erwähnte nachträgliche Ausbau des Asparagins und Glutamins zu empfehlen.

Die Erfahrungen der obigen Versuche benutzend synthetisierten wir das geschützte Oxytocin-Nonapeptid mit der Anwendung von BOC-Aminosäuren und DCC-Kondensation. Das BOC-Glutamin und BOC-Asparagin wurde mit *p*-Nitrophenylester gekoppelt, die Seitenketten des Cysteins und Tyrosins wurden mit Benzylgruppen geschützt. Die Vollständigkeit der Kopplungen wurde durch Titrieren nach DORMAN und gleichzeitige Aminosäuren-Analyse kontrolliert. Letztere Methode hat bekanntlich Nachteile (sie ist verhältnismäßig langsam, ergibt in ihrer ursprünglichen Form infolge der Zersetzung mehrerer Aminosäuren keine genauen Resultate, der Träger begünstigt die Zersetzung der Aminosäuren), dagegen ist sie bei der Bestimmung vieler Aminosäuren (Glycin, Prolin, Leucin, Isoleucin, usw.) sehr zuverlässig und genau. Im Falle der an den Seitenketten geschützten trifunktionellen Aminosäuren werden die Schutzgruppen bei der üblichen Hydrolysemethode gewöhnlich teilweise entfernt; deshalb ist bei der Berechnung der wahren Tyrosin- und Cysteinmenge die während der Hydrolyse unverändert gebliebene Menge der entsprechenden Benzylderivate zu den freien Aminosäuren zu addieren. (O-Benzyl-Tyrosin und S-Benzyl-Cystein werden nämlich während Aminosäureanalyse von der kurzen Säule mit den basichen Aminosäuren vor Histidin eluiert). Das Problem

wird dadurch kompliziert, daß das Tyrosin und sogar das Cystein während der Hydrolyse teilweise zersetzt wird. Die Zersetzung dieser und anderer Aminosäuren kann durch eine von uns ausgearbeitete neue Hydrolysemethode größtenteils vermieden werden, indem statt der Mischung von Salzsäure und Dioxan oder Salzsäure und Essigsäure 3*N* Merkaptoäthansulfonsäure (in 50%-iger Essigsäure gelöst) angewandt wird. Es wurden für alle von uns benützten Aminosäuren die Korrektionsfaktoren berechnet, deren Anwendung die genaue quantitative Bestimmung aller empfindlichen und an Seitenketten geschützten Aminosäuren ermöglicht [17]. Dadurch lassen sich die infolge der vom Träger verursachten und spontanen Zersetzung entstehenden Fehler vermeiden und die Bestimmungsmöglichkeit auf zahlreiche geschützte Aminosäurederivate erweitern. Die Aminosäurenanalyse wurde von uns zu einer für die Kontrolle der Peptidsynthese an fester Phase routinemäßig verwendbaren Methode entwickelt, die sich zwar langsamer, aber in vielen Fällen zuverläßiger als die Dorman-Titration erweist.

Bei den Kopplungsreaktionen, in denen mehr als 5% der Aminogruppen frei bleibt [Glu(NH_2), Asp(NH_2), Ile, Tyr (Bzl)] kann nach unter denselben Bedingungen wiederholter Kopplungsreaktion 3-Nitrophthalsäureanhydrid als Blocker angewandt werden [18]. Die *p*-Nitrophenylester des BOC-Glutamins und Asparagins werden auch bei großem, fünffachem Überschuß und wiederholter Reaktion nur bis zu 75—80% gekoppelt. Deshalb haben wir die Reaktionsgeschwindigkeit der sich bei klassischen Peptidsynthesen [19] durch hohe Reaktionsfähigkeit auszeichnenden Pentafluorphenylester der BOC-Aminosäuren an fester Phase untersucht [20]. Nach unseren Versuchen zeigen die Pentafluorphenylester auch an fester Phase weit größere Reaktionsfähigkeit als die *p*-Nitrophenylester; deshalb haben wir bei späteren Oxytocin-Synthesen zur Kopplung des BOC-Asparagins und Glutamins deren Pentafluorphenylester verwendet.

Die geschützten Nonapeptide wurden vom Träger durch Ammonolyse abgespaltet. Die in Dimethylformamid gelösten Rohprodukte wurden durch Fällung mit Äther bzw. Methanol gereinigt. In einem Falle war es infolge der Verwendung von 3-Nitrophthalsäureanhydrid als Blocker möglich, das geschützte Nonapeptid mittels Ionenaustausches von den Fehlsequenzen zu reinigen [18]. Infolge der sehr schlechten Wasserlöslichkeit des Oxytocin-Nonapeptids versuchten wir die Ionenaustauschchromatographie in Dimethylformamid-Methanol-Gemisch, mit Anwendung der von YOUNG [21] angegebenen Methode, mit einem makroporösen Ionenaustauscher (Amberlyst A-26) durchzuführen. Leider ist der Ionenaustausch unter solchen Bedingungen so langsam, daß wir keine effektive Reinigung erzielen konnten. (Bei anderen, in Wasser oder Methanol besser löslichen Peptiden läßt sich diese Methode erfolgreicher anwenden.) Nach der erwähnten Reinigung wurden die Schutzgruppen von den Nonapeptiden durch Reduktion mit Natrium in flüssigem Ammonia entfernt, dann das freie Nonapeptid durch Einführung von Luft bei pH=7 oxidiert [22]. Die Oxytocin-Aktivität der Lösung (~70—80 Einheit/ml) war niedriger, als die des mit der klassischen Synthese gewonnenen Produktes, was auf Verunreinigung des Rohproduktes durch Fehlsequenzen hinweist. Nach unserer Meinung ist die Synthese an fester Phase in seiner gegenwärtigen Form ohne jeden besonderen Reinigungsschritt für die Synthese von Oxytocin von etwa 100 Einheit/mg Aktivität geeignet. Auch eine weitere Reinigung ist durchführbar [23].

* * *

Für die Unterstützung unserer Forschungen und die Durchführung der biologischen Untersuchungen sind wir der Pharmazeutischen Fabrik GEDEON RICHTER (Budapest) zu aufrichtigem Dank verpflichtet.

Experimentelles

Oxytocin-Synthesen an fester Phase

a) *Versuch mit NPS-Aminosäuren.* NPS-Glycin wurde in der durch MERRIFIELD beschriebenen Weise an chlormethyliertes, 2% Divinylbenzol enthaltendes Polystyrol-Harz gebunden. Die Menge des Glycins wurde durch Aminosäurenanalyse und Stickstoffbestimmung des Harzes zu etwa 0,70—0,80 mMol/g bestimmt. Die Herstellung des Oxytocins wurde mit dem folgenden Synthesezyklus durchgeführt:

Waschen des Peptidträgers (7 g, ~5 mMol) mit CH_2Cl_2. 5 Min. Schütteln mit 5% Trifluoressigsäure in CH_2Cl_2, dann 15 Min. mit 0,5*N* HCl in Essigsäure — CH_2Cl_2 (1:1), um die NPS-Gruppe zu entfernen. Je 3×Waschen mit CH_2Cl_2, Äthanol und CH_2Cl_2. 10 Min. Behandeln mit 10% Triäthylamin in CH_2Cl_2, zur Freisetzung der Aminogruppen. 3×5 Min. Waschen mit CH_2Cl_2. 10 Min. Äquilibrieren mit der CH_2Cl_2 Lösung der entsprechenden NPS-Aminosäure (15 mMol, 3×Überschuß). Nach Zugabe von 15 ml 1 Mol Dicyclohexylcarbodiimid-Lösung in CH_2Cl_2, 2 Std. Schütteln. Abschließend je 3×Waschen mit CH_2Cl_2, Dimethylformamid und CH_2Cl_2, Kopplungskontrolle durch DORMAN-Titration und Aminosäuren Analyse.

Bei Anwendung von NPS-Aminosäuren ergaben die Kopplungsreaktionen bis zur Synthese des C-terminalen Tetrapeptides ständig Ausbeuten über 95%; so wurde kein Blocker angewendet. Die *p*-Nitrophenylester des NPS-Asparagins und NPS-Glutamins ergaben auch bei 6×Überschuß eine so niedrige Ausbeute (50—60%), daß die Synthese nach dem Einbau des NPS-Glutamins unterbrochen werden mußte, da das eingebaute Glutamin nur 25% der ursprünglichen Menge des C-terminalen Glycins betrug.

b) *Versuch mit BOC-Aminosäuren, mit nachträglichem Ausbau der Amidgruppen des Asparagins und Glutamins.* Die Synthese erfolgte im wesentlichen nach dem unter a) beschriebenen Zyklus. Die erste Beladung des Trägers betrug 0,55 mMol Glycin/g Harz (8 g, etwa 4,5 mMol). Der einzige Unterschied bestand darin, daß die BOC-Schutzgruppen mit 25%-iger Trifluoressigsäure in CH_2Cl_2 in Reaktionszeiten von 30 Min. entfernt wurden. Die Reihenfolge der angewandten Aminosäurederivate war wie folgt: BOC-Leu, BOC-Pro, BOC-Cys (Bzl), BOC-Asp (OMe), BOC-Glu (OMe), BOC-Ile, BOC-Tyr (Bzl) und Z-Cys (Bzl). Die Kopplung von BOC-Ile und BOC-Tyr (Bzl) wurde wiederholt. Auf Grund der Dorman-Titration bzw. der Aminosäurenanalyse wurden die Aminosäuren in folgenden Prozent-Anteilen in das Molekül eingebaut: (Glycin 100%) Leu 97—98%, Pro 95—96%, Cys 95%, Asp 90—91%, Glu 85—87%, Ile 75—80%, Tyr 75—78%, Cys 65—70%.

c) *Synthese mit BOC-Aminosäuren, mit Anwendung von 3-Nitrophthalsäureanhydrid als Blocker.* Sie Synthese erfolgte im wesentlichen wie unter b) mit folgenden Unterschieden: zum Einbau des BOC-Asparagins und BOC-Glutamins wurden ihre *p*-Nitrophenylester in 6×Überschuß mit 12 Std. Reaktionszeit angewandt und der Kopplungsprozeß in beiden Fällen wiederholt. Die Ergebnisse der Dorman-Titrierung und der Aminosäurenanalyse waren die Folgenden: (Gly=100%) Leu

95—96%, Pro 95—96%, Cys 92—94%, Asp(NH_2) 80—85%, Glu(NH_2) 75—80%, Ile 70—75%, Tyr 65—70%, Cys 65—70%. Nach der Kopplung von BOC-Asparagin, BOC-Glutamin, BOC-Isoleucin und BOC-Tyrosin-Benzyläther wurden die unreagierten Aminogruppen mit 3-Nitrophthalsäureanhydrid in der folgenden Weise blockiert: nach der Dorman-Titrierung wurde das Polymer mit Dimethylformamid gewaschen, dann mit der Lösung von äquivalenter Menge (5 mMol) 3-Nitrophthalsäureanhydrid in 20 ml Pyridin behandelt. Der Überschuß des Blockers wurde durch waschen mit Triäthylamin in Dimethylformamid entfernt.

Analytische Kontrolle der Kopplungsreaktionen

a) *Mit Dorman-Titration.* Die Vollständigkeit der Kopplungsreaktion wurde mit der Dorman-Methode kontrolliert, jedoch statt Pyridin-Hydrochlorid nach LOSSES Vorschlag [25] Pyridin-Hydrobromid verwendet.

b) *Mit Aminosäuren-Analyse.* Nach der Peptidbindung wurde das Polymer durch gründliches Waschen (s. Synthesezyklus) von den Nebenprodukten und Verunreinigungen befreit, dann ein Muster von etwa 8—10 mg getrocknet. Das Muster wurde in ein Bombenrohr (Pyrex, 80×12 mm) eingemessen und 1 ml 3*N* Merkaptoäthansulfonsäure (in 50%-iger Essigsäure gelöst) zugegeben. Die Lösung wurde auf −70 °C abgekühlt, das Bombenrohr mit dem eingefrorenen Material in Vakuum (~50 μHg) zugeschmolzen; nach 22stündiger Hydrolyse (110±2 °C) das Rohr geöffnet und der Inhalt quantitativ auf ein kleines Glasfilter übertragen, das Polymer abfiltriert, und mit 1,00 ml pH 5,28 Natriumcitrat-Puffer nachgewaschen. Von der erhaltenen 2 ml Lösung wurden Anteile von 0,2 ml zur Aminosäuren-Analyse benützt. (Wir arbeiteten mit einem automatischen Aminosäure-Analysator, Modell HD-1200 E, mit Zweikolumnen-System, mit Chromex KG—50 als Ionenaustauscher.)

Herstellung und Reinigung der Oxytocin-Cyclopeptide

a) *Nach der Peptidsynthese mit Methode* b) wurde das Polymer gründlich getrocknet, in 50 ml abs. Dimethylformamid gequollen und 50 ml mit Ammoniak gesättigtes Methanol zugegeben. Durch die Mischung wurde 2 Stunden lang, bei 0 °C, NH_3 geleitet, dann wurde sie über Nacht stehengelassen. Das Polymer wurde abfiltriert, mit Dimethylformamid nachgewaschen, und die Ammonolyse noch zweimal wiederholt. Die vereinigten Dimethylformamid-Methanol Lösungen wurden eingedampft, das erhaltene Öl in 20 ml Dimethylformamid gelöst und das geschützte Nonapeptid mit Äther gefällt. Das Rohprodukt (3,2 g, 55% auf das ursprüngliche Glycin bezogen) war noch nicht chromatographisch rein, deshalb wurde es in 15 ml Dimethylformamid gelöst und durch Ausfällen mit 500 ml Methanol gereinigt. Dieser Reinigungsprozeß wurde wiederholt und so 2,0 g (33%) Produkt von etwas unscharfem Schmelzpunkt (215—220 °C) erhalten, dessen Aminosäuren-Analyse (Gly 1,00) Leu 0,98; Pro 0,92; Cys 1,84; Asp 0,97; Glu 0,97; Ile 0,82; Tyr 0,75 ergab.

Analyse: Ber. $C_{65}H_{88}O_{15}N_{12}S_2$ (1341,51) C 58,30; H 6,70; N 12,53%; Gef. C 57,72; H 6,53; N 12,70%. $[\alpha]_D^{22} = -43{,}5°$ (c=1, DMF).

Durch Dünnschichtchromatographie (in *n*-Butanol-Essigsäure-Wasser 4:1:1, bzw. Essigester-Pyridin-Essigsäure-Wasser 60:20:6:11) konnten 4—5 Peptide von einander sehr nahe liegenden R_f-Werten nachgewiesen werden, eines davon ist

auf Grund des R_f-Wertes das gesuchte Oxytocin-Nonapeptid, das durch Säulenchromatographie weder an Silicagel noch an Sephadex LH-20 (DMF-EtOH Gradient) von den chemisch sehr ähnlichen Verunreinigungen getrennt werden konnte. Die Oxytocin-Aktivität nach Reduktion der Schutzgruppen mit Natrium in flüssigem NH_3 und Oxidation (2 Stunden, pH=7, Lufteinführung) betrug ~5 Einheit/mg.

b) *Nach der Synthese mit der Methode* c) wurde das Nonapeptid mit der unter a) beschriebenen Methode mittels Ammonolyse vom Polymer abgespalten und durch Fällung gereinigt. Nach der Reinigung wurde ein chromatographisch fast reines Produkt mit ziemlich scharfem Schmelzpunkt (229—230 °C) erhalten. Ausbeute 1,00 g (18%).

Anal. Ber. $C_{65}H_{88}O_{15}N_{12}S_2$ (1341,51) C 58,30; H 6,70; N 12,53%; Gef. C 57,84; H 7,00; N 12,40%. $[\alpha]_D^{22} = -51{,}5°$ (c=0,6 DMF).

Die Aminosäurenanalyse ergibt etwas niedrige Werte für Glutaminsäure und Tyrosin. (Gly=1,00) Leu 0,96; Pro 0,95; Cys 1,75; Asp 0,92; Glu 0,87; Ile 0,92; Tyr 0,65. Von 0,50 g des Materials wurden die Schutzgruppen durch Reduktion mit Natrium in flüssigem Ammoniak entfernt, dann das freie Nonapeptid durch Lufteinführung bei pH 7 zwei Stunden lang oxidiert. Die Oxytocin-Aktivität der Lösung wurde unmittelbar gemessen, und auf Grund der Konzentration der Lösung (1 mg/ml) 70,8 Einheit/ml gefunden.

Literature

[1] *Merrifield, R. B.:* Federation Proc. **21**, 412 (1962).
[2] *Yamashiro, D., C. H. Li:* J. Amer. Chem. Soc. **95**, 1310 (1973).
[3] *Ives, D. A.:* Can. J. Chem. **46**, 2318 (1968).
[4] *Bayer, E., H. Hagenmaier:* Tetrahedron Letters 2037 (1968).
[5] *Bayer, E., H. Hagenmaier:* Peptides 1968, North-Holland Publishing Co., Amsterdam (1968) S. 162
[6] *Manning, M.:* J. Amer. Chem. Soc. **90**, 1348 (1968).
[7] *Beyerman, H. C., R. A. In t'Veld:* Rec. Trav. Chim. **88**, 1019 (1969).
[8] *Inukai, N. u.A.:* Bull. Chem. Soc. Japan **41**, 182 (1968).
[9] *Phocas, I. u.A.:* J. Chem. Soc. 1506 (1967).
[10] *Paul, R., A. S. Kende:* J. Amer. Chem. Soc. **86**, 741, 4162 (1964).
[11] *Ressler, C.:* J. Amer. Chem. Soc. **78**, 5956 (1956).
[12] *Fruton, J. S., M. Bergman:* J. Biol. Chem. **127**, 627 (1939).
[13] *Miller, H. K., H. Waelsch:* Arch. Biochem. Biophys. **35**, 176 (1952).
[14] *Kovács, J., K. Medzihradszki, V. Bruckner:* Acta Chim. Acad. Sci. Hung. **6**, 183 (1955).
[15] *Hanson, R. W., H. N. Rydon:* J. Chem. Soc. 836 (1964).
[16] *Battersby, A. R., J. J. Reynolds:* J. Chem. Soc. 524 (1961).
[17] *Kovács, K., R. Ferenczi, B. Penke:* Monatshefte, im Druck
[18] *Wieland, T. u.A.:* Annalen **727**, 130 (1969).
[19] *Kovács, J., L. Kisfaludy:* J. Org. Chem. **35**, 3563 (1970).
[20] *Penke, B., K. Kovács:* Peptides 1972, North-Holland Publishing Co., Amsterdam (1973) S. 187.
[21] *Young, G. T.:* Chem. Comm. 1057 (1971).
[22] *Du Vigneaud, V., u.A.:* J. Amer. Chem. Soc. **75**, 4879 (1953).
[23] *Manning, M. u.A.:* J. Chrom. **38**, 396 (1968).
[24] *Losse, G.:* Persönliche Mitteilung.

ТВЕРДОФАЗНЫЙ СИНТЕЗ ОКСИТОЦИНА

П. Паллаи, К. Ковач, Б. Пэнке

С целью изучения синтеза пептидов на твердой фазе нами был синтетизирован окситоцин тремя разными методами. Было установлено, что при исключительном применении аминокислот *NPS* нельзя синтезировать чистый окситоцин. Из-за побочных реакций транспептидации так же нельзя решить дополнительное образование группы амида кислот аспарагина и глутамина путём аминолиза соответствующих эфиров. Для проверки реакции присоединения нами был выработан новый метод гидролиза, способствующий точному количественному определению всех аминокислот при помощи анализатора аминокислот.

STEROIDS, XXIII.
Synthesis of 2- and 4-Hydroxy and 2,4-Dihydroxy Derivatives of Estrone and Estradiol

By
KATALIN KOVÁCS, Z. RAKONCZAY AND B. MATKOVICS
Biochemical and Genetical Groups, Attila József University, Szeged

(Received May 19, 1973)

The following hydroxy derivatives of estrone and estradiol were prepared during this work[1]: 2,3-dihydroxyestrone, 2,3-dihydroxyestradiol, 3,4-dihydroxyestrone, 3,4-dihydroxyestradiol, 2,3,4-trihydroxyestrone and 2,3,4-trihydroxyestradiol. The syntheses were performed *via* the corresponding mono and dinitro derivatives, and all intermediates were isolated and described.

A number of authors have dealt with the direct synthesis of the group of compounds mentioned in the title [1—4], while others have strived to synthesize the monomethoxy derivatives [5] in order to identify the methoxy intermediates occurring among natural estrogens [6—7].

As regards the hydroxylated estrogens accumulating during pregnancy, many authors attribute importance exclusively to the compounds mentioned, but primarily to 2-hydroxyestrone [8].

In the case of estrogens bound to protein, and possibly to glutathion, on the other hand, the important intermediate role of these compounds [9—11] is assumed.

Valuable results have been obtained recently on the isolation of this group of compounds, and on the study of their properties and role in the intermediate metabolism [12, 13].

The synthesis of these compounds has already been dealt with for purposes of identification of the derivatives obtained in previous non-specific enzymatic hydroxylation experiments [14].

[1] Abbreviations used: 2-nitroestrone means 2-nitro-3-hydroxy-1,3,5(10)-triene-17-one; 2-aminoestrone and 2-hydroxyestrone mean the 2-amino and 2-hydroxy derivatives of this same compound; similarly, 2-nitroestradiol means 2-nitro-3,17ß-dihydroxyestra-1,3,5(10)-triene, while 2-aminoestradiol and 2-hydroxyestradiol mean the corresponding 2-amino and 2-hydroxy derivatives, and so on.

Experimental[2]

2- and 4-nitroestrones and *2,4-dinitroestrone* were prepared and purified as described by WERBIN and HOLOWAY [1]. The reduction of mono- and dinitroestrones was carried out with sodium borohydride to the corresponding estradiols, just as for the mono- and diamino and the mono- and dihydroxy substituted derivatives, by the method of PATTON [4].

In the identification an effort was made to attain the chemical and physicochemical properties for the compounds described in the literature, and also to obtain materials which were chromatographically (TLC) completely pure by running them in a number of well-known solvent pairs. Separations were performed under the usual conditions, on silica gel adsorbent prepared according to Stahl (Merck or Reanal) in an ascending system.[3]

2-Nitroestrone (I) [1]. M.p.: 178—80 °C (Lit.: 183.5—184 or 155 °C). Anal.: Calc.: $C_{18}H_{21}O_4N$ C 68.55 H 6.71 N 4.44; Found: C 68.65 H 6.70 H 4.41. $[\alpha]_D = +30 \pm 1°$ (c=1.0; $CHCl_3$). ν_{max}^{KBr} 3350 (OH), 1750, 1640 (CO), 1530 (Ar-NO_2), 880, 760, 650 (C-NO_2) cm^{-1}. (The IR spectra were taken with a UNICAM SP 1000 spectrophotometer in all cases.)

2-Nitroestradiol (II) [4]. The sodium borohydride reduction of I gave the diol. M.p.: 162—3 °C (Lit.: 167—8 °C). Anal.: Calc.: $C_{18}H_{23}O_4N$ C 68.11 H 7.30 N 4.41; Found: C 68.15 H 7.23 N 4.48. $[\alpha]_D = +160 \pm 2°$ (c=1.0; $CHCl_3$). ν_{max}^{KBr} 3490, 3300, 2950 (OH), 1630, 1525 (Ar-NO_2), 965, 990, 760 (C-NO_2) cm^{-1}.

2-Aminoestrone (III). It was reduced to amine by the method of KRAYCHY and GALLAGHER [15] with an aqueous solution of alkaline sodium hydrosulphite ($Na_2S_2O_4$). The yield was very good. M.p.: 192—93 °C (Lit.: 220 °C). Anal.: Calc.: $C_{18}H_{23}O_2N$ C 75.75 H 8.14 N 4.91; Found: C 75.80 H 8.18 N 4.67. $[\alpha]_D = -40 \pm 2°$ (c=0.5; $CHCl_3$). ν_{max}^{KBr} 3500, 3390, 3350 (NH_2, OH), 1730 (CO), 1290 (NH_2) cm^{-1}.

2-Aminoestradiol (IV). Sodium borohydride reduction of an alkaline methanolic solution of III led to IV. M.p.: 188—90 °C. Anal.: Calc.: $C_{18}H_{25}O_2N$ C 75.23 H 8.76 N 4.87; Found: C 75.30 H 8.80 N 4.72. $[\alpha]_D = -130 \pm 2°$ (c=0.1; $CHCl_3$). ν_{max}^{KBr} 3390, 3320, 2950 (NH_2, OH), 1290 1220 (NH_2) cm^{-1}.

2-Hydroxyestrone (V). Prepared from III by diazotation and boiling the diazo compound with urea (by a combination of the methods of NIEDERL and VOGEL [2] and KRAYCHY and GALLAGHER [15]). The 2-hydroxyestrone formed was purified from the by-products by preparative thick layer chromatography on a silica gel adsorbent mentioned before. The end-product of the above reaction was dissolved in $CHCl_3$ and transferred in a band to a 500 μ thick adsorbent layer. The plate was run in a 1:2:2 mixture of acetone—cyclohexane—chloroform. The identified band, with the appropriate R_f value, was scraped off together with the adsorbent. The adsorbent containing the substance was repeatedly extracted with acetone—chloroform (1:2). The adsorbent was removed by filtration on a G5 glass filter and the solvent

[2] Melting points are uncorrected.

[3] We wish to publish the detailed TLC properties of the compounds in the near future elsewhere.

was evaporated in N_2 atmosphere. (As formation of quinone was observed, it is very important to avoid contact of the material with air as far as possible.) The product thus isolated was pure by TLC. M.p.: 116—18 °C (Lit.: 200 °C). Anal.: Calc.: $C_{18}H_{22}O_3$ C 75.52 H 7.74; Found: C 75.60 H 7.80. $[\alpha]_D = +190 \pm 2°$ (c=1.0; EtOH). ν_{max}^{KBr} 3350 (OH), 1730, 1710 (CO), 1610, 1290 (Ar) cm^{-1}.

2-Hydroxyestradiol (VI). Prepared by the previously mentioned reduction of V. M.p.: 194—96 °C. Anal.: Calc.: $C_{18}H_{24}O_3$ C 75.00 H 8.39; Found: C 75.05 H 8.43. $[\alpha]_D = +110 \pm 2°$ (c=0.1; EtOH). ν_{max}^{KBr} 3400 (OH), 1510, 1450, 1260 (Ar) cm^{-1}.

4-Nitroestrone (VII). M.p.: 277—78 °C (Lit.: 279—80 °C or 258 °C). Anal.: Calc.: $C_{18}H_{21}O_4N$ (as for I); Found: C 68.60 H 6.78 N 4.41. $[\alpha]_D = -299 \pm 2°$ (c=0.3; $CHCl_3$). ν_{max}^{KBr} 3350 (OH), 1730 (CO), 1530 (Ar-NO_2), 1030, 825, 800 (C-NO_2) cm^{-1}.

4-Nitroestradiol (VIII). Prepared from VII by the method used for II. M.p.: 192—93 °C (Lit.: 220 °C). Anal.: Calc.: (as for II); Found: C 68.08 H 7.20 N 4.72. $[\alpha]_D = +250 \pm 2°$ (c=0.1; $CHCl_3$). ν_{max}^{KBr} 3200, 2950 (OH), 1530 (Ar-NO_2), 1050, 825 (C-NO_2) cm^{-1}.

4-Aminoestrone (IX). Prepared from VII, analogously as for III. M.p.: 250—52 °C. Anal.: Calc.: (as for III); Found: C 75.70 H 8.09 N 4.67. $[\alpha]_D = +50 \pm 1°$ (c=0.1; dimethylsulphoxide)

4-Aminoestradiol (X). Prepared from IX as for III and IV. M.p.: 266—68 °C. Anal.: Calc.: (as for IV); Found: C 75.20 H 8.72 N 4.72. $[\alpha]_D = -90 \pm 2°$ (c=0.1; dimethylsulphoxide). ν_{max}^{KBr} 3390, 3320, 2950 (OH, NH_2), 1620, 1300, 800 (NH_2) cm^{-1}.

4-Hydroxyestrone (XI). Prepared from IX by the combined method given for V. M.p.: 233—35 °C. Anal.: Calc.: (as for V); Found: C 75.58 H 7.78. $[\alpha]_D = +100 \pm 2°$ (c=0.1; EtOH). ν_{max}^{KBr} 3400, 3350 (OH), 1740 (CO), 1290 (Ar) cm^{-1}.

4-Hydroxyestradiol (XII). Prepared from XI as for VI. M.p.: 168—70 °C. Anal.: Calc.: (as for VI); Found: C 75.04 H 8.40. $[\alpha]_D = +140 \pm 2°$ (c=0.1; EtOH). ν_{max}^{KBr} 3400 (OH), 1510, 1250 (Ar) cm^{-1}.

2,4-Dinitroestrone (XIII). Prepared as described by WERBIN and HOLOWAY [1]. M.p.: 185—87.5 °C. Anal.: Calc.: $C_{18}H_{20}O_6N_2$ C 59.99 H 5.59 N 7.78; Found: C 60.05 H 5.62 N 8.10. $[\alpha]_D = +120 \pm 2°$ (c=1.0; $CHCl_3$). ν_{max}^{KBr} 3350, 3320 (OH), 1750 (CO), 1730, 1535 (Ar-NO_2), 1320 (NO_2), 750 (C-NO_2) cm^{-1}.

2,4-Dinitroestradiol (XIV). Prepared from XIII similarly as previously. M.p.: 263—65 °C. Anal.: Calc.: $C_{18}H_{22}O_6N_2$ C 59.11 H 6.12 N 7.78; Found: C 59.20 H 6.18 N 8.10. $[\alpha]_D = +100 \pm 2°$ (c=0.1; $CHCl_3$). ν_{max}^{KBr} 3220, 2940 (OH), 1320 (NO_2), 800, 745 (C-NO_2) cm^{-1}.

2,4-Diaminoestrone (XV). Prepared as above, by reduction, from XIII. M.p.: 207—9 °C. Anal.: Calc.: $C_{18}H_{24}O_2N_2$ C 71.97 H 8.05 N 9.03; Found: C 80.02 H 8.10 N 9.40. $[\alpha]_D = +200 \pm 2°$ (c=0.1; MeOH). ν_{max}^{KBr} 3390, 3350 (NH_2, OH), 1745 (CO), 1615, 1290 (NH_2) cm^{-1}.

2,4-Diaminoestradiol (XVI). Prepared from XV by further reduction. M.p.: 198—200 °C. Anal.: Calc.: $C_{18}H_{26}O_2N$ C 71.52 H 8.66 N 9.26; Found: C 71.57

H 8.60 N 9.40. $[\alpha]_D = +160 \pm 2°$ (c=0.1; dimethylsulphoxide). ν_{max}^{KBr} 3380, 3320 (NH_2, OH), 1290 (NH_2) cm^{-1}.

2,4-Dihydroxyestrone (XVII). Prepared from XV in accordance with the above. M.p.: 228—30 °C. Anal.: Calc.: $C_{18}H_{22}O_4$ C 71.51 H 7.33; Found: C 71.48 H 7.30. $[\alpha]_D = +128 \pm 2°$ (c=0.1; EtOH). ν_{max}^{KBr} 3420, 2940 (OH), 1740 (CO), 1610, 1290 (Ar) cm^{-1}.

2,4-Dihydroestradiol (XVIII). Prepared from XVII by sodium borohydride reduction. M.p.: 223—25 °C. Anal.: Calc.: $C_{18}H_{24}O_4$ C 71.04 H 7.95; Found: C 71.10 H 7.90. $[\alpha]_D = +300 \pm 2°$ (c=0.1; EtOH). ν_{max}^{KBr} 3420, 2940 (OH), 1380, 1260 (Ar) cm^{-1}.

The authors wish to acknowledge the assistance of the Analytical Laboratory of the Institute of Organic Chemistry, Attila József University, Szeged, for the analyses, and to express their thanks for the starting material (estrone) to the Pharmaceutical Works GEDEON RICHTER Budapest).

References

[1] *Werbin, H., C. Holoway:* J. Biol. Chem. **223**, 651 (1965).
[2] *Niederl, J. B., H. J. Vogel:* J. Amer. Chem. Soc. **71**, 2566 (1949).
[3] *Könyves, I., A. Olsson:* Acta Chem. Scand. **18**, 483 (1964).
[4] *Patton, T. L.:* J. Org. Chem. **24**, 1795 (1959).
[5] *Kraychy, S.:* J. Amer. Chem. Soc. **81**, 1702 (1959).
[6] *Layne, D. S., R. H. Common, W. A. Maw, R. M. Fraps:* Nature **181**, 351 (1958).
[7] *Axelrod, L. R., P. N. Rao, J. W. Goldzicher:* Arch. Biochem. Biophys. **87**, 152 (1960).
[8] *Yoshizawa, I., J. Fishman:* J. Clin. Endocr. **32**, 3 (1971).
[9] *Brown, B. J., P. H. Jellinck:* Biochem. J. **124**, 91 (1971).
[10] *Elce, J. S.:* Biochem. J. **126**, 1067 (1972).
[11] *Lyttle, C. R., P. H. Jellinck:* Biochem. J. **127**, 481 (1972).
[12] *Knuppen, R., O. Haupt, H. Breuer:* Biochem. J. **128**, 1369 (1972).
[13] *Gelbke, H. P., R. Knuppen:* J. Chromatogr. **71**, 465 (1972).
[14] *Matkovics, B., S. E. Rajki, D. G. Szőnyi:* Steroids Lipids Res. **3**, 118 (1972).
[15] *Kraychy, S., T. F. Gallagher:* J. Biol. Chem. **229**, 523 (1957).

СТЕРОИДЫ XXIII. СИНТЕЗ 2- И 4-ГИДРОКСИ-, 2,4-ГИДРОКСИ ЭСТРОНА И ЭСТРАДИОЛА

К. Ковач, З. Ракоцаи, Б. Маткович

Синтетизированы, через соответствующие нитросоединения, все С-2 и С-4 однозамещенные гидроксипроизводные эстрона и эстрадиола. Продукты всех ступеней синтеза выделены и характеризованы.

RHEOLOGICAL PROPERTIES AND THIXOTROPIC BEHAVIOUR OF KAOLINITE SUSPENSIONS

By

F. SZÁNTÓ and M. GILDE

Institute of Colloid Chemistry, Attila József University, Szeged

(Received July 21, 1973)

The rheological properties of Ca-Na-kaolinite and of monocationic Na-kaolinite were investigated as a function of the concentration of the suspension and of the electrolyte used as coagulating agent. The structure of aggregates of both types is changed by bivalent cations present in the electrolyte, as reflected by rheological curves and hysteresis loop.

Introduction

Structure formation of particles and rheological properties of suspensions of clay minerals, such as kaolinite, can be varied between wide limits by modifying the interactions between the particles. In connection with the formation of structure, VAN OLPHEN [1] supposes aggregated or flocculated states and their combinations. He defines the aggregated state as coming about by face-to-face interaction, whereas in flocculation edge-to-face or edge-to-edge associations are characteristic. He takes into account the double layers of positive charge formed at the edges under suitable conditions. The changes of rheological properties are explained — especially in the case of sols and gels of montmorillonite — by changes in character and strength of the interactions between the double layers of positive charge at the edges and those of negative charge present at basic faces. MICHAELS and BOLGER [2] consider the flocs as stable flow units forming larger aggregates. At low shear rates the aggregates form a loose network, which determines the plastic and structural properties of the suspension. At high shear rates the aggregates break down into individual flocs. FLEGMANN, GOODWIN and OTTEWILL [3] stated that the yield stress of monocationic kaolinite suspensions, plotted as a function of pH, changes according to a maximum curve. The maximum observed appeared to occur at a zero point of charge of the kaolinite edges.

Materials and methods

For preparing the material, Zettlitz kaolin was desaggregated with Na_2CO_3. On the basis of our earlier investigations, addition of 0.2 g Na_2CO_3 to 100 g kaolin was found optimal. The material treated with Na_2CO_3 solution was dried over water bath. A suspension of 4% concentration was prepared from the sample and

the particles of $d \leqq 2\,\mu m$ were separated by sedimentation. The fraction to be used was separated from the supernatant containing particles of colloidal dimensions by centrifugating only once. The sample obtained can be considered as Ca-Na-kaolinite, as according to our earlier experiences no total ion exhange occurs with Na_2CO_3 [4].

From the Ca-Na-kaolinite, monocationic Na-kaolinite was obtained by acidic and subsequent NaCl treatment as follows. The pH of the suspension was adjusted with HCl to pH=4, thus decomposing the Na_2CO_3. Then the material was treated with $2N$ NaCl and purified by centrifugation until the Cl^- ion concentration of the supernatant decreased to $1.5 \cdot 10^{-3}$ mole. The rheological properties and thixotropic behaviour of both Ca-Na- and monocationic Na-kaolinite were studied in suspensions of different concentrations, as well as with constant kaolinite concentration in the presence of different quantities of coagulating electrolyte.

The measurements were made with a viscometer type "Rotovisco". The Bingham yield stresses τ_B were obtained by extrapolating the linear sections of the flow curves in the usual way. We used principally these data for rheological characterization of the materials.

Results and discussion

Na-kaolinite suspension of relatively lower concentration (20%) exhibits a low yield stress ($\tau_B = 20$ dynes/cm^2) without showing a hysteresis loop (Fig. 1). With increasing concentrations the yields stress increases; from 30% concentration this increase is more important and a hysteresis loop appears, the area of the latter also increases with concentration.

In the case of Ca-Na-kaolinite the hysteresis loop can be observed already at 20% concentration, but is of opposite sense. The τ values obtained with decreasing r.p.m. being higher then those increasing r.p.m. (Fig. 2), the system exhibits "anti-

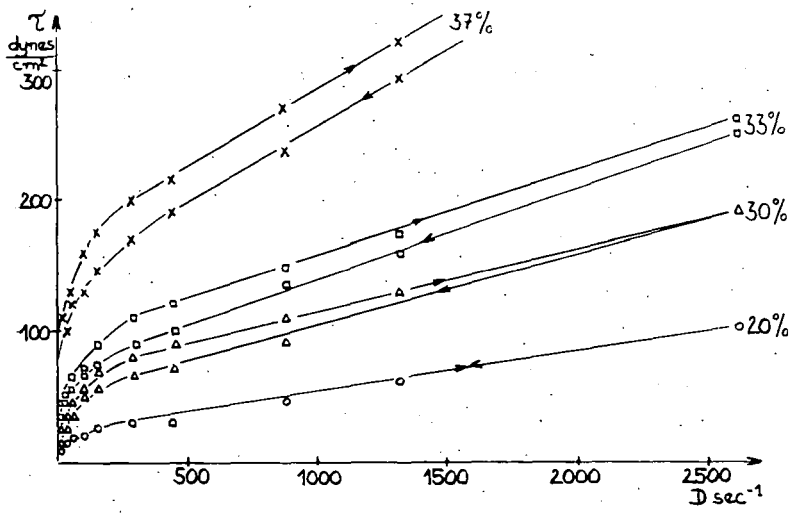

Fig. 1. Flow curves of Na-kaolinite suspensions of different concentration

thixotropy". With increasing concentration, this phenomenon becomes more pronounced. In suspensions of this type the effect of prolonged shear on flow properties was also studied. After determining the flow curves in the usual way (lower curves in

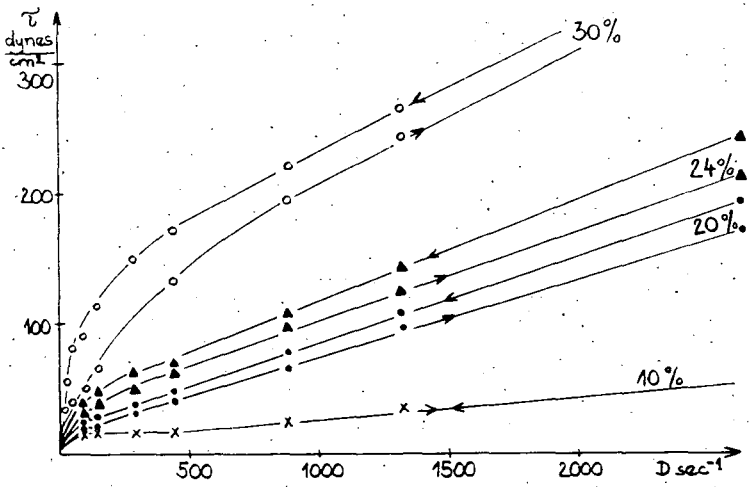

Fig. 2. Flow curves of Ca-Na-kaolinite suspensions of different concentration

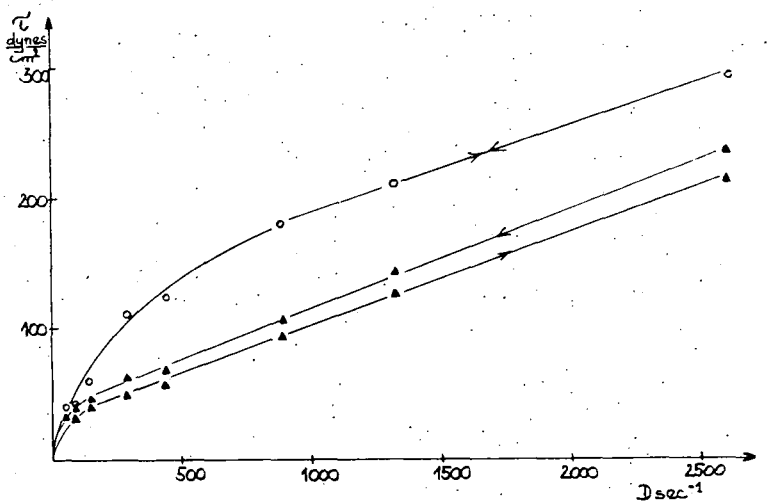

Fig. 3. Effect of shear on the flow curves of 24% Ca-Na-kaolinite suspension

Fig. 3), the suspension was sheared with the highest r.p.m. ($D=2620\ sec^{-1}$) for 30 minutes, and the flow curves were recorded again (upper curve in the figure). As a result, the τ values become significantly higher, whereas the hysteresis loop disappeared.

This difference in behaviour can be explained with the different rates of aggregation and differences in the interactions (adhesive forces) between the particles. The bonds between the particles of the Na-kaolinite suspension, in which the adhesion is low, can be more easily interrupted by shearing and regenerate more slowly, thus giving a regular hysteresis loop. In contrary, in the Ca-Na-kaolinite suspensions, the adhesive forces between the particles being higher, the system will be in more aggregated state. On the mechanical impact of the shearing, disaggregation, possibly also orientation of the particles will occur. At the same time, while the number of the particles is increased by the shear, the tendency of the system to rebuild the structure is comparatively high; thus higher τ values are obtained in the descending branch of the curve than in the ascending branch. The significant increase of the τ values after shearing with the maximum r.p.m. shows that the disaggregation proceeded further. The number of the particles forming the structure having thus reached a maximum, no further increase can be found in the descending branch, and thus the hysteresis loop disappears.

The influence of Ca^{2+} ions on the rheological properties of Ca-Na- and Na-kaolinite was also studied. The Bingham yield stress of 20% suspensions of different $CaCl_2$ concentrations is shown in Fig. 4. The τ_B values of the Ca-Na-kaolinite,

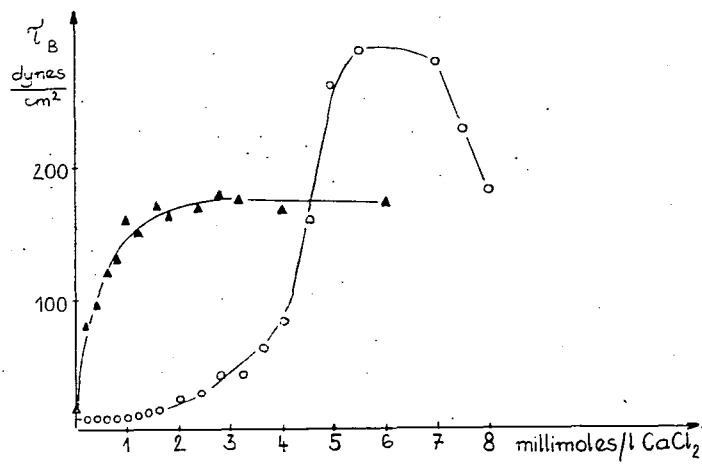

Fig. 4. Bingham yeld stress of 20% Ca-Na-kaolinite and Na-kaolinite suspensions of different $CaCl_2$ concentrations. ▲ Ca-Na-kaolinite, o Na-kaolinite

which is, as we have seen, in a slightly aggregated state, increase steeply in the presence of small quantities of $CaCl_2$, but reach a constant value at 2 mmole/l $CaCl_2$ concentration. The flow curves show antithixotropy at all $CaCl_2$ concentrations studied. At the same time, the effect of the $CaCl_2$ on a thoroughly washed Na-kaolinite suspension (of $0.3 \cdot 10^{-3}$ mole Cl^- ion concentration) is minimal up to 2 mmole/l concentration added. With further increasing $CaCl_2$ concentrations the τ_B values show, however, a steep increase exceeding the maximum observed

with Ca-Na-kaolinite. The τ_B *vs.* $CaCl_2$ concentration curve of a Na-kaolinite suspension of 40% washed in a usual way (of $1.5 \cdot 10^{-3}$ mole Cl^- ion concentration) shows an essentially similar curve (Fig. 5). Some difference can be observed in the beginning of the curve, a well expressed minimum at low $CaCl_2$ concentrations being observable in the latter case.

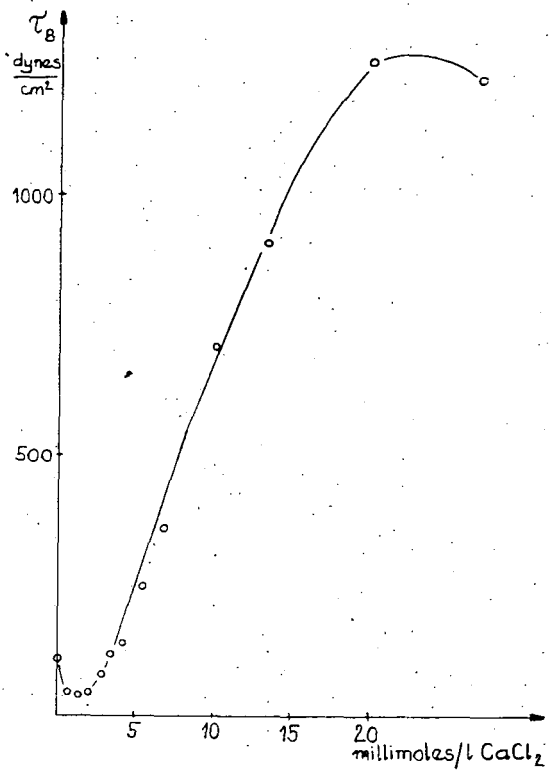

Fig. 5. Bingham yield stress of 40% Na-kaolinite suspensions of different $CaCl_2$ concentration

The differences in the effect of the Ca^{2+} ions on the rheological behaviour of the samples can be interpreted by taking into account the different states of aggregation of the starting material. The strength of the network of the Ca-Na-kaolinite suspensions, more aggregated from the beginning, will be increased by the influence of small quantities of $CaCl_2$, resulting in a steep τ_B curve. The increase of the adhesion may be attributed to a decrease of the thickness of the double layer rather then to ion exchange. In Na-kaolinite suspensions the flocculation process expressed by the increase of the yield stress starts at comparatively higher $CaCl_2$ concentrations. The minimum of the curve shown in Fig. 5 can be interpreted with changes of the charges (+) at the edges and (−) on the faces, caused by electrolyte, as presented by VAN OLPHEN in connection with montmorillonite. The steep ascension of the curve after the minimum represents the flocculation process as a result of increasing van der Waals forces.

We studied also the effect of $CaCl_2$ on the thixotropic behaviour of a 40% Na-kaolinite suspension. The thixotropy found at low $CaCl_2$ concentrations increases at higher concentrations, as shown by the broadening of the hysteresis loop at 3.3 mmole/l concentration (Fig. 6). Maximum thixotropy seems to be connected with a mild flocculating effect. With further increasing $CaCl_2$ concentration, the interactions between the particles become more intense and the breadth of hysteresis loop decreases; finally the loop disappears at 13.4 mmole/l concentration (Fig. 7). So no thixotropy is found in the system with maximum τ_B values. At $CaCl_2$ concentrations exceeding that corresponding to the maximum of τ_B, antithixotropy appears, similarly as in Ca-Na-kaolinite suspensions. The character of thixotropy or antithixotropy and their degree can be systematically varied by changing the interactions (adhesive forces) between the particles.

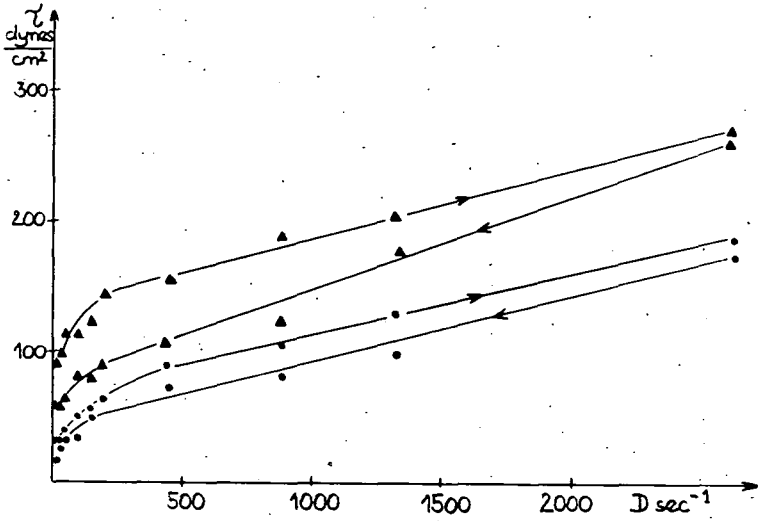

Fig. 6. Effect of $CaCl_2$ on the thixotropic behaviour of 40% Na-kaolinite suspension. $CaCl_2$ concentration: ● 0.67 mmole/l; ▲ 3.3 mmole/l

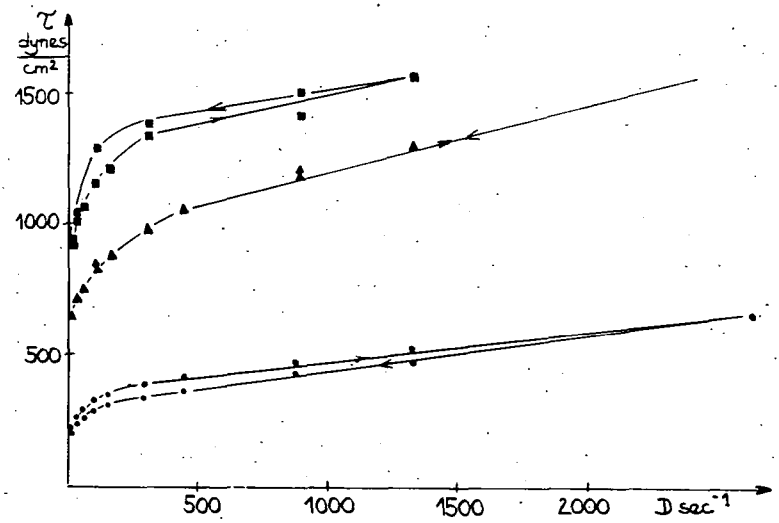

Fig. 7. Effect of $CaCl_2$ on the thixotropic behaviour of 40% Na-kaolinite suspension. $CaCl_2$ concentration: ● 6.7 mmole/l; ▲ 13.4 mmole/l; ■ 26.8 mmole/l

References

[1] *van Olphen, H.:* An Introduction to Clay Colloid Chemistry, Chap. 7, John Wiley, New York, 1963.
[2] *Michaels, A. S., J. C. Bolger:* Ind. Eng. Chem. Fundamentals **1**, 153 (1962).
[3] *Flegmann, A. W., J. W. Goodwin, R. H. Ottewill:* Proceedings of the British Ceramic Society 1969.
[4] *Szántó, F., M. Gilde, B. Várkonyi, J. Balázs:* Acta Geol. Acad. Sci. Hung. **11**, 409 (1967).

РЕОЛОГИЧЕСКИЕ СВОЙСТВА И ТИКСОТРОПИЯ КАОЛИНИТОВЫХ СУСПЕНЗИЙ

Ф. Санто, М. Гильде

Изучены реологические свойства Ca-Na-каолинита и монокатионного Na-каолинита в зависимости от концентрации суспензии и коагулирующего электролита. Структура агрегатов, образующихся из образцов обеих типов, изменялась под влиянием двухвалентного катиона прибавляемого электролита. Происходящие изменения отразились в реологическом поведении и на виде гистерезисных петель.

INVESTIGATIONS INTO THE POROSITY OF CAPILLAR SYSTEMS

By

M. GILDE and F. SZÁNTÓ

Institute of Colloid Chemistry, Attila József University, Szeged

(Received July 21, 1973)

The dependence on time of the diffusion of an electrolyte into tubes of known cross section and length was followed by conductivity measurements. Comparing the results with the corresponding theoretical relation, the length and the cross section of the tubes were calculated and found to be in good accordance with their real dimensions. The method was applied to a capillar system of unknown porosity, thus permitting the tortuosity factor to be determined.

Since the already classic work of MANEGOLD [1], the study of the porosity of capillar systems was the object of numerous investigations [2—5]. This problem is of high practical importance, being closely related with the permeability of foils, dyestuff films and other anticorrosive coatings. The permeability of rocks may be important from the point of view of oil field exploration.

The porosity of a capillar system is due to capillar tubes and holes of different diameteres and directions. The porosity is generally characterized by the quotient of the volume of these cavities and the total volume of the porous system. As the internal cavities and capillaries of the system are of different cross sections, lengths, ramification, etc., therefore a single numerical characteristic will not always be sufficient for describing the porous system, and further data are desirable. The tortuosity factor (see *e.g.* FATT [6]) is a step in this direction.

In an earlier paper [7] we described a method of determining the porosity by measuring the electric conductivity. We applied this method, based on the mentioned results of MANEGOLD and FATT, to measure the porosity of dyestoff films with the aid of a conductivity cell. In this cell the electrolyte of conductivity $\varkappa_0$ between two platinum electrodes in the distance l was divided into two parts by a dyestoff film of thickness l_x. To obtain the total resistance, the resistance of the electrolyte enclosed in the capillaries of the dyestoff film has to be added to the resistance of the electrolyte divided by the film. Therefore, if the conductivity measured in the cell containing the film is $\varkappa_f$, the porosity due to the capillaries traversing the film can be expressed by

$$\varepsilon = \frac{\varkappa_f}{\varkappa_0 - \varkappa_f} \frac{l_x}{l}. \tag{1}$$

If all capillaries were perpendicular to the surface of the film, the porosity given by Eq. (1) would be equal to the exact value of the quotient of the total cross section of the capillaries traversing the film and the total surface area of the film. Thus the capillaries in an electric insulator could be characterized by a single figure.

However, this characteristic does not give information about the course which the capillary, starting from one surface of the film, takes to arrive to the opposite surface. It seemed therefore desirable to elaborate a method capable to yield more, though not full, information on the porous system. We tried to find a method giving also the true, or at least the mean length of the capillaries traversing the film. Starting from FATT's quoted investigations, we modified the method based on the measurement of electric conductivity to permit the so-called tortuorsity factor to be determined, too. The method essentially consists in measuring the time dependence of the diffusion of the electrolyte into the porous system.

The diffusion of an electrolyte into a tube of given cross section and length through both ends of the tube can be exactly followed theoretically. Thus it is possible to express the time dependence of the conductivity of the electrolyte present in the tube by a closed formula [8]. On the other hand, the changes in time of this conductivity can be measured by the cell mentioned above.

Description of the apparatus

In our measurements we used a cylindrical cell, containing electrolyte of known concentration divided by the sample to be examined, and closed on both ends by platinum electrodes. This cell was connected with a conductometer type RADELKISZ OK—102.

Investigations on plexiglass samples

To check the theoretical formula, we used plexiglass discs, provided with perforations of known dimensions, to separate the electrolyte in the cell. The discs, closely fitting into the cell, were made of a plexiglass plate of 9.73 mm (±0.4%) mean thickness. In each disc a cylidrical hole of 1, 2 or 4 mm diameter was drilled perpendicularly to the surface (samples No. 1, 2 and 3, respectively), while sample No. 4 contained 13 holes of 1 mm diameter. The holes were filled with 1% agar gel. The samples prepared in this way were placed between the two parts of the cell, previously filled up with 1% agar gel containing 0.1*N* KCl. The measurements were made at 24±2 °C. Fig. 1 shows the time dependence of the conductivity of the cell separated by sample No. 1. The upper curve gives the results of the measurements made at 24 °C, the lower curve those at 22 °C. The time dependence of the measurements with samples No. 2 and 3 was very similar. Figure 2 shows the results obtained with sample No. 4, containing 13 holes, at 24 and 23 °C, respectively.

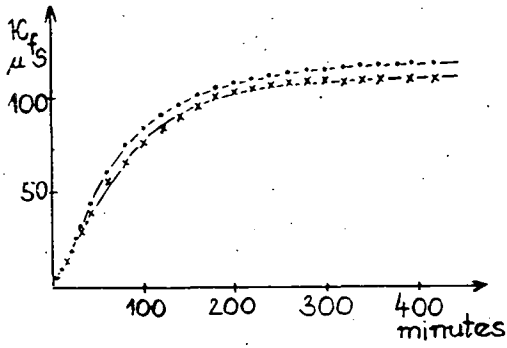

Fig. 1. Time dependence of conductivity for sample No. 1

On the base of theoretical considerations [8], the relative conductivity was calculated. Denoting by $\varkappa_\infty$ the conductivity evolved in the cell after a long time and show-

ing no further changes, the relative conductivity is defined as the quotient $\sigma_r = \varkappa_f / \varkappa_\infty$. The mean values of the relative conductivities obtained with different samples are plotted in Fig. 3 as a function of time. In order to compare this curve of relative conductivity with the theoretical curve, the former has to be reduced. Let us read from the theoretical curve some values of σ_r and the respective values of the independent variable τ. As τ depends on the diffusion constant D of the electrolyte, the length l of the tube and the time t according to

$$\tau = D\left(\frac{\pi}{l}\right)^2 t, \qquad (2)$$

the corresponding time t can be read from the measured curve of relative conductivity pertaining to the same value of σ_r. Some corresponding data are listed in Table I. From these, the values of l can be calculated using Eq. (2) (column 4 in Table I). The mean of the values of l obtained in this way was 9.53 mm. This differs from the true length of the tube by 0.2 mm ($\sim$2%). Using the mean value of l, the relative conductivity σ_r can be plotted as a function of τ. This plot, together with the theoretical curve, is shown in Fig. 4.

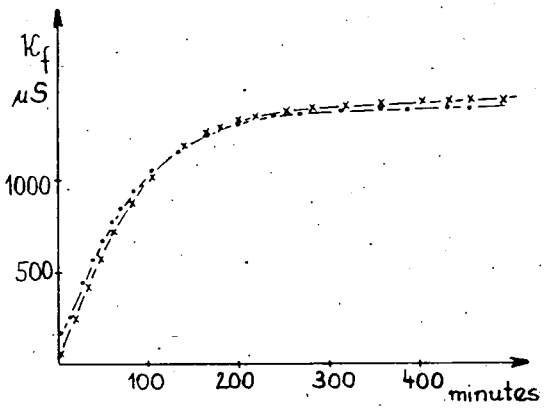

Fig. 2. Time dependence of conductivity for sample No. 4

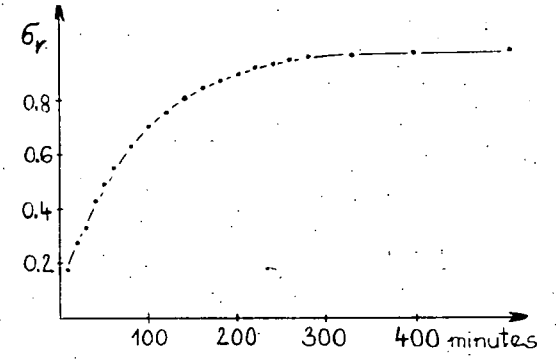

Fig. 3. Mean values of relative conductivity obtained with different samples as a function of time

It can be seen that the kinetic determination of the conductivity results in a good approximation of the length of the tube.

Table I

σ_r	τ	t minutes	l mm
0.70	1.31	100	9.23
0.75	1.48	117	9.39
0.80	1.69	139	9.58
0.85	1.97	165	9.67
0.90	2.34	199	9.74
0.95	3.06	252	9.59

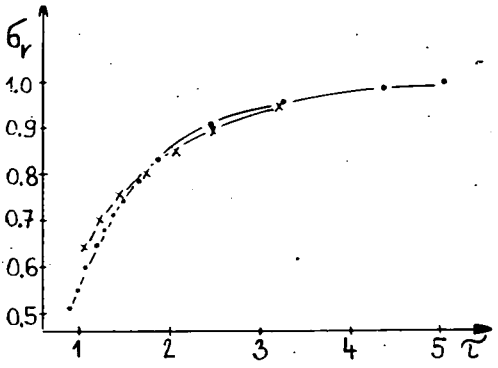

Fig. 4. Measured and theoretical curve of relative conductivity as a function of τ: × measured curve; ● theoretical curve

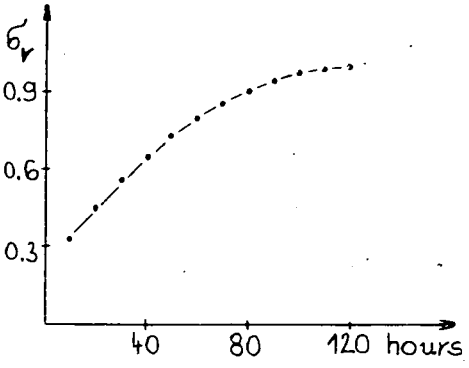

Fig. 5. Time dependence of relative conductivity of Sarmatian limestone

The $\varkappa_\infty$ read from the measurement can be considered as identical with the $\varkappa_f$ in Eq (1). By measuring also $\varkappa_0$ the porosity ε_k can be calculated using Eq. (1) (see Table II). This $\varkappa_0$ is the conductivity of the cell containing no sample if the distance of the electrodes of the cell filled with 1% agar gel containing 0.1N KCl is the same as in measuring $\varkappa_f$. The porosity can be determined also by filling the hole of the sample with the same electrolyte as used in the cell. In this case the value of $\varkappa_f$ can be read and the porosity ε_s can be calculated immediately after filling the cell. In Table II, column 1 gives the diameter of the holes in the sample, and column 2 the porosity ε_g calculated from the diameter of the holes.

Table II

Diameter of holes mm	ε_g	ε_s	ε_k
1	0.0020	0.0021	0.0022
2	0.0082	0.0078	0.0075
4	0.0330	0.0278	0.0273
13×1	0.0269	0.0281	0.0275

Table III

σ_r	τ	t hours	l mm
0.55	0.98	29	44.5
0.60	1.03	35	44.8
0.65	1.16	41	48.9
0.70	1.31	47	49.0
0.75	1.48	54	48.8
0.80	1.69	60	48.6
0.85	1.97	66	47.4
0.90	2.34	77	47.0
0.95	3.06	94	45.3

Measurements on a sample of Sarmatian limestone

A sample of 8.6 mm mean thickness, prepared of Érd limestone, was studied. The disc was boiled in distilled water to fill the pores. The cell was filled with 0.1 N KCl solution. The time dependence of the relative conductivity is shown in Fig. 5.

The mean length of the capillaries in the limestone was determined as in the case of the plexiglass samples (Table III). The length l obtained was 46.9 mm.

Dividing this by the thickness of the sample, the value 5.5 was obtained for the tortuosity factor. We also determined the porosity ε applying Eq. (1), obtaining the value 0.0085.

References

[1] *Manegold, E.:* Kapillarsysteme. Chemie und Technik Verl.-Ges.m.b.H., Heidelberg, Bd. 1, (1955), und Bd. 2, (1960).
[2] *Brasher, B. M., J. J. Nurse:* J. Appl. Chem. **9**, 96 (1959).
[3] *Glass, A. L., J. Smith:* J. Paint Technology **38**, 203 (1966).
[4] *Maitland, C. C., J. E. O. Mayne:* Paint Technology **29**, 25 (1965).
[5] *Mysels, K. J., D. Stigter:* J. Phys. Chem. **57**, 104 (1953).
[6] *Fatt, I.:* J. Phys. Chem. **63**, 751 (1959).
[7] *Gilde, M., F. J. Gilde, F. Szántó:* Study of the Porosity of Films. Lecture (in Hungarian) presented at the Meeting of the Ist Conference on Colloid and Surface Chemistry, Mátrafüred, 24 May, 1971.
[8] *Gilde, F. J.:* Acta Phys. et Chem. Szeged. **19**, 201 (1973).

ИЗУЧЕНИЕ ПОРИСТОСТИ КАПИЛЛЯРНЫХ СИСТЕМ

М. Гильде, Ф. Санто

Изучена диффузия электролита в капилляр известной длины и сечения определением электропроводности в зависимости от времени. Сопоставлением полученных данных и теоретических соотношений были рассчитаны длина и сечение капилляра, которые получились соответствующими действительным размерам. Метод был распространён на капиллярную систему с неизвестными параметрами и таким образом нам удалось рассчитать для нее параметр пористости.

МЕХАНИЗМ ОБРАЗОВАНИЯ ЧАСТИЦ В ГРАНУЛЬНОЙ ПОЛИМЕРИЗАЦИИ

И. АНДОР, А. Э. ШАМРАКОВА

Институт общей и физической химии университета им. Аттилы Йожефа, Сеге
Кафедра физико-химии полимеров и коллоидов Одесского госуниверситета

(Поступило в редакцию 20 июля 1973 г.)

Изучен механизм образования полистирольных частиц из мономерной эмульсии, стабилизованной полиметакриловой кислотой. Показано, что в полимеризующихся эмульсиях дисперсность полимерных частиц, при прочих равных условиях, не определяется однозначно ни поверхностной активностью, ни вязкостью раствора применяемого диспергатора. В системах, достаточно стабильных для образования гранул необходимой степени чистоты и дисперсности, критическая фаза процесса завершается при тем более ранних стадиях полимеризации, чем сильнее стабилизующее действие диспергатора.

Введение

Одной из основных технических проблем проведения гранульной (суспензионной) полимеризации является обеспечение необходимой стабильности полимеризующейся мономерной эмульсии в течение процесса [1, 2]. Патентная литература, описывающая различные способы осуществления гранульной полимеризации разных мономеров с получением продукта требуемой степени дисперсности, исключительно широка [3—5]. Вследствие большого практического значения вопроса неудивительно, что научные публикации появлялись относительно редко и опубликованных данных еще недостаточно для составления теории гранульной полимеризации. Между тем, до настоящего времени в производстве гранульных полимеров и, в особенности, различных сополимеров, нередки весьма серьезные затруднения, избежать которых стремятся все еще эмпирическим подбором условий проведения процесса.

В литературе до сих пор нет единого мнения относительно механизма образования и стабилизации мономерно-полимерных капель в процессе гранульной полимеризации [1, 3, 6, 7]. Мнения авторов противоречат друг-дгуру даже в таких основных вопросах, как влияние межфазного поверхностного натяжения, вязкости дисперсионной среды и динамическом равновесии в полимеризующейся эмульсии [8—11].

Ранее нами было рассмотрено, на примере полимеризации стирола в присутствии полиметакриловой кислоты (ПМАК), влияние вязкости водной фазы [12, 13] и молекулярного веса диспергатора [14] на стабилизацию полимеризующейся эмульсии. Было установлено, что определяющим фактором стабилизующего действия в полимеризующихся системах, при подходящем

гидрофильно-гидрофобном балансе [15], является конформационное состояние, т. е. гибкость макромолекул диспергатора. Связь некоторых кинетических и коллоидно-химических особенностей гранульной полимеризации была рассмотрена в работах [16, 17].

Задача данного исследования заключалась в установлении механизма образования полимерных частиц в процессе гранульной полимеризации и в определении причин возникновения загрязнения полимерных гранул раствором диспергатора.

Экспериментальные данные

Подготовка исходных веществ и методика проведения опытов описана в работе [12]. Оценку эффективности стабилизации полимеризующейся эмульсии проводили по защищенной поверхности образовавшихся полимерных гранул, которую рассчитывали согласно работы [18]. Для установления механизма образования полимерных частиц из эмульсии мономера (стирола), полимеризации проводились в закрытых стеклянных дилатометрах с магнитным перемешиванием [19], позволивших непосредственное визуальное наблюдение происходящих процессов с одновременной регистрацией глубины полимеризации. Диспергирующая система (растворы ПМАК) и скорость перемешивания были подобраны таким образом, чтобы за происходящими изменениями макроскопического состояния капель мономера, ярко окрашенных „Суданом III", возможно было следить невооруженным глазом. Соотношение фаз в этих опытах мономер: вода составляло 1:4.

В табл. I представлены данные, показывающие на каких глубинах превращения происходят в основном слипание и сплошная агломерация частиц в гранульной полимеризации стирола при разных условиях стабилизации.

Таблица I

Критическая фаза гранульной полимеризации стирола, завершающаяся сплошной агломерацией

Концентр. ПМАК, г/дл	0	0,05	0,10	0,25	0,50
Критич. фаза, % полимериз.	10—20	15—25	20—35	30—50	нет агл.

Полученные экспериментальные результаты показывают, что период наступления в завершения так называемой „критической фазы" определяется не столько вязкостью мономерно-полимерных капель, сколько стабилизирующим действием применяемого диспергатора. В слабо стабилизованных системах, как это следует из данных табл. I, с увеличением концентрации ПМАК необратимое слипание, приводящее к агломерации всей мономерно-полимерной массы, происходит при все более высоких степенях полимеризации. Наконец, в достаточно стабильной системе (0.5 г/дл ПМАК) наблюдается визуально трудно устанавливаемый период частичного слипания частиц, не завершающийся сплошной агломерицией.

Таблица II

Состав полистирольных гранул по окраске при последующем добавлении подкрашенного мономера

№п/п	Диспергатор		Степень полим., % в момент введения	Средний состав гранул, %		
	$C_{ПМАК}$	α		Красный	Розовый	Бесцветн.
1.	0,5	0	20	100	–	–
2.	0,25	0,3	20	100	–	–
3.	0,5	0,3	25	75	20	5
4.	1,0	0,4	25	60	30	10
5.	2,0	0,4	25	40	30	30
6.	1,0	0,4	40	30	50	20

На рис. 1 представлены данные, показывающие внешний вид полимерных гранул, полученных при разных условиях стабилизации, когда сплошная агломерция уже предотвращена а также при высоких эффективностях стабилизации полимеризационной системы. Соответственно: *а, б, в* и *г, д, е.*

Данные рис. 1 убедительно показывают, что при улучшении стабилизации, наряду с уменьшением размеров частиц, исчезают явления загрязнения раствором диспергатора, деформации и слипания гранул на поздних стадиях процесса.

В табл. II представлены данные, показывающие состав полистирольных гранул по окраске при введении в полимеризационные системы по 5 мл окрашенного „Суданом III" мономера к 15 мл уже частично заполимеризовавшейся бесцветной эмульсии, при разных стабильностях системы.

Из данных табл. II следует, что чем лучше стабилизация и чем выше уже достигнутая степень полимеризации, тем меньшая часть мономерно-полимерных капель принимает участия в динамическом равновесии диспергирования и коалесценции при стационарном перемешивании полимеризующейся эмульсии.

В работах [12, 13] нами было показано отсутствие непосредственной корреляции между величинами вязкости и поверхностной активности растворов диспергатора и их стабилизующим действием. Приведенные в табл. III срав-

Таблица III

Эффективность стабилизации полимеризующейся эмульсии стирола в присутствии ПМАК

№п/п	$C_{ПМАК}$ г/дл	α	$\eta_{с(уд)}$	$\sigma_с$, дин/см	S_0, $см^2$	d_s, см
1.	0,25	0,4	20,2	68,6	32	0,16
2.	0,5	0,3	18,5	68,4	55	0,09
3.	1,0	0,25	19,0	67,9	79	0,07
4.	0,5	0,5	50	68,4	46	0,12
5.	1,0	0,35	51	68,0	96	0,05
6.	2,0	0,27	50	66,8	140	0,03
7.	1,0	0	0,6	66,5	27	0,17
8.	3,0	0	2,1	65,0	108	0,04

нительные данные свидетельствуют, что стабилизующее действие, или соответственно средний размер образовавшихся гранул, не определяется однозначно ни величиной поверхностного натяжения, ни вязкостью раствора диспергатора.

Данные табл. III показывают, что эффективность стабилизации (S_0) имеет значения отличающиеся в системах №№ 1—3 более чем в два раза, а в системах №№ 4—6 более чем в три раза, несмотря на весьма близкие величины вязкости сред в сериях. Данные поверхностного натяжения, в особенности

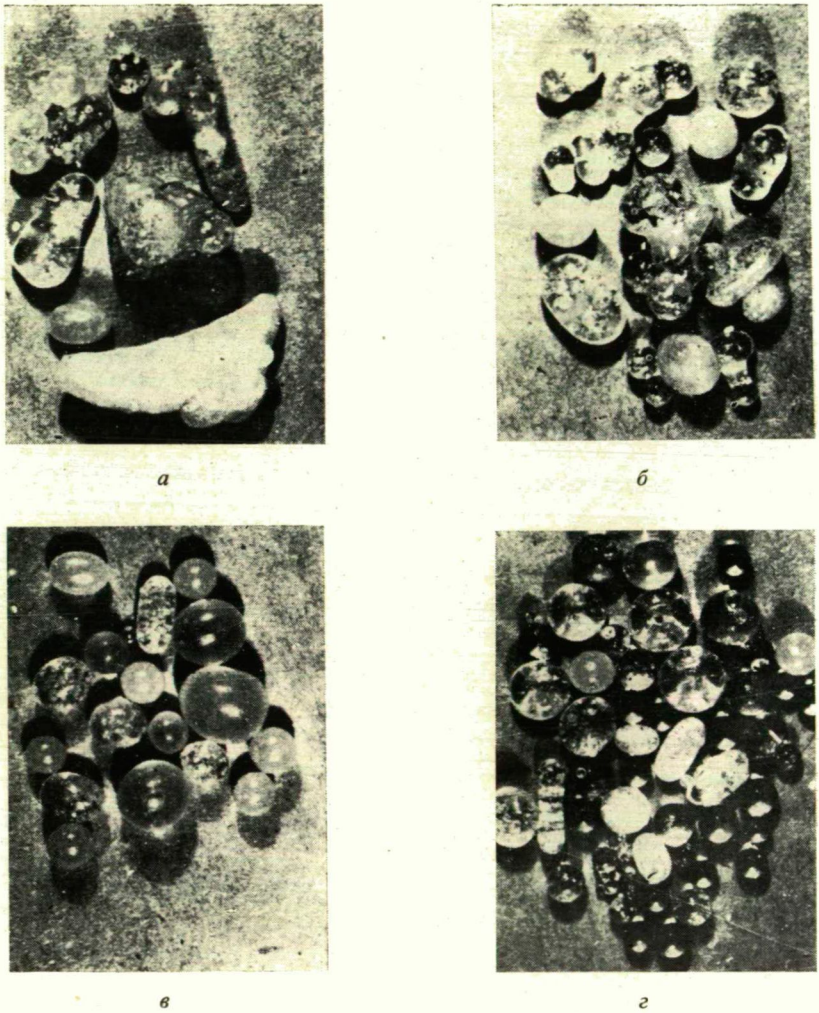

Рис. 1. Фотографии полистирольных гранул, полученных при разных эффективностях стабилизации полимеризующейся эмульсии: $C_{пмак}$ (г/дл) *а* — 0.25; *б* — 0.5; *в* — 0.75; *г* — 1.0 ($\alpha = 0.1$); *д* — 0.25 ($\alpha = 0.3$); *е* — 1.0 ($\alpha = 0.3$).

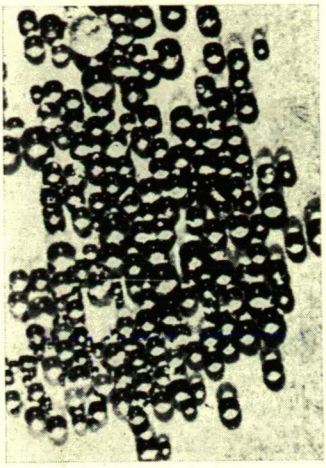

д

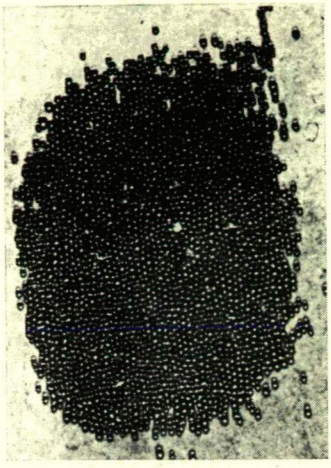

е

систем №№ 7 и 8 отчетливо показывают, что большая поверхностная активность не означает в этих системах высокого стабилизующего действия.

В табл. IV представлена зависимость средних размеров гранул от длительности проведения процесса полимеризации при достаточно сильной стабилизации системы.

Данные таблицы IV показывают практическую неизменность средних размеров полимерных гранул при достаточной эффективности стабилизации, несмотря на более чем шестикратное увеличение времени достижения конца критической фазы.

Таблица IV

Время окончания критической фазы и средние размеры полистирольных гранул, полученных в присутствии разных концентраций инициатора (инициатор — перекись бензоила (ПБ), $C_{\text{пмак}}=0{,}5$ г/дл, $\alpha=0{,}3$)

Концентрация ПБ, моль/л	0,164	0,082	0,041	0,020	0,010
Критич. фаза, минуты	60	110	180	260	390
d, см	0,097	0,099	0,10	0,097	0,095

Обсуждение полученных результатов

Динамическое равновесие диспергирования и коалесценции, устанавливающееся при стационарном перемешивании двух взаимонерастворимых жидкостей, известно из общей теории эмульсий [20] и экспериментально было подтверждено также и для случая гранульной полимеризации [6, 21]. Однако, механизм и длительность перехода динамического равновесия в статическое

состояние формы и размеров капель мономерно-полимерной эмульсии разными исследователями рассматривается по-разному. Некоторые авторы [3, 4, 8] считают, что в гранульной полимеризации при достижении определенной глубины превращения наступает „критическая фаза" или „липкое состояние" при котором происходит односторонний процесс коалесценции, приводящий к агломерции всей мономерно-полимерной массы. При наличии в системе надлежащего диспергатора происходит только частичная коалесценция. В этом случае распределение гранул по размеру устанавливается в критической фазе процесса и определяется рядом фактором из числа которых наиболее важным является качество применяемого диспергатора.

Другие авторы [11, 22] считают, что распределение размеров частиц, при надлежащей стабилизации, устанавливается сразу же в начале процесса вместе с достижением динамического равновесия эмульсионной системы.

На наш взгляд, противоречие двух мнений только кажущееся. Как это следует из данных таблицы I и рис. 1 очевидно, что необходимо разграничить два случая возникновения критической фазы. Первый случай — слабая стабилизация, когда критическая фаза заканчивается тем позже, чем относительно лучше стабилизована система, т. е. сплошная агломерация происходит на более глубоких стадиях превращения (табл. I). С улучшением стабилизации, когда в системе уже не происходит сплошной агломерации, но критическая фаза завершается при все более высоких степенях превращения, то все же образующиеся полимерные частицы представляют собой более или менее крупные агломераты и деформированные гранулы, содержащие в себе захваченный при слипании раствор диспергатора (рис. 1 фото *а*, *б*, *в*). Эти условия стабилизации еще далеко не удовлетворяют требованиям технического осуществлеия гранульной полимеризации. Второй случай — сильная стабилизация, когда дальнейшее улучшение стабилизации в полимеризующейся системе начинает сдвигать завершение критической фазы в противоположную сторону, т. е. образование дискретных мономерно-полимерных частиц, заканчивается тем раньше, чем лучше [12] стабилизована система (рис. 1 фото *г*, *д*, *е*, и табл. II). Таким образом становятся ясными причины возникновения противоречивых литературных данных. Авторы работ [3 8] пришли к обобщающим выводам на основании изучения относительно слабо стабилизованных систем, а авторы [11, 22] наблюдали системы при весьма высоких эффективностях стабилизации, что и следует из анализа условий проведения их опытов.

Как известно [23, 24], в стационарно перемешиваемой эмульсионной системе средний диаметр капель ($\bar{d}$), характеризующее дисперсность внутренней фазы, является функцией геометрических, механических и физических параметров, которую можно записать в общем виде:

$$\bar{d} = f(\varrho_c, \varrho_\Phi^0, \eta_c, \eta_\Phi^0, \sigma_{c\Phi}^0, V_\Phi, H, n, g) \qquad (1)$$

где ϱ_c и ϱ_Φ^0 — плотность дисперсионной среды и дисперсной фазы соответственно,

η_c и η_Φ^0 — вязкость фаз,

$\sigma_{c\Phi}^0$ — поверхностное натяжение на границе раздела фаз,

V_Φ — объемная доля дисперсной фазы,

H — многокомпонентный параметр, включающий размеры и форму сосуда и перемешивающего устройства,
n — число оборотов мешалки,
g — ускорение силы тяжести.

В случае полимеризующейся эмульсии положение с применением уравнения (1) усложняется тем, что величины $\varrho_{ф}^{0}$, $\eta_{ф}^{0}$ и $\sigma_{сф}^{0}$ являются функциями глубины полимеризации. При этом изменение величины $\eta_{ф}^{0}$ по ходу полимеризационного процесса достигает несколько порядков. Эти изменения прекращают динамическое равновесие диспергирования и коалесценции и приводят о образованию дискретных полимерных частиц. Из этого следует, что распределение мономерно-полимерных капель по размеру должно постоянно меняться до тех пор пока рост величин $\eta_{ф}^{0}$ и $\sigma_{сф}^{0}$ не приведет к прекращению динамического равновесия.

Согласно работы [25], средний диаметр капель в стационарно перемешиваемой эмульсии определяется соотношением величин, которое м. б. выражено уравнением:

$$\bar{d} = kH^{p}\frac{\eta_{ф}^{a}\sigma_{сф}^{b}}{\eta_{c}^{h}\Delta\varrho^{i}n^{m}V_{ф}^{r}} \qquad (2)$$

где k—константа, $\Delta\varrho$—разность плотностей фаз и a, b, h, i, m, r, p—экспериментально определяемые показатели степеней при соответствующих параметрах. Применение уравнения (2) для расчета среднего диаметра полимерных частиц затруднено не только вследствие функциональной зависимости величин $\varrho_{ф}$, $\eta_{ф}$ и $\Delta\varrho$ от степени полимеризации, но и в результате того, что два из основных факторов, определяющих дисперсность полимеризующейся эмульсии, — эмульгирующая (дисперсность) и стабилизирующая („время жизни" капли) способность применяемого диспергатора не находятся в явном виде в уравнении. Эти свойства диспергатора отражаются в величинах ϱ_{c}, η_{c} и $\sigma_{сф}$, однако, как это следует из данных табл. III, при неизменных механических условиях, но при разных эффективностях стабилизации, несмотря на весьма близкие значения величин η_{c} и σ_{c} (что пропорционально величине $\sigma_{сф}$), средние диаметры гранул могут значительно различаться. Эти данные подтверждают высказанное нами ранее положение [12, 13], что в полимеризующихся эмульсиях стабилизующее действие не может быть однозначно характеризовано поверхностной активностью или вязкостью раствора применяемого диспергатора. Авторы работ [26], исходя из противоположной этому предпосылки, провели тщательное исследование влияния геометрических и физических параметров системы на гранулометрический состав полиметилметакрилата, получаемого в присутствии частично ацеталированных поливиниловых спиртов, также обнаружили в своих последних работах невозможность применения частных решений равенства (1) в более широком интервале концентраций применяемых ими диспергаторов [27].

Во многих работах, например [3, 4, 6] авторы рекомендовали для получения высококачественного полимерного продукта, как возможно быстрее провести полимеризующуюся эмульсию через стадию „липкого состояния". Этот весьма важный в техническом отношении вопрос может быть рассмотрен

с точки зрения вышеизложенных представлений о механизме образования полимерных гранул. Действительно, если система недостаточно стабильна, то длительность критической фазы, которая заканчивается при относительно высоких степенях полимеризации, легко может отразиться на внешнем виде, чистоте и размерах полимерных гранул. Это является естественным следствием более высокого числа соударений частиц при при большей длительности критической фазы. Вероятность слипания гранул при соударениях является прямой функцией нестабильности системы.

В присутствии высокоэффективного диспергатора, когда критическая фаза завершается на ранних стадиях полимеризационного процесса, т. е. мономерно-полимерные капли еще не обладают очень высокой вязкостью, длительность критической фазы не должно неблагоприятно отразиться на продукте гранульной полимеризации. Экспериментально подтерждается это данными представленными в табл. IV.

Таким образом, можно прийти к выводу, что, в соответствии с литературными данными, полимерные частицы в гранульной полимеризации образуются в результате перехода первоначального динамического равновесия диспергирования и коалесценции мономерной эмульсии в статическое состояние дискретных полимерных частиц при определенных глубинах полимеризации, зависящих от условий стабилизации полимеризационной системы. До настоящего времени нет такой теории, которая позволила бы составить математическое выражение функциональной зависимости среднего размера полимерных гранул от различных параметров системы для разных диспергаторов. В полимеризационных системах, достаточно стабильных для того, чтобы получить продукт необходимой чистоты и дисперсности, критическая фаза процесса завершается при тем более ранних стадиях полимеризации, чем сильне стабилизующее действие диспергатора при прочих равных условиях проведения процесса. При техническом осуществлении гранульной полимеризации помимо этого необходимо учитывать, что скорость полимеризации уже при относительно больших средних размерах капель (от 0.05 см и меньше) может значительно превысить скорость гомогенной полимеризации в массе мономера [16, 17]. Следовательно, с улучшением стабилизации системы растет скорость полимеризации, т. е. степень дисперсности выступает как кинетический фактор в процессе.

Загрязнение полимера раствором диспергатора, образование деформированных частиц и частичная агломерация происходят в тех случаях, когда вследствие недостаточной эффективности стабилизации критическая фаза процесса заканчивается на относительно больших глубинах превращения. В этих случаях слипание мономерно-полимерных капель не всегда сопровождается их дроблением, вследствие высокой вязкости и поверхностного натяжения частиц. В результате этого, слипшиеся частицы могут содержать включения раствора диспергатора и могут деформироваться под действием гидродинамических сил.

Литература

[1] *Wenning H.:* Kunst. Plast. **5**, 328 (1958).
[2] *Хувинк Р., А. Ставерман:* Химия и технология полимеров, т. 2, часть I. Изд. Химия, Москва, 1965.
[3] *Trommsdorf E., C. E. Schildknecht:* High Polymers, vol 10., Intersci. Publ. N-Y., L. 1956.
[4] *Karásek B.:* Chemické listy **55**, 673 (1961).
[5] *Николаев А. Ф.:* Синтетические полимеры и пластические массы на их основе. Изд. Химия, Москва, 1964.
[6] *Hohenstein W. P., H. Mark:* High Molecular Weight Organic Compounds, vol. 6., Intersci. Publ. N-Y. 1949.
[7] *Winslow F. H., W. Matreyek:* Ind. Engng. Chem. **43**, 1108 (1951).
[8] *Hohenstein W. P., H. Mark:* J. Polymer Sci. **1** 127 (1946).
[9] *Trommsdorf E.:* Makromol. Chem. **13**, 76 (1954).
[10] *Hopff H., E. Lutz:* Kunst. Plast. **5**, 341 (1958).
[11] *Gerspacher P.:* Dokt. Diss. ETH Zürich. Juris Verlag. 1963.
[12] *Юрженко А. И., И. А. Андор:* Коллоидн. ж. **32**, 130 (1970).
[13] *Андор И. А., А. И.Юрженко:* Коллоидн. ж. **33**, 492 (1971).
[14] *Андор И. А., А. И.Юрженко, А. Э. Шамракова:* Коллоидн. ж. **32**, 644 (1970).
[15] *Юрженко А. И., И. А. Андор:* Докл. АН СССР **181**, 658 (1968).
[16] *Иванчев С. С., И. А. Андор, Н. И. Соломко:* Докл. АН СССР **199**, 1343 (1971).
[17] *Андор И., А. Э. Шамракова, А. И. Юрженко:* Acta Phys. et Chem. Szeged **18**, 245 (1972).
[18] *Юрженко А. И., И. А. Андор, Н. Н. Заяц:* Коллоидн. ж. **30**, 455 (1968).
[19] *Пучин В. А., Т. И.Юрженко:* Зав. лаб. **21**, 205 (1955).
[20] *Ребиндер П. А.:* Коллоидн. ж. **8**, 157 (1946).
[21] *Рутовский Б. Н., Г. С. Гончаров, Я. Г. Муравин:* Хим. промышл. № 4, 106 (1951).
[22] *Hoppff H., H. Lüssi, E. Hammer:* Makromol. Chem. **82**, 184 (1965).
[23] *Кремнев Л. Я., А. А. Равдель:* Коллоидн. ж. **16**, 17 (1954).
[24] *Павлушенко И. С., А. В. Янишевский:* Ж. прикл. химии **31**, 1348 (1958).
[25] *Павлушенко И. С., А. В. Янишевский:* Ж. прикл. химии **32**, 1495 (1959).
[26] *Hopff H., H. Lüssi, P. Gerspacher:* Makromol. Chem. **78**, 24, 37 (1964).
[27] *Hopff H., H. Lüssi, E. Hammer:* Makromol. Chem. **82**, 175 (1965).

THE MECHANISM OF PARTICLE FORMATION IN BEAD POLYMERIZATION

J. Andor and *A. E. Shamraková*

We have investigated the mechanism of formation of polystyrene particles from emulsion stabilized by polymetacrylic acid, and shown that the dispersity of particles formed from polymerizing emulsions under the same circumstances is not unambigously determined either by the surface activity nor by the viscosity of the dispersing solution used. In systems having high stability for the formation of beads of adequate purity and dispersion grade, the stronger the stabilization effect of the dispersing agent, the earlier the critical period of the process comes to an end.

BOOK REVIEW

New developments in semiconductors, edited by P. R. Wallace, R. Harris, M. J. Zuckerman, 584 pages, Noordhoff International Publishing, Leiden, The Netherlands, 1973.

The rapid development of semiconductor physics, the appearence of new trends in research, and the high number of scientific publications as well as application in industry and technics make necessary to publish books giving a good review of recent development. This publication, which contains the re-edited versions of lectures held at the 1971 Summer Schol of the Department of Physics, McGill University Montreal, Canada, satisfies these exigences. 14 authors of different countries contributed lectures on recent problems and developments in the field of semiconductor physics.

Canada having traditional ties both with the USA and with some of the European countries, the selection of topics throws a good light on the different trends of modern research in these countries. In spite of the freedom given to the lectures in the choice of the topic, the Summer School gave a comprehensive review of the problems dealt with in different research centres.

According to the main lines of semiconductor research, the chapters of the book discuss such topics as hyperquantum phenomena, amorphous materials, metal-semiconductor transitions, which are not readily available in standard books.

Though the publication deals in general with the theoretical foundations of modern investigation, several chapters give also the most important experimental results and their interpretation.

The book satisfies high standards, nevertheless the clearness of its language and precisity of style make it easily comprehensible for readers in possession of the necessary knowledge in this line. The authors are scientists working at a high level on these modern problems and are able to sum up the recent development of their field of research.

Part I is devoted to *magnetic semiconductors* [Dr. C. Haas (Laboratorium voor Anorganische Chemie, R. U. Groningen, The Netherlands): *Band structure and transport properties of magnetic semiconductors;* Dr. S. Methfessel (Ruhr-Universität, Bochum, Federal Republic of Germany): *Ferromagnetic and semiconducting chalcogenides;* P. Leroux—Hugon (CNRS, Bellevue, France): *Transport phenomena in magnetic semiconductors;* J. B. Goodenough (Lincoln Laboratory, M. I. T., Cambridge, Mass., USA): *Valence bond approach to magnetic semiconductors;* W. Baltensperger (Eidg. Technische Hochschule, Zürich, Switzerland): *Electrons in magnetic crystals*].

Part II deals with *metal—semiconductor—insulator phase transitions.* [L. M. Facilov (University of California, Berkeley, California, USA): *Semiconductor metal and magnetic phase transitions in transition metal and rare earth compounds,* D. C. Mattis (Yeshiva University, New York, New York USA): *Phonons and the metal-insulator phase transition.*]

Part III treats the topic of *amorphous semiconductors* [Dr. S. F. Edwards (The Schuster Laboratory, University of Manchester, Manchester, England): *The electronic structure of amorphous materials;* E. N. Economou (James Frank Institute, Chicago, Illinois, USA): *Amorphous semiconductors; theoretical foundations of existing models*].

Lectures of part IV deal with *transport properties in strong magnetic fields.* [Dr. S Askenazy (Faculté des Sciences, l'Université Paul Sabatier, Toulouse, France): *Phénomènes de transport dans le domaine quantique et ultraquantique;* Dr. R. A. Stradling (Clarendon Laboratory, Oxford, England): *The influence of optical phonons on electron transport in semiconductors;* W. Zawadzki (Polish Academy of Sciences, Warsaw, Poland): *Spin properties of conduction electrons in small-gap semiconductors.*]

Part V and part VI are devoted to the problems of *Raman scattering* and *narrow bandgap semiconducting alloys,* respectively. [Dr. Z. Yafet (Bell Laboratories, Murray Hill, New Yersey, USA): *Raman scattering in semiconductors by electronic excitations:* Dr. C. Verie (CNRS, Bellevue, France): *Zero bandgap transition in semiconducting alloys.*]

This book will give the reader up to date and well-arranged knowledge in semiconductor physics, therefore it can be warmly recommended to specialists, advanced students and to young research workers entering the field to the most important recent developments in the major areas of modern semiconductor research.

A. SÜLI

(Institute of Experimental Physics,
Attila József University, Szeged)

INDEX

A kiadásért felelős: Dr. Leindler László
1974
A kézirat a nyomdába érkezett: 1973. okt. 14. Megjelenés: 1974. február
Példányszám: 550 Ábrák száma: 51 Terjedelem: 11,2 (A/5) ív
Készült monó szedéssel, íves magasnyomással, az MNOSZ 5601–54 és az MNOSZ 5602–50 A szabványok szerint
73-4424 — Szegedi Nyomda

TOMI PRIORES

Acta Chemica, Mineralogica et Physica,	Tom.	I,	Fasc.	1—2,	1928—29.
Acta Chemica, Mineralogica et Physica,	Tom.	II,	Fasc.	1—2,	1932.
Acta Chemica, Mineralogica et Physica,	Tom.	III,	Fasc.	1—3,	1934.
Acta Chemica, Mineralogica et Physica,	Tom.	IV,	Fasc.	1—3,	1934.
Acta Chemica, Mineralogica et Physica,	Tom.	V,	Fasc.	1—3,	1937.
Acta Physica et Chemica, Nova series	Tom.	VI,	Fasc.	3—4,	1938.
Acta Chemica, Mineralogica et Physica,	Tom.	VII,	Fasc.	1—3,	1939.
Acta Chemica et Physica,	Tom.	I,	Fasc.	1—2,	1942.
Acta Chemica et Physica,	Tom.	II,	Fasc.	1—6,	1948—50.
Acta Physica et Chemica, Nova series	Tom.	I,	Fasc.	1—4,	1955.
Acta Physica et Chemica, Nova series	Tom.	II,	Fasc.	1—4,	1956.
Acta Physica et Chemica, Nova series	Tom.	III,	Fasc.	1—5,	1957.
Acta Physica et Chemica, Nova series	Tom.	IV,	Fasc.	1—2,	1958.
Acta Physica et Chemica, Nova series	Tom.	IV,	Fasc.	3—4,	1958.
Acta Physica et Chemica, Nova series	Tom.	V,	Fasc.	1—2,	1959.
Acta Physica et Chemica, Nova series	Tom.	V,	Fasc.	3—4.	1959.
Acta Physica et Chemica, Nova series	Tom.	VI,	Fasc.	1—4,	1960.
Acta Physica et Chemica, Nova series	Tom.	VII,	Fasc.	1—2,	1961.
Acta Physica et Chemica, Nova series	Tom.	VII,	Fasc.	3—4,	1961.
Acta Physica et Chemica, Nova series	Tom.	VIII,	Fasc.	1—2,	1962.
Acta Physica et Chemica, Nova series	Tom.	VIII,	Fasc.	3—4,	1962.
Acta Physica et Chemica, Nova series	Tom.	IX,	Fasc.	1—2,	1963.
Acta Physica et Chemica, Nova series	Tom.	IX,	Fasc.	3—4,	1963.
Acta Physica et Chemica, Nova series	Tom.	X,	Fasc.	1—2,	1964.
Acta Physica et Chemica, Nova series	Tom.	X,	Fasc.	3—4,	1964.
Acta Physica et Chemica, Nova series	Tom.	XI,	Fasc.	1—2,	1965.
Acta Physica et Chemica, Nova series	Tom.	XI,	Fasc.	3—4,	1965.
Acta Physica et Chemica, Nova series	Tom.	XII,	Fasc.	1—2,	1966.
Acta Physica et Chemica, Nova series	Tom.	XII,	Fasc.	3—4,	1966.
Acta Physica et Chemica, Nova series	Tom.	XIII,	Fasc.	1—2,	1967.
Acta Physica et Chemica, Nova series	Tom.	XIII,	Fasc.	3—4,	1967.
Acta Physica et Chemica, Nova series	Tom.	XIV,	Fasc.	1—2,	1968.
Acta Physica et Chemica, Nova series	Tom.	XIV,	Fasc.	3—4,	1968.
Acta Physica et Chemica, Nova series	Tom.	XV,	Fasc.	1—2,	1969.
Acta Physica et Chemica, Nova series	Tom.	XV,	Fasc.	3—4,	1969.
Acta Physica et Chemica, Nova series	Tom.	XVI,	Fasc.	1—2,	1970.
Acta Physica et Chemica, Nova series	Tom.	XVI,	Fasc.	3—4,	1970.
Acta Physica et Chemica, Nova series	Tom.	XVII,	Fasc.	1—2,	1971.
Acta Physica et Chemica, Nova series	Tom.	XVII,	Fasc.	3—4,	1971.
Acta Physica et Chemica, Nova series	Tom.	XVIII,	Fasc.	1—2,	1972.
Acta Physica et Chemica, Nova series	Tom.	XVIII,	Fasc.	3—4,	1972.
Acta Physica et Chemica, Nova series	Tom.	XIX,	Fasc.	1—2,	1973.